Mine Impact Burial Prediction From One to Three Dimensions

Peter C. Chu

***Abstract*—The Navy's mine impact burial prediction model (IBPM) creates a time history of a cylindrical (or near-cylindrical) mine as it falls through air, water, and sediment. The output of the model is the predicted burial depth and orientation of the mine in the sediment, as well as height, area, and volume protruding. Model inputs consist of environmental parameters and mine characteristics, as well as parameters describing the mine's release. This paper reviews the following model advances from one to three dimensions: 1) 1-D models predict the vertical position of the mine's center of mass (COM) with the assumption of constant falling angle, 2) 2-D models predict the COM position in the (x, z)-plane and the rotation around the y-axis, and 3) 3-D models predict the COM position in (x, y, z)-space and the rotation around x-, y-, and z-axes. These models are verified using the data collected from recent mine impact burial experiments. The 1-D model only solves one momentum equation (in the z-direction); it cannot predict the mine trajectory and burial depth well. The 2-D model restricts the mine motion in the (x, z)-plane (which requires motionless *[AU: Requires motionless what?]* for the environmental fluids), and uses incorrect drag coefficients and inaccurate sediment dynamics. The prediction errors are large in the mine trajectory and burial depth prediction (6–10 times larger than the observed depth in sand bottom of the Monterey Bay, CA). The 3-D model predicts the trajectory and burial depth relatively well for cylindrical and near-cylindrical mines, but not for the operational mines such as Manta and Rockan. Future improvements should include the shape effects, especially the operational mines.**

***Index Terms*—Burial depth, drag and lift forces and torques, impact burial prediction model (IBPM), IMPACT25/28, IMPACT35, Kirchhoff–Kelvin equation, mine impact burial prediction, orientation, sediment dynamics, translation velocity, triple coordinate system.**

NOMENCLATURE

(C_{d1}, C_{d2})	Drag coefficients along and across the cylinder.
C_l	Lift coefficient.
C_{tl}	Translational lift coefficient (kg s^{-1}).
e_v	Void ratio.
(f_1, f_2, f_3)	Added-mass ratios for drag and lift forces.
f_r	Added-mass ratio for moment of drag and lift forces.
(f_{rd2}, f_{rd3})	Rotational drag force (N).
$\mathbf{F}_b$	Buoyancy force (N).
$\mathbf{F}_d$	Drag force (N).
$(\mathbf{F}_{d1}, \mathbf{F}_{d2}, \mathbf{F}_{d3})$	Drag force in the F-coordinate (N).
$\mathbf{F}_l$	Lift force (N).
$(\mathbf{F}_{l1}, \mathbf{F}_{l2}, \mathbf{F}_{l3})$	Lift force in the F-coordinate (N).
$(\mathbf{i}_E, \mathbf{j}_E, \mathbf{k}_E)$	Unit vectors in the E-coordinate.
$(\mathbf{i}_F, \mathbf{j}_F, \mathbf{k}_F)$	Unit vectors in the F-coordinate.
$(\mathbf{i}_M, \mathbf{j}_M, \mathbf{k}_M)$	Unit vectors in the M-coordinate.
(J_1, J_2, J_3)	Moments of gyration (kg m^2).
$(J_1^{(i)}, J_2^{(i)}, J_3^{(i)})$	Moments of gyration for cylindrical part-i (kg m^2).
L	Length of the cylinder (m).
$\mathbf{M}_b$	Torque due to the buoyancy force (kg m^2 s^{-2}).
$\mathbf{M}_h$	Torque due to the hydrodynamic force (kg m^2 s^{-2}).
$(\mathbf{M}_{d1}, \mathbf{M}_{d2}, \mathbf{M}_{d3})$	Torques due to the drag force in the M-coordinate (kg m^2 s^{-2}).
$\mathbf{r}$	Position vector (in the M-coordinate) of point on the cylinder's surface.
R	Radius of the cylinder.
Re	Reynolds number.
$\mathbf{V}$	Translation velocity (m s^{-1}).
$\mathbf{V}_r$	Water-to-cylinder velocity (m s^{-1}).
$\mathbf{V}_1$	Component of $\mathbf{V}_r$ along the cylinder (m s^{-1}).
$\mathbf{V}_2$	Component of $\mathbf{V}_r$ perpendicular to the cylinder (m s^{-1}).
$\mathbf{V_w}$	Water velocity (m s^{-1}).

Manuscript received June 5, 2005; revised October 4, 2005; accepted October 15, 2005. This work was supported by the U.S. Office of Naval Research Coastal Geosciences Program under the Grants N0001403WR20178 and N0001404WR20067, by the Naval Oceanographic Office, and by the Naval Postgraduate School. **Guest Editor: M. D. Richardson**.

The author is with the Naval Ocean Analysis and Prediction Laboratory, Naval Postgraduate School, Monterey, CA 93943 USA (e-mail: pcchu@nps.edu).

Color versions of one or more of the figures in this paper are available online at http://ieeexplore.ieee.org.

Digital Object Identifier 10.1109/JOE.2007.890941

ν	Molecular viscosity of the water ($m^2\ s^{-1}$).
Π	Volume of the cylinder (m^3).
ρ	Density of the cylinder (kg m^3).
ρ_w	Density of the water (kg m^3).
χ	Distance between COM and COV (m).
(ψ_1, ψ_2, ψ_3)	Angles determining the cylinders' orientation.
$\boldsymbol{\omega}$	Angular velocity (s^{-1}).
$(\omega_1, \omega_2, \omega_3)$	Angular velocity components in the M-coordinate (s^{-1}).
$(\omega_1^F, \omega_2^F, \omega_3^F)$	Angular velocity components in the F-coordinate (s^{-1}).

I. Introduction

In mine hunting, success often hinges on knowing as much as possible about the mines that have been placed and the effects the environment has had on that placement. Since bottom mines cannot be searched visually, and are often difficult to locate with conventional sonar, an estimate of area or height of the mine protruding from the sediment, or the burial depth, is crucial information for the planning and execution of mine clearance operations. Determining the likely mine burial depth requires numerical models of the burial process and knowledge of the environment, including sediment properties, waves, tides, and water depth.

Sea-deployed mines currently used by the United States and other nations fall into three general categories: bottom, moored, and drifting mines. Bottom mines rest on the ocean floor and are generally deployed in littoral regions. Common placements for bottom mines include shipping channels, harbors, anchorages, rivers, and estuaries. Bottom mines are deployed in one of three ways: aircraft, surface ship, or submarine. Mine impact burial models have been developed to predict mine's motion in air and water and to determine the burial depth when the mine comes to rest in the sediment.

The 1-D impact burial prediction model (IBPM) was developed by Arnone and Bowen [1] to predict the vertical position of the cylindrical mine's center of mass (COM) as it falls through air, water, and sediment. The burial depth of the mine in marine sediment is then calculated from the mine's velocity and the sediment characteristics. IBPM only solves the vertical momentum equation with the assumption of an unchanged orientation in the fluid.

Satkowiak [2], [3] modified Arnone and Bowen's [1] pioneering work including corrected reference flow used in drag calculation and corrected added-mass term in equations; reworked equations for sediment-cavity regime, drag due to cylindrical and rounded noses, and retarding forces in semisolid sediment; and included water temperature effect on the water viscosity. The major weakness of the 1-D model is the mine's orientation (or the falling angle) assumed constant as it falls through the fluid.

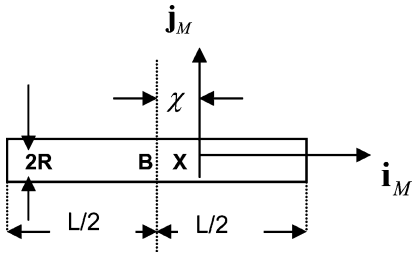

Fig. 1. M-coordinate with the COM as the origin $\mathbf{X}$ and (i_m, j_m) as the two axes. Here, χ is the distance between the COV ($\mathbf{B}$) and COM ($\mathbf{X}$) and (L, R) are the cylinder's length and radius (after [13]).

The 2-D models were developed first by Hurst to overcome major weakness of IBPM (constant falling angles) ([4]), and written in Basic (IMPACT25) and in Matlab (IMPACT28). The models contain three equations with two momentum equations (in x- and z-directions) and a moment-of-momentum equation (in y-direction), and predict mine COM position in the (x, z)-plane and the rotation (i.e., mine orientation) around the y-axis. The models include Mulhearn's [5] formulation for sediment bearing strength and uses multilayered sediments.

Although the 2-D (x, z)-models advance our knowledge on the mine by including mine rotation around the y-axis, it is very difficult to include the motion of fluid. This is because it is hard to assume the fluid (air, water, and sediment) movement strictly in the (x, z)-plane. Any fluid motion in the y-direction induces drag force, and in turn, causes the mine movement (in the y-direction), which breaks the 2-D scenario [6], [7]. In fact, it is impossible to lay a mine in the same vertical plane of the fluid velocity. Sensitivity studies on IMPACT25/28 burial depth show the insensitivity of the mine-releasing height and the water temperature ([8]). A mine drop experiment at Monterey Bay, CA ([9]–[11]) shows that IMPACT25/28 overpredicts the burial depth.

The 3-D model (IMPACT35) has been developed with the support from the U.S. Office of Naval Research (ONR, Arlington, VA) through mine burial prediction program [12]–[15]. The model contains six equations with three momentum equations and three moment-of-momentum equations, and predicts the mine's COM position in the (x, y, z)-space and the rotation (i.e., mine's orientation) around the three axes. Several mine drop experiments conducted at the Naval Postgraduate School (Monterey, CA), Naval Undersea Warfare Center—Carderock (West Bethesda, MD), and Baltic Sea (by the German Navy) are used to evaluate the 2-D and 3-D models. The results show great improvement of the 3-D modeling.

The 1-D, 2-D, and 3-D models are reviewed in the following sections. Basic physics, formulation, strength, and weakness of each model are presented. The purpose is to provide an overall picture of more than two decades' effort on predicting the mine movement in air, water, and sediment.

II. Mine Location and Orientation

Consider an axially symmetric cylinder with the COM $\mathbf{X}$ [or called gravity center (GC) in literature] and center of volume (COV) $\mathbf{B}$ on the main axis (Fig. 1). Let (L, R, χ) represent cylinder length, radius, and the distance between the two points

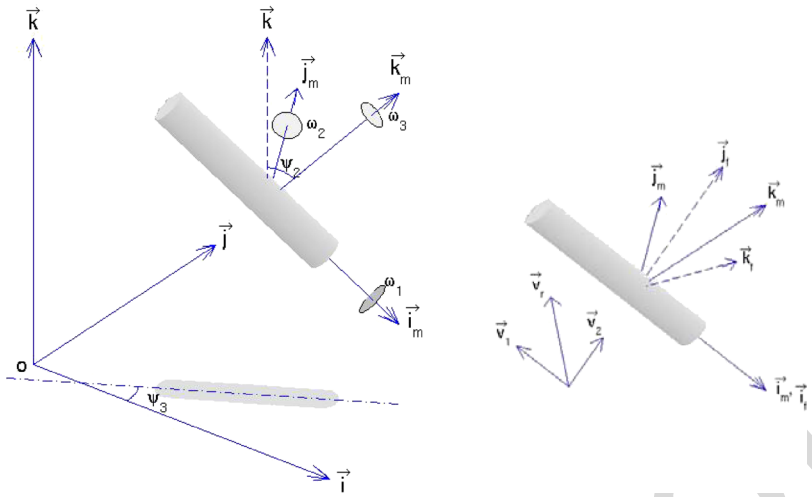

Fig. 2. Mine's COM position (x, z) and orientation ψ_2 (after [16]).

$(\mathbf{X}, \mathbf{B})$. The positive χ-values refer to nose-down case, i.e., the point $\mathbf{X}$ is lower than the point $\mathbf{B}$. Let $F_E(O, \mathbf{i}, \mathbf{j}, \mathbf{k})$ be the earth-fixed coordinate (E-coordinate) with the origin "O", and three axes: x- and y-axes (horizontal) with the unit vectors $(\mathbf{i}, \mathbf{j})$ and z-axis (vertical) with the unit vector $\mathbf{k}$ (upward positive). The position of the cylinder is represented by the position of the COM

$$\mathbf{X} = x\mathbf{i} + y\mathbf{j} + z\mathbf{k} \tag{1}$$

which is translation of the cylinder. The translation velocity is given by

$$\frac{d\mathbf{X}}{dt} = \mathbf{V}, \qquad \mathbf{V} = (u, v, w). \tag{2}$$

The orientation of the cylinder main axis (pointing downward) is given by $\mathbf{i}_M$. The angle between $\mathbf{i}_M$ and $\mathbf{k}$ is denoted by $\psi_2 + \pi/2$ (Fig. 2). The angle ψ_2 is the mine-falling angle. In the 1-D and 2-D modeling, only the E-coordinate system is used. In 3-D modeling, two extra-coordinate systems (main-axis-following and force-following coordinates) are also used.

III. Triple Coordinate Systems

The following three coordinate systems are used in mine impact burial prediction modeling: earth-fixed coordinate (E-coordinate), main-axis-following coordinate (M-coordinate), and force-following coordinate (F-coordinate) systems. All three coordinate systems are 3-D, orthogonal, and right-handed [16]. Projection of the mine's main-axis vector $\mathbf{i}_M$ onto the (x, y)-plane creates angle (ψ_3) between the projection and the x-axis (Fig. 2). The M-coordinate is represented by $F_M(\mathbf{X}, \mathbf{i}_M, \mathbf{j}_M, \mathbf{k}_M)$ with the origin "$\mathbf{X}$" (i.e., the COM location), unit vectors $(\mathbf{i}_M, \mathbf{j}_M, \mathbf{k}_M)$, and coordinates (x_M, y_M, z_M). The unit vectors of the M-coordinate system are given by

$$\mathbf{j}_M = \mathbf{k} \times \mathbf{i}_M \quad \mathbf{k}_M = \mathbf{i}_M \times \mathbf{j}_M. \tag{3}$$

The M-coordinate system is solely determined by orientation of the cylinder's main axis $\mathbf{i}_M$.

The F-coordinate is represented by $F_F(X, i_F, j_F, k_F)$ with the origin $\mathbf{X}$, unit vectors $(\mathbf{i}_F, \mathbf{j}_F, \mathbf{k}_F)$, and coordinates (x_F, y_F, z_F). Let $\mathbf{V}_w$ be the fluid velocity. The water-to-mine velocity is represented by

$$\mathbf{V}_r = \mathbf{V}_w - \mathbf{V} \tag{4}$$

which can be decomposed into two parts

$$\mathbf{V}_r = \mathbf{V}_1 + \mathbf{V}_2 \quad \mathbf{V}_1 = (\mathbf{V}_r \cdot \mathbf{i}_F)\mathbf{i}_F \quad \mathbf{V}_2 = \mathbf{V}_r - (\mathbf{V}_r \cdot \mathbf{i}_F)\mathbf{i}_F \tag{5}$$

where $\mathbf{V}_1$ is the component paralleling to the cylinder's main axis (i.e., along $\mathbf{i}_M$), and $\mathbf{V}_2$ is the component perpendicular to the cylinder's main-axial direction. The unit vectors for the F-coordinate are defined by (column vectors)

$$\mathbf{i}_F = \mathbf{i}_M \quad \mathbf{j}_F = \mathbf{V}_2/|\mathbf{V}_2| \quad \mathbf{k}_F = \mathbf{i}_F \times \mathbf{j}_F. \tag{6}$$

Transforms among the three coordinate systems can be found in [16].

IV. The 1-D Modeling

The 1-D models assume that the cylinder is not rotating about any axis, nor is there a net fluid dynamic lift; consequently, it can be reasonably applied to stable motion of the body along one of its major axes (horizontal or vertical). The models predict the COM location (i.e., z) using the Kirchhoff–Kelvin theory. Only the E-coordinate system is used for 1-D modeling.

A. Kirchhoff–Kelvin Theory

In the later half of the 19th century, Kirchhoff and Lord Kelvin showed that the motion of a solid moving through an ideal fluid could be represented by a compact system of equations describing the coupled fluid-body dynamics [17], [18]. Publications about the implications and extensions of this theory (cited as the Kirchhoff–Kelvin equations hereafter) were frequent from the 1870s until the 1900s, when experimental aerodynamics showed the limitations of the idealized models in representing the coupled dynamics of bodies and complex turbulent boundary layer regimes. Interest in the subject also

waned due to the daunting nonlinearity of the governing equations. Recently, there has been a resurgence of interest in the Kirchhoff–Kelvin theory, since the widespread availability of highly capable computers has allowed numerical analysis of problems involving nonlinear dynamics [19]–[21]. Even when analytical closure is not practical, the general results of the Kirchhoff–Kelvin equations aid heuristic explanations of the observed dynamics of more complex shapes, such as coins (very short cylinders) sinking in water [22] and tumbling cards [23]. In [24], excellent introductory can be found to the Kirchhoff–Kelvin equations and implications.

In general, the Kirchhoff–Kelvin equations predict the coupled dynamic response of arbitrary solid bodies to various forces and torques within inviscid, incompressible flow. For high Reynolds number regimes ($\mathrm{Re} = UD/\nu > 10^4$, where U is velocity, D is either the length or diameter of the cylinder depending on release orientation, and ν is kinematic viscosity), the direct effect of viscosity is small such that coherent structures of the turbulent boundary layer diminish. The typical value of Re for mine falling through the water column is around 10^5 [15]. This condition allows the generalized dynamics of falling bodies to be characterized in terms of a simplified form of the Kirchhoff–Kelvin theory where buoyancy forces and turbulent drag are balanced by the inertia of the cylinder and displaced water. For a freely sinking cylinder of diameter d and length l, the combined effect of gravity and buoyancy per unit volume is

$$B = (\rho - \rho_w)g \tag{7}$$

where g is the gravity and $(\rho - \rho_w)$ is the density difference of the cylinder and the water. The flow over the cylinder surface yields pressure distributions that result in a net drag force on the body, empirically represented as proportional to the square of the body's speed through the water

$$F \approx \frac{1}{2}\rho_w C_d U^2 \Lambda \tag{8}$$

where C_d is the drag coefficient, U is mine's fall speed, and Λ is an effective cross-sectional area normal to the flow. Under the assumption that the torques exerted by wake pressure fluctuations are insignificant, the phenomenological representation of the total drag force on the cylinder can be used in an approximation for the falling motion where the rate of change in kinetic energy is parameterized by the rate of change of the cylinder momentum and the acceleration of the "virtual mass" of the displaced water (which depends upon the geometric characteristics of the body). Thus, the force balance on the cylinder is given by

$$\frac{d^2z}{dt^2} = \frac{\rho_w C_d \Lambda}{2\rho\Pi(1+f)}\left(\frac{dz}{dt}\right)^2 - \frac{(\rho - \rho_w)}{\rho}g + \frac{F}{\rho\Pi} \tag{9}$$

where Π is the volume of the mine, f is the effective added-mass factor or the virtual mass coefficient of the system due to the acceleration of water around the moving body, and F is the additional sediment force which is zero in air and water.

Full implementation of the theory is not the focus of this paper; however, stability analysis of particular variants of the Kirchhoff–Kelvin equation provide useful insights. We can characterize the generalized dynamics governing the motions of mines falling through water under the following hypothetical situations: vertical descent with the axis of the cylinder aligned parallel to the flow or vertical descent with the axis of the cylinder aligned perpendicular to the flow. For the simplest case where the axis of the cylinder is aligned with the fall direction, body motions will be stable unless they are significantly disturbed in a direction normal to the motion. This means that a vertically oriented cylinder dropped freely will maintain this orientation until external forces, such as variable turbulent drag, cause the motion to become unstable resulting in changes in orientation. With the axis of the cylinder oriented horizontally, or normal to the trajectory, the motion is also stable. An alterative scenario where the axis of the cylinder is not initially aligned either parallel or perpendicular to the flow makes application of the above equations difficult, but has been addressed in [25] where it is established that with time, the falling body will assume a horizontal orientation where the torque exerted on the body by the water turns the main axis of the cylinder, so that it is normal to the relative flow (broadside). This configuration is stable when the exposed area is normal to the flow and is significantly greater than the cross-sectional area of the "nose-on" attitude. Slight variations of this stable mode also exist including regular oscillations, glide tumble motions, and helical motions.

B. IBPM

The 1-D model is the first generation of the U.S. Navy's mine impact burial model [1]–[3], called the IBPM. This model is used to predict the vertical location and orientation of a cylindrical mine falling through air, water, and sediment through solving the Kirchhoff–Kelvin equation (9). The model consists of four major components: 1) steady falling attitude (ψ_2), 2) drag computation, 3) cavity regimes, and 4) additional sediment forces.

1) Constant Falling Angle in Single Media: IBPM does not use the moment-of-momentum equation to predict the mine orientation. After the mine passes the interface of two contacted media, the falling angle is assumed [1] to have a steady value determined by the moments of the vertical force $(\rho g - f_1\rho_w \cos^2\psi_2)$ and of the horizontal force $(\rho g - f_2\rho_w \sin^2\psi_2)$,

$$\tan\psi_2 = \frac{\mathrm{moment}(\rho g - f_1\rho_w\cos^2\psi_2)}{\mathrm{moment}(\rho g - f_2\rho_w\sin^2\psi_2)}. \tag{10}$$

An iteration method is used to calculate the attitude ψ_2. Equation (10) is not correct since the orientation of the moment is not the same as the orientation of mine.

In IBPM, the falling angle is treated as a given parameter, which means that the orientation of the mine does not change in the single medium. The effective cross-sectional area (or sometimes called projected area) Λ is calculated by

$$\Lambda = 2LR\sin\psi_2 + \pi R^2\cos\psi_2. \tag{11}$$

For an attitude of 0° (vertical), Λ equals πR^2. For an attitude of 90° (horizontal), Λ is the product of the length (L) and diameter $(2R)$.

The effective added-mass factors in the along and across mine's axis direction f_1 and f_2 are given by

$$f_1 = \frac{\alpha_0}{2-\alpha_0} \quad f_2 = \frac{\beta_0}{2-\beta_0} \tag{12}$$

where

$$\begin{aligned} \alpha_0 &\equiv \frac{4}{\delta}\left(\frac{4}{\delta^2}-1\right) - \left[\frac{1}{2}\ln\left(\frac{2+\delta}{2-\delta}\right) - \frac{\delta}{2}\right] \\ \beta_0 &\equiv \frac{4}{\delta^2} - \frac{1}{\delta}\left(\frac{4}{\delta^2}-1\right)\ln\left(\frac{2+\delta}{2-\delta}\right) \\ \delta &\equiv \frac{2R}{L}. \end{aligned} \tag{13}$$

δ is the aspect ratio. The effective added-mass factor is computed by

$$f = f_2 \sin\psi_2 + f_1 \cos\psi_2. \tag{14}$$

For an attitude of 0° (vertical), f equals f_1. For an attitude of 90° (horizontal), f equals f_2.

2) Drag Coefficient: Drag on a cylinder is proportional to the forces acting on the cylinder as if it were falling both vertically and horizontally. Thus, attitude during fall is important. Simply put, the total drag coefficient is a sum of the drag coefficient due to flow plus the drag coefficient due to cross flow as a function of attitude. This becomes somewhat more complicated because the character of the flow across the cylinder changes based on the magnitude of the Reynolds number of the cylinder. When the Reynolds number is small (<1), skin friction dominates but as the Reynolds number increases, a more laminar flow occurs and pressure drag dominates. At a certain and critical Reynolds number (10^4), flow becomes turbulent and drag abruptly decreases. Reynolds number is thus dependent on velocity of the cylinder and must be constantly recalculated as the cylinder falls through each medium. Let the Reynolds number (Re) be defined by

$$\mathrm{Re} = \frac{2UR}{\nu} \tag{15}$$

where ν is the kinematic viscosity of the fluid.

The axial and cross drag coefficients (C_{da}, C_{dc}) are calculated by [1]

$$C_{dc} = 1.1\eta C_{d\infty}\sin^2\psi_2 \quad C_{da} = 1.1C_{d*}\frac{\Lambda}{2RL} \tag{16}$$

where (17), shown at the bottom of the page, is the cross flow drag coefficient for the cylinder with infinite length $(C_{d\infty})$, and

$$C_{d*} = 0.33\delta + \frac{3.984}{\sqrt{\mathrm{Re}}}\left[\frac{1}{\delta} + \delta^{1/2}\right] \tag{18}$$

is the axial drag coefficient with no surface imperfections. The coefficient of 1.1 in (16) is used to account for imperfections of the cylinder with the correction factor η given by

$$\eta = 0.52238 + 0.02119\frac{1}{\delta} - 0.00048\left(\frac{1}{\delta}\right)^2. \tag{19}$$

The total drag coefficient (C_d) for computing the drag force on a mine moving through the fluid is calculated by

$$C_d = C_{da} + C_{dc}\sin^2\psi_2. \tag{20}$$

3) Air–Water Cavity: Upon impacting the water, the cylindrical mine enters the air–water cavity. The properties of the fluid in the water cavity are combination of air and water fluid properties and are continuously changing with time. Thus, it becomes extremely difficult to accurately predict the forces acting on a body in a fluid of changing properties [1], [26]. The changing properties around the cylinder through the cavity are the fluid density and kinematic viscosity. For example, the fluid density changes from air ($\rho_a = 1.29$ kg m^{-3}) to seawater ($\rho_w = 1025$ kg m^{-3}).

Within the air–water cavity regime, a percentage of each of these densities is used in determination of the resulting average density. This is represented by the ratio (called the void ratio) of the volume of water in the cavity to the total cavity volume. Although it is difficult to actually determine these volumes, the trend of this ratio is known. For example, the void ratio equals 0 for the cylinder in the air, and equals 1 for the cylinder totally wetted in the water. The void ratio n_0 is calculated by

$$n_0(t) = \sqrt{\frac{p_D(t)}{p_S(t)}} \tag{21}$$

in the IBPM. Here

$$p_D(t) = p_a + \frac{1}{2}\rho_w\left[U(t)\right]^2 \quad p_S(t) = p_a - \rho_w g z(t) \tag{22}$$

are the dynamic and static pressures, $z = 0$ denotes the air–water interface, and $p_a(= 100$ kPa) is the atmospheric pressure at the air–water interface. The air–water cavity density (ρ_w^{cav}) and viscosity (ν_w^{cav}) are calculated by

$$\rho_w^{\mathrm{cav}} = \rho_a(1-n_0) + \rho_w n_0, \quad \frac{1}{\rho_w^{\mathrm{cav}}\nu_w^{\mathrm{cav}}} = \frac{(1-n_0)}{\rho_a\nu_a} + \frac{n_0}{\rho_w\nu_w}. \tag{23}$$

The dynamic effect of cavitation on the body is through the change of the Reynolds number (in turn the change of the drag coefficient). The Reynolds number for the air–water cavity is calculated by

$$\mathrm{Re}_w^{\mathrm{cav}} = \frac{2UR}{\nu_w^{\mathrm{cav}}}$$

$$C_{d\infty} = \begin{cases} 0.84864 + 5.81939/\mathrm{Re}, & \text{if } \mathrm{Re} \le 4\times10^3 \\ (0.5833\times10^{-4})\mathrm{Re} + 0.61677, & \text{if } 4\times10^3 < \mathrm{Re} \le 10^4 \\ 1.2, & \text{if } 10^4 < \mathrm{Re} \le 8\times10^4 \\ 1.19381 + (0.65828\times10^{-6})\mathrm{Re} - 10^{-11}\mathrm{Re}^2, & \text{if } 8\times10^4 < \mathrm{Re} \le 5\times10^5 \\ 8\times10^{-7}\mathrm{Re} - 0.15, & \text{if } \mathrm{Re} \ge 5\times10^5 \end{cases} \tag{17}$$

Substitution of $\mathrm{Re}_w^{\mathrm{cav}}$ into (16)–(20) leads to the drag coefficient for the air–water cavity.

4) Water–Sediment Cavity: Upon impacting the sediment, the cylindrical mine enters the water–sediment cavity. Similar to the air–water cavity regime, the properties of the water–sediment cavity are combination of water and sediment properties and are continuously changing with time. In the water–sediment cavity regime, the fluid density changes from water ($\rho_w = 1025$ kg m^{-3}) to sediment ρ_s. Within the water–sediment cavity, the void ratio n_1 is calculated by

$$n_1(t) = \sqrt{\frac{p_D(t)}{p_S(t)}} \tag{24}$$

where

$$\begin{aligned} p_D(t) &= p_a + \rho_w g h + \frac{1}{2}\rho_s \left[U(t)\right]^2 \\ p_S(t) &= p_a + \rho_w g h - \rho_s g \left[z(t) + h\right] \end{aligned} \tag{25}$$

are the dynamic and static pressures and h is the water depth. The water–sediment cavity density (ρ_s^{cav}) and viscosity (ν_s^{cav}) are calculated by

$$\rho_s^{\mathrm{cav}} = \rho_w(1-n_1) + \rho_s n_1 \quad \frac{1}{\rho_s^{\mathrm{cav}}\nu_s^{\mathrm{cav}}} = \frac{(1-n_1)}{\rho_w \nu_w} + \frac{n_1}{\rho_s \nu_s}. \tag{26}$$

The kinematic viscosity of the sediment is determined by

$$\nu_s = \nu_w + \frac{S}{\rho_s dU/dz} \tag{27}$$

where S is the shear strength of the sediment. Substitution of ν_s into (15) leads to a new Reynolds number; and then, use of (16)–(20) leads to the drag coefficient for the water–sediment cavity.

5) Additional Sediment Forces: It is noted that there are forces acting on the mine in the sediment which are different from those forces determined in the air and water. The hydrodynamic forces do not impose or account for the retarding force on a mine moving in sediment. The compressive and shearing stress forces of a sediment, which are not included in the hydrodynamic forces, are important in affecting the mine movement. The following equations

$$F = F_C + F_S \quad F_C = 2S\Lambda_f \quad F_S = S\Lambda_s \tag{28}$$

are used to compute the sediment resistant force [1]. Here, Λ_f and Λ_s are the frontal and side areas of the cylinder. The sediment resistant force is also dependent on the velocity of cylinder [3]

$$F = E_s S(N_b\Lambda_f + S_{af}\Lambda_s/S_t) \tag{29}$$

where E_s is the sediment strain effect (i.e., ratio of the sediment strength for a given velocity of the cylinder), $N_b(=10)$ is the bearing capacity factor, S_{af} is the side adhesive factor (0.3 for the cavity and 1.0 for sediment), and $S_t(=3)$ is the sediment sensitivity coefficient.

Thus, the sediment shear strength and density data are required to solve the Kirchhoff–Kelvin equation (9) for mine movement in the sediment since they are needed for determination of the sediment's compressive and shearing forces, buoyancy force, added-mass, drag force, and kinematic viscosity. Since the properties of sediment change with depth, the sediment density and shear strength profiles with 5-cm vertical resolution are used in the IBPM.

C. Sensitivity Studies

For a single medium, after the attitude (ψ_2) is determined from (10), the effective cross-sectional area Λ and effective added-mass factor f can be calculated using (11) and (12), and then, the total drag coefficient C_d can be computed using (20). For sediment, the compressive and shear stress forces (F) are computed from the density and shear strength. With the known parameters (Λ, f, C_d, F), the Kirchhoff–Kelvin equation (9) can be solved for mine movement. For mine penetration into the air–water and water–sediment interfaces, the total drag coefficient C_d^{cav} is calculated from the cavity density (ρ_w^{cav} or ρ_s^{cav}) and viscosity (ν_w^{cav} or ν_s^{cav}).

Arnone and Bowen [1] conducted a model sensitivity study on the mine air weight (or wet weight), length, and radius. The model (9) was integrated with various combinations of these parameters and the following three different attitudes: $\psi_2 = 0°$ (horizontal), 45°, abd 90° (vertical). The water impact velocity has the following features: 1) For mine movement in the air, as one would expect, the more streamlined the falling attitude is (i.e., $\psi_2 = 90°$, vertical), the higher velocity of the cylindrical mine falls; 2) the water impact velocity varies drastically with the attitude for light mines; such an effect reduces as the mass increases; and 3) the water impact velocity is not sensitive to mine length and radius.

The mine-falling velocity in water has the following characteristics.

1) It varies drastically with attitude and wet weight. For the same wet weight, the mine falls faster for $\psi_2 = 90°$ (vertical) than for $\psi_2 = 0°$ (horizontal). For the same ψ_2, the mine falls faster for heavier wet weight.
2) It is not sensitive to attitude for short mines and is very sensitive to attitude for long mines.
3) It is not sensitive to mine length for horizontal release $(\psi_2 = 0°)$ and is very sensitive to mine length for vertical release $(\psi_2 = 90°)$.
4) It is not sensitive to attitude for small R and is very sensitive to attitude for large R.***[AU: Last item of this list was removed, because it was exactly the same as point 4). Please check.]***

D. Strength and Weakness

IBPM can simulate mine-falling velocity in the air and water columns. As mentioned in Section IV-C, the model provides the following useful results: 1) the mine has higher falling velocity for vertical release $(\psi_2 = 90°)$ than for the horizontal release $(\psi_2 = 0°)$; 2) the water impact velocity varies drastically with the attitude for light mines, but does not for heavy mines; and 3) the mine-falling velocity in water column is sensitive to attitude, wet weight, mine length, and mine radius. For the same mine, the falling velocity in the water has a minimum in horizontal orientation and a maximum in vertical orientation.

Weakness of the IBPM is to assume the constant attitude (ψ_2) during the mine falling through air, water, and sediment (Fig. 3),

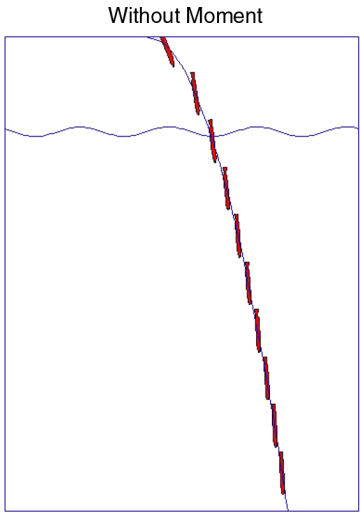

Fig. 3. Mine's orientation is assumed constant by the 1-D model when it falls through a single fluid (after [12]).

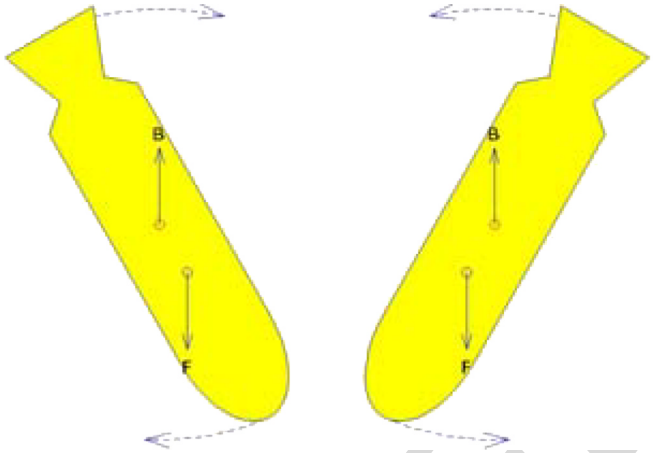

Fig. 4. Change of mine orientation caused by moment of momentum due to the buoyancy force (after [27]).

which is not physically realistic [12]. In fact, the orientation changes for any solid object falling through fluid (air and water). When COV is not colocated with COM, the buoyancy force ($\mathbf{B}$) has a moment of momentum exerted on mine (Fig. 4) [27]. If the mine slants toward left (right), the moment of momentum due to the buoyancy force will rotate the mine clockwise (counterclockwise), respectively. This causes the spiral motion for mine falling through fluid.

V. The 2-D Modeling

To overcome the major weakness of the 1-D model (i.e., constant falling angle), Hurst [4] modified the IBPM model allowing the cylinder to move both vertically and horizontally [in (x, z)-plane] as well as rotating about y-axis. These changes mandated the use of more complicated dynamical system than the IBPM. Two coordinate systems (E- and M-coordinates) are used in the 2-D modeling.

A. Dynamical System

Let the cylinder be moving in (x, z)-plane. The momentum equations in the (x, z)-directions are given by

$$\frac{d^2x}{dt^2} \equiv \frac{du}{dt} = \frac{F_h^x}{\rho\Pi} \tag{30}$$

$$\frac{d^2z}{dt^2} \equiv \frac{dw}{dt} = -g + \frac{B + F_h^z}{\rho\Pi} \tag{31}$$

where B is the buoyancy force, and F_h^x and F_h^z are the components of the hydrodynamic force $\mathbf{F}_h$. Since the cylinder is in the (x, z)-plane, the only possible rotation is around y-axis, which is described by the attitude ψ_2. The moment-of-momentum equation in the M-coordinate is given by

$$J_2 \frac{d^2\psi_2}{dt^2} = B\chi \cos\psi_2 + M_h^y \tag{32}$$

where J_2 is the moment of inertia in the y-axis and M_h^y is called the braking torque in [4].

B. IMPACT25/28

The 2-D models, usually called IMPACT25 (written in Basic) and IMPACT28 (written in Matlab), are the second generation of the Navy's mine IBPMs and were based on (30)–(32) for obtaining x, z, and ψ_2. The external forcing for IMPACT25/28 consists of drag force (F_h^x and F_h^z) and braking torque (M_h^y). Since the mine movement is restricted in the (x, z)-plane, it is very hard to include the motion of the fluids (air or water). If the fluid has velocity in the y-direction, the mine's motion cannot be 2-D. Thus, in IMPACT25 and IMPACT28, the fluid (air or water) is assumed motionless.

1) Drag Force: The drag force for the whole cylinder is calculated in two directions: along the cylinder's main axis ($\mathbf{i}_M$) and across the cylinder ($\mathbf{k}_M$)

$$\mathbf{F}_d = -F_d(\mathbf{i}_M \sin\psi_2 - \mathbf{k}_M \cos\psi_2) \tag{33}$$

where F_d is computed using the drag law

$$F_d = \frac{1}{2}\rho_w \hat{C}_d(u^2 + w^2)\Lambda. \tag{34}$$

The drag coefficient $\hat{C}_d$ is computed by

$$\hat{C}_d = C_d + C_{dn} \tag{35}$$

where C_d is computed in the same way as in the 1-D model [i.e., (20)] and C_{dn} is the drag coefficient for the nose.

2) Braking Torque: The braking torque M_h^y in (32) is calculated by

$$M_h^y = -\frac{1}{6}C_{dc}R\rho_w\omega_2 L^3 V_c \tag{36}$$

where

$$V_c = u\cos\psi_2 + w\sin\psi_2 \tag{37}$$

is the cross-cylinder velocity. Equation (36) is only used when the mine is fully immersed in a single fluid. During the cavity regimes, a different calculation is applied. Furthermore, the torque is opposite in sign to rotation, and thus, it acts to brake the rotation of mine. For a single fluid, the basic (30)–(32) are integrated with (33) and (36).

3) Sediment: In the 1-D models, IPBM and its modifications treat the sediment as fluid that is characterized by the following two parameters: sediment density and shear strength. Different from the 1-D models, the 2-D model treats the sediment as a solid that undergoes plastic deformation [4]. The pertinent parameters become sediment density and bearing strength. Bearing strength is the load bearing capacity of the sediment and defined as the pressure in front of the object penetrating the sediment. It is related to the shear strength, typically larger by a factor of about ten. The following three mechanisms contributing to the sediment resistance on the penetration of a falling mine are included in IMPACT25/28: bearing strength of the sediment (70%), hydrodynamic drag (25%), and buoyancy (5%) [4].

As the mine penetrates the sediment, the hydrodynamic drag that retards the penetration is calculated by

$$F_d = \frac{\rho_s \Lambda (u^2 + w^2)}{2} \left(C_1 \frac{h}{L} + C_2 \right) \tag{38}$$

where C_1 and C_2 are drag coefficients for low Reynolds number and h is the depth in sediment. The buoyancy force comes into play when the mine impacts the sediment. A crater is formed and the force that is required to create and enlarge the crater is given by [4]

$$B = \pi g h (\rho_w - \rho) \Lambda. \tag{39}$$

Two assumptions are made regarding the mine. First, the buoyancy force acts uniformly on the portion of the mine in contact with the sediment. Second, cavity is formed, and remains at the aft end of the mine, leading the mine surface to the buoyancy force. The second is not always true. For some cases, the cavity collapses under the weight of the sediment. The collapse limit is defined and approximated as the depth where the buoyancy force is 20% of the bearing force. Besides, the drag, buoyancy, and bearing strength of sediment all depend on the mine contact area Λ.

4) Air–Water Cavity: As mentioned before, when the mine penetrates the air–water interface, it forms a cavity behind the mine that changes the drag forces. Throughout the cavity regimes, nonsymmetric forces are acting on the mine that generate torque and affect the rate of rotation. The cavity parameterization is different between the 2-D models (IMPACT25/28) and 1-D model (IPBM). The cavity formation in the 2-D models is controlled by a cavitation number (N_{cav}) defined by

$$N_{\text{cav}} = \frac{2(p_{\text{out}} - p_{\text{in}})}{\rho_w (u^2 + w^2)} \tag{40}$$

where p_{out} and p_{in} are the hydrodynamic pressure outside (i.e., water) and inside the cavity, respectively. Pressure difference between outside and inside of the cavity increases or the mine's velocity decreases; the cavitation number increases until the eventual collapse of the cavity. The drag coefficient of the cavity is the function of the cavitation number

$$C_d(N_{\text{cav}}) = \hat{C}_d(1 + bN_{\text{cav}}). \tag{41}$$

When the air–water cavity collapses, $N_{\text{cav}} = 0$, $C_d(0)$ is the water drag coefficient. The torque in the air–water cavity can be computed after the drag coefficient is determined.

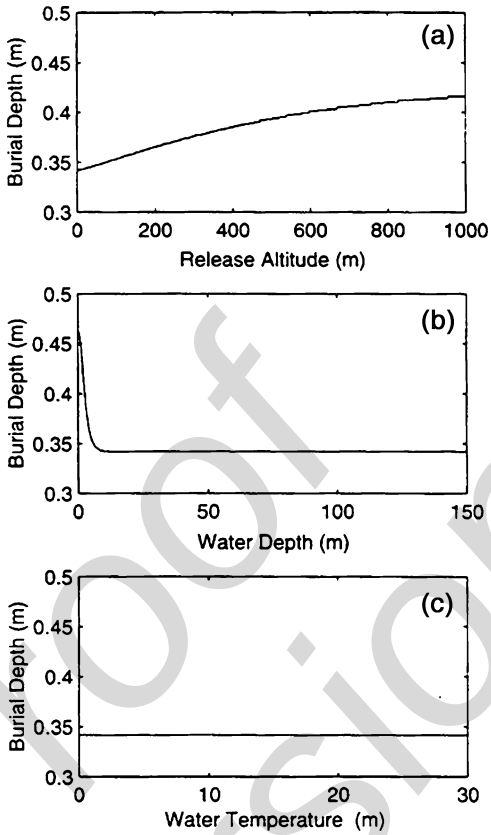

Fig. 5. Effect of (a) release attitude, (b) water depth, and (c) water temperature on burial depth. Values are preliminarily chosen to represent all conditions under which IMPACT25 and IMPACT28 may be used (after [28]).

C. Sensitivity Study

Sensitivity studies [8], [28] were conducted on the 2-D model (IMPACT25/28) to ascertain which parameters the model is most sensitive to and which can be simplified or eliminated to simplify its use. The model was altered to allow most parameters to be set and a loop run for one variable at a time. All model runs were made with preset mine profile, which has a dry weight of 538 kg, a wet weight of 251 kg, and a uniform diameter of 0.475 m.

1) Sensitivity to Release Parameters: Fig. 5 demonstrates the sensitivity of the release altitude and model parameters such as water depth and water temperature. Altitude, when varied from 0 to 1000 m, has a small effect on burial depth (relative difference of 18%). When a more realistic upper limit of 300 m for a mine laying aircraft is applied, the relative difference drops to just 9%. Water depth affects the burial depth only if a mine reaching the terminal velocity (in this case, about 20 m). Although temperature varies the water density up to 3%, and in

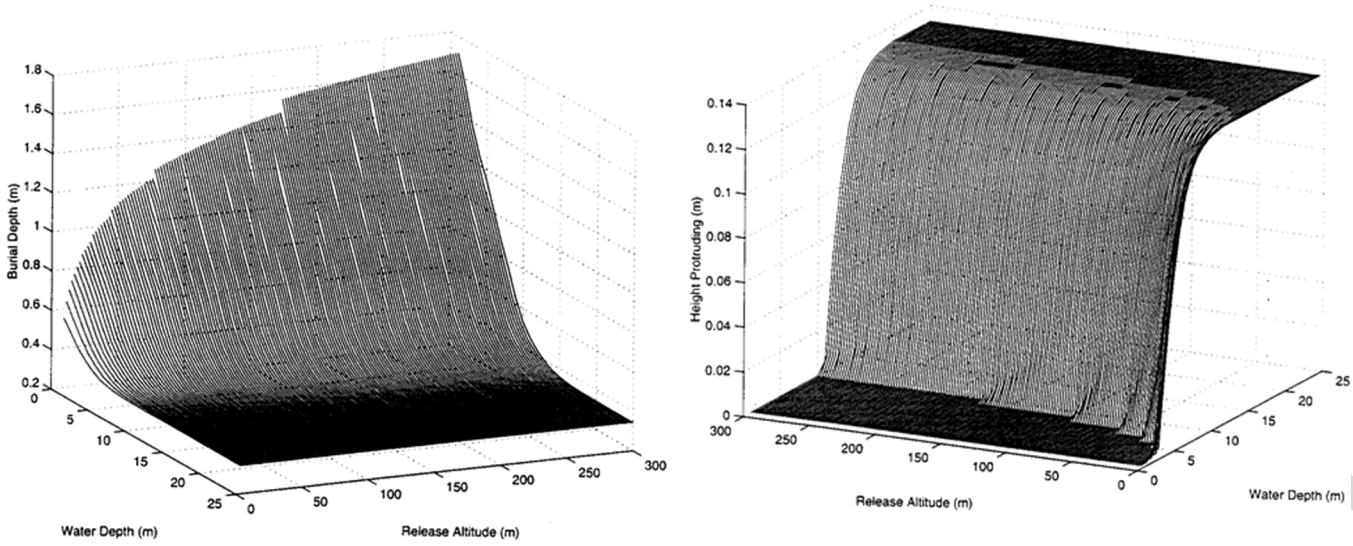

(a) (b)

Fig. 6. Dependence of (a) burial depth and (b) height protruding on release altitude and water depth (all in meters). Protruded height is illustrated here to clarify the levels at which these parameters become less influential in the 2-D models (after [28]).

turn, changes the viscosity [29], it does not affect the burial depth and orientation.

For vertical initial falling angle (Fig. 6) with zero rotation rate, the mine is heading directly downward, resulting in the maximum burial depth. When the release height is 150 m, the mine burial depth is 2.405 m for the vertical initial falling angle and 0.359 m for the horizontal initial falling angle. Such a difference in burial depth decreases as the release height decreases. When the release height is 1.5 m, the mine burial depth is 0.977 m for the vertical initial falling angle and 0.342 m for the horizontal initial falling angle.

2) Sensitivity to Sediment Characteristics: Fig. 7 shows the sensitivity of sediment density and shear strength on burial depth. For the shear strength of 1 kPa (extremely soft sediment), the burial depth changes 37% for sediment density varying from 1000 to 2000 kg m^{-3} ***[AU: "kg/m^{3}" was changed to "kg m^{-3}" to be consistent. Please check.]***. At the more common values of shear strength (5–15 kPa), the sediment density has very little effect, just 3.7% Fig. 7(a). As shear strength increases, the influence of sediment density reduces. For constant sediment density (1.5 kg m^{-3}), the impact burial depth drastically reduces from 0.55 m for the shear strength of 1 kPa to 0.1 m for shear strength of 10 kPa [Fig. 7(b)].

A power law is used

$$S = \alpha \rho_s^{\beta} \tag{42}$$

to represent the relationship between sediment density (ρ_s) and shear strength (S) [30]. Here, the two coefficients α and β are determined experimentally. Considering a homogeneous sediment layer $(\rho_s = \text{const})$, the shear strength is a function of (α, β). For a given ρ_s, increasing α or β enhances the shear strength (S), and in turn, decreases the burial depth. These features are well simulated by the model (Fig. 8).

D. Strength and Weakness

The improvement of the 2-D model versus the 1-D model is its capability to predict the mine rotation in the (x, z)-plane, i.e., ψ_2. In the 2-D model, the momentum equation for the (x, z)-directions and the moment-of-momentum equation for the y-direction are used to predict the position and orientation around the y-axis [i.e., in the (x, z)-plane]. The basic physics for the spiral motion described in Fig. 4 is included in the 2-D model, but strictly in the (x, z)-plane [31], [32].

Since the mine movement is strictly in the (x, z)-plane, it is very hard to include the motion of fluid in the 2-D model, because it is impossible to lay a mine in the same direction of the fluid velocity. In littoral zone, the water velocity is not negligible. The application of the 2-D model for the operational use is limited. Besides, the drag coefficients for the axial and cross directions have similar dependence on the Reynolds number Re and the aspect ratio (δ) [see (17) and (18)]. However, the drag coefficients in the axial and cross directions are independent [33]. Besides, a mine drop experiment shows that IMPACT25/28 overpredicts (5–10 times larger) the mine burial in the sandy bottom [9], [31], [32]. This indicates that the sediment dynamics is too simple in the 2-D model.

VI. The 3-D Modeling

To overcome the major weaknesses of the 2-D model, i.e., 1) environmental fluid assumed motionless, 2) similar drag coefficients in the axial and cross directions, and 3) nonrealistic sediment dynamics, Chu *et al.*[10]–[16], [34]–[38] modified IMPACT25/28 allowing the cylinder to move in 3-D space. These changes mandated the use of more complicated dynamical system than IMPACT25/28. The three coordinate systems (E-, F-, and M-coordinates) are used in the 3-D modeling.

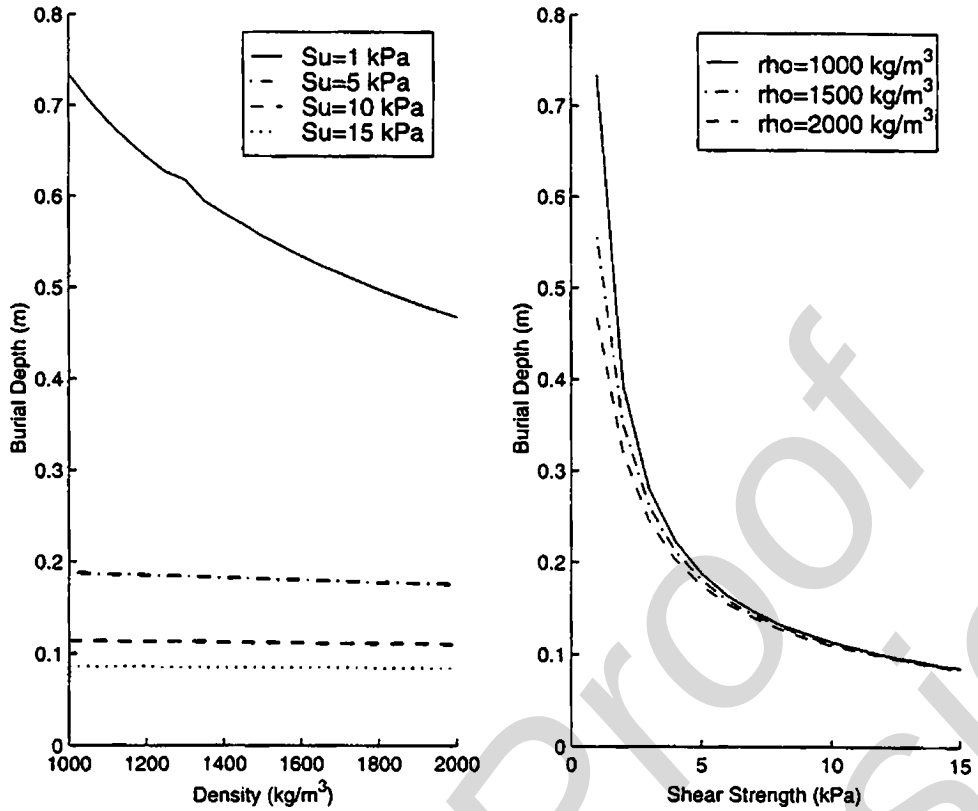

Fig. 7. Effect of sediment (a) density and (b) shear strength on burial depth. Density change only impacts the predicted burial depth in very soft sediments. As expected, shear strength has a dramatic impact on predicted burial depth (after [31]).***[AU: Please change units in the fig. to be consistent with the text]***

A. Dynamical System

The three momentum equations (in the E-coordinate system) are given by

$$\frac{d}{dt}\begin{bmatrix} u \\ v \\ w \end{bmatrix} = -\begin{bmatrix} 0 \\ 0 \\ g \end{bmatrix} + \frac{\mathbf{F}_b + \mathbf{F}_h}{\rho \Pi} \tag{43}$$

and the three moment-of-momentum equations (in the M-coordinate system) are written in vector form

$$\mathbf{J} \bullet \frac{d\boldsymbol{\omega}}{dt} = -2\mathbf{J} \bullet (\boldsymbol{\Omega} \times \boldsymbol{\omega}) + \mathbf{M}_b + \mathbf{M}_h. \tag{44}$$

Here, $(\mathbf{F}_b, \mathbf{M}_b)$ are the buoyancy force and torque and $(\mathbf{F}_h, \mathbf{M}_h)$ are the hydrodynamic force and torque including drag, lift, and impact ($\mathbf{F}_d$, $\mathbf{F}_l$, $\mathbf{F}_i$; $\mathbf{M}_d$, $\mathbf{M}_l$, $\mathbf{M}_i$). The vectors $(\boldsymbol{\omega}, \boldsymbol{\Omega})$ are the angular velocity of mine and M-coordinate system

$$\boldsymbol{\Omega} = \omega_2 \mathbf{j}_M + \omega_3 \mathbf{k}_M. \tag{45}$$

The first term in the right-hand side of (44) is an apparent torque (similar to the Corilois term in Earth science) due to the use of the rotating coordinate system (i.e., the M-coordinate). If $\omega_1 = 0$, then $\boldsymbol{\Omega} = \boldsymbol{\omega}$. The apparent torque is given by

$$-2\mathbf{J} \bullet (\boldsymbol{\Omega} \times \boldsymbol{\omega}) = \begin{cases} 0, & \text{if } \omega_1 = 0 \text{ (i.e., } \boldsymbol{\Omega} = \boldsymbol{\omega}) \\ -2J_2\omega_1\omega_3\mathbf{j}_M & \\ \quad +2J_3\omega_1\omega_2\mathbf{k}_M, & \text{if } \omega_1 \neq 0. \end{cases} \tag{46}$$

The gravitational force, passing the COM, does not induce the moment. In the M-coordinate system, the moment of gyration tensor for the axially symmetric cylinder is a diagonal matrix

$$\mathbf{J} = \begin{bmatrix} J_1 & 0 & 0 \\ 0 & J_2 & 0 \\ 0 & 0 & J_3 \end{bmatrix} \tag{47}$$

where J_1, J_2, and J_3 are the moments of inertia. The buoyancy force induces the moment in the $\mathbf{j}_M$ direction if the COM does not coincide with the COV (i.e., $\chi \neq 0$)

$$\mathbf{M}_b = |\mathbf{F}_b| \chi \cos\psi_2 \mathbf{j}_M. \tag{48}$$

B. IMPACT35

The 3-D model, usually called IMPACT35 (written in Matlab), is the third generation of the Navy's mine IBPM. It was developed to solve the six scalar (43) and (44) to obtain (x, y, z, ω_1, ω_2, ω_3). From the angular velocity (ω_1, ω_2, ω_3), the three angles determining the mine orientation (ψ_1, ψ_2, ψ_3) can be obtained

$$\frac{d\psi_1}{dt} = \omega_1 \quad \frac{d\psi_2}{dt} = \omega_2 \quad \frac{d\psi_3}{dt} = \omega_3.$$

The external forcing for IMPACT35 consists of drag force $\mathbf{F}_d$ and torque $\mathbf{M}_d$, as well as lift force $\mathbf{F}_l$ and torque $\mathbf{M}_l$. All these external forces and torques are calculated in the F-coordinate system. The model includes cylindrical and noncylindrical

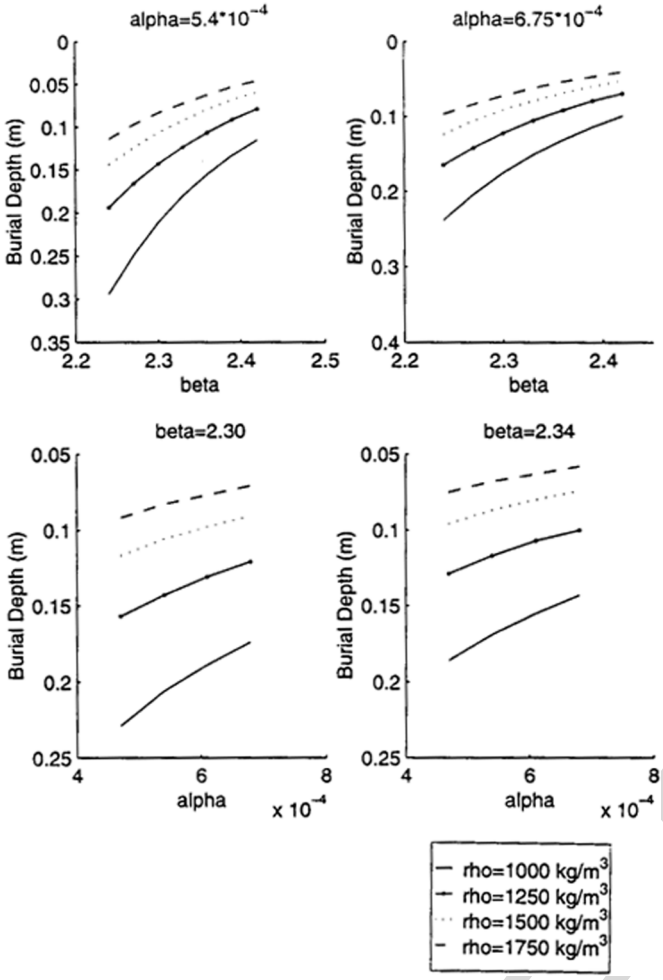

Fig. 8. Effect of α and β on predicted burial depth (meters) for different values of sediment density (after [31]). ***[AU: Please change units in the figure to as they are in text]***

mines. In this section, the cylindrical mine is taken as an example for illustration.

1) Drag and Lift Forces: Two features of the drag and lift coefficients (Reynolds-number-dependent and asymmetry in along- and across-mine main axis) distinguish IMPACT35 from IMPACT25/28. The drag and lift forces are calculated using the F-coordinate system. Let (C_{d1}, C_{d2}) be the drag coefficients along- and across-mine main axis and (f_1, f_2, f_3) be the added-mass corrections (f_1, f_2, f_3) in the three directions of the F-coordinate system.

The total drag force along-$\mathbf{i}_F$ (i.e., relative flow along the cylinder's main axis) is calculated by

$$F_{d1} = C_{td1}(t)V_1, \quad C_{td1}(t) \equiv C_{d1}\frac{\pi R^2}{2}\frac{\rho_w}{(1+f_1)}\left|V_1(t)\right|. \tag{49}$$

C_{d1} is almost independent on the axial Reynolds number (Re) when $Re > 10^4$, but dependent on the cylinder's aspect ratio [33],

$$C_{d1} = \begin{cases} 1.0, & \text{if } \delta > 8 \\ 0.75 + \delta/32.1934 + 0.09612/\delta^2, & \text{if } 8 \geq \delta > 0.5 \\ 1.15, & \text{if } \delta \leq 0.5. \end{cases} \tag{50}$$

The total drag force along-$\mathbf{j}_F$ (i.e., relative flow across the cylinder) is calculated by

$$F_{d2} = R\int_{-\frac{L}{2}-\chi}^{\frac{L}{2}-\chi} C_{d2}\left(V_2'\right)^2\frac{\rho_w}{(1+f_2)}d\eta \quad V_2'(\eta) = V_2 - \omega_3^F\eta$$

where V_2' is the water-to-cylinder velocity at the surface in the $\mathbf{j}_F$ direction and an empirical formula is used for calculating C_{d2} [39], as shown in (51) at the bottom of the page.

The drag force along-$\mathbf{k}_F$ is calculated by

$$\mathbf{F}_{d3} = \left[C_{d2}R\frac{\rho_w}{(1+f_2)}\omega_2^F\left|\omega_2^F\right| \times\left(\int_0^{\frac{L}{2}-\chi}\eta^2 d\eta - \int_{-\frac{L}{2}-\chi}^{0}\eta^2 d\eta\right)\right]\mathbf{k}_F. \tag{52}$$

The water-to-cylinder velocity determines the lift force [40],

$$\mathbf{F}_l = \left[\frac{C_{tl}(t)}{L}\int_{-\frac{L}{2}-\chi}^{\frac{L}{2}-\chi} V_2'(\eta)d\eta\right]\mathbf{k}_F$$
$$C_{tl}(t) \equiv C_l LR\frac{\rho_w}{(1+f_2)}|V_2| \tag{53}$$

where C_l is the lift coefficient. An empirical formula is used for calculating C_l [41]

$$C_l = \begin{cases} 2\omega_1 R/V_2, & \text{if } \omega_1 R/V_2 \leq 4 \\ 8 + 0.24(\omega_1 R/V_2 - 4), & \text{if } \omega_1 R/V_2 > 4. \end{cases} \tag{54}$$

2) Drag and Lift Torques: For an axially symmetric cylinder, the moment of the hydrodynamic force in $\mathbf{i}_F$ direction is not

$$C_{d2} = \begin{cases} 1.9276 + 8/\mathrm{Re}, & \text{if } \mathrm{Re} \leq 12 \\ 1.261 + 16/\mathrm{Re}, & \text{if } 12 < \mathrm{Re} \leq 180 \\ 0.855 + 89/\mathrm{Re}, & \text{if } 180 < \mathrm{Re} \leq 2000 \\ 0.84 + 0.00003\mathrm{Re}, & \text{if } 2000 < \mathrm{Re} \leq 12\,000 \\ 1.2 - 4/\delta & \text{if } 12\,000 < \mathrm{Re} \leq 150\,000, \quad \delta \geq 10 \\ 0.835 - 0.35/\delta, & \text{if } 12\,000 < \mathrm{Re} \leq 150\,000, \quad 2 \leq \delta < 10 \\ 0.7 - 0.08/\delta, & \text{if } 12\,000 < \mathrm{Re} \leq 150\,000, \quad \delta < 2 \\ 1.875 - 0.0000045\mathrm{Re}, & \text{if } 150\,000 < \mathrm{Re} \leq 350\,000 \\ 1/(641\,550/\mathrm{Re} + 1.5), & \text{if } \mathrm{Re} > 350\,000. \end{cases} \tag{51}$$

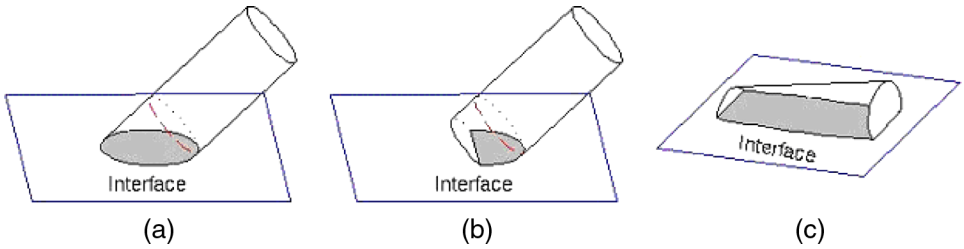

Fig. 9. Three patterns of cylinder penetration with the cross section being (a) a complete ellipse, (b) a cutoff ellipse with one side straight line, and (c) a cutoff ellipse with two sides straight lines (after [36]).

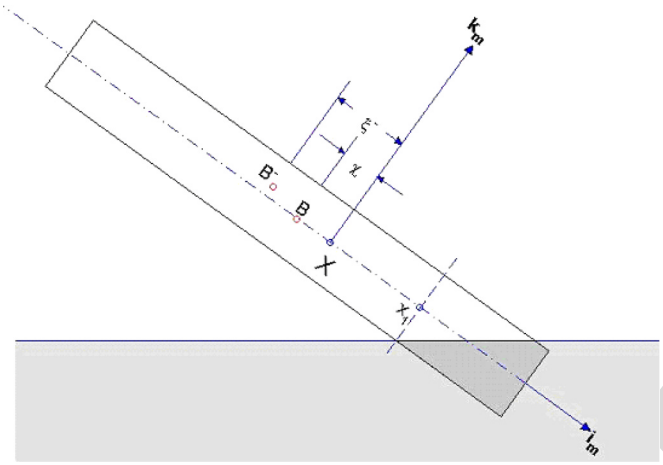

Fig. 10. Illustration of PCOV (B^-), x_1, and ξ^- for the tail part $[C^{(1)}, D^{(1)}]$ for the case in Fig. 9(a) (after [36]).

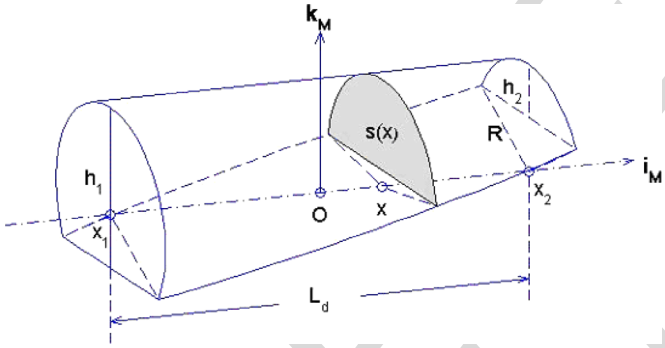

Fig. 11. Geometry of the part $D^{(1)}$ (after [36]).

caused by the drag and lift forces, but by the viscous fluid. The moment of the viscous force of steady flow between two rotating cylinders with the common axis is calculated by [42]

$$M = 4\pi\mu \frac{r_1^2 \cdot r_0^2}{r_1^2 - r_0^2}(\omega_1 - \omega_0)$$

where (r_1, r_0) and (ω_1, ω_0) are the radii and angle velocities of the inner and outer cylinders and μ is the viscosity. Moment of the viscous force on one rotating cylinder is the limit case of the two rotating cylinders as $r_0 \to \infty$ and $\omega_0 = 0$. The moment of the viscous force around $\mathbf{i}_F$ is calculated by

$$\mathbf{M}_{v1} = -C_{m1}\omega_1 \mathbf{i}_F \quad C_{m1} \equiv \pi\mu L d^2. \tag{55}$$

Same as the hydrodynamic forces, the torques along $\mathbf{j}_F$ and $\mathbf{k}_F$ axes, ($\mathbf{M}_{d1}$, $\mathbf{M}_{d2}$, $\mathbf{M}_l$), are calculated. When the cylinder rotates around $\mathbf{j}_F$ with the angular velocity ω_2^F, the drag force causes a torque on the cylinder in the $\mathbf{j}_F$ direction

$$\mathbf{M}_{d2} = \left[-\omega_2^F \left|\omega_2^F\right| \int_{-\frac{L}{2}-\chi}^{\frac{L}{2}-\chi} C_{d2} R \frac{\rho_w}{(1+f_r)} \eta^2 |\eta| d\eta \right] \mathbf{j}_F \tag{56a}$$

where f_r is the added-mass factor for the moment of drag and lift forces. If the water-to-cylinder velocity or the cylinder mass distribution is nonuniform ($\chi \neq 0$), the drag force causes a torque on the cylinder in the $\mathbf{k}_F$ direction

$$\mathbf{M}_{d3} = \left[\int_{-\frac{L}{2}-\chi}^{\frac{L}{2}-\chi} C_{d2} R \frac{\rho_w}{(1+f_r)} \left(V_2 - \omega_3^F \eta\right)^2 \eta d\eta \right] \mathbf{k}_F. \tag{56b}$$

The lift force exerts a torque on the cylinder in the $\mathbf{j}_F$ direction

$$\mathbf{M}_{l2} = \left[-\int_{-\frac{L}{2}-\chi}^{\frac{L}{2}-\chi} C_l R \frac{\rho_w}{f_{kr}} \left(V_2 - \omega_3^F \eta\right) \eta d\eta \right] \mathbf{j}_F. \tag{57}$$

3) Interfacial Treatment: Computation of buoyancy and hydrodynamic forces ($\mathbf{F}_b$, $\mathbf{F}_h$) and torques ($\mathbf{M}_b$, $\mathbf{M}_h$) is more complicated for a cylinder penetrating through air–water and water–sediment interfaces than falling through a single medium such as water. At the instance when the cylinder penetrates into an interface, three situations may exist as follows: 1) the cross section is a complete ellipse [Fig. 9(a)], 2) a cutoff ellipse with one side straight line [Fig. 9(b)], or 3) a cutoff ellipse with two straight lines [Fig. 9(c)]. The interface separates the cylinder to two parts. Each part contains a noncylinder D and a subcylinder C (Fig. 10). Let (L_c, L_d), (Ω_c, Ω_d), and (Π_c, Π_d) be the lengths, surfaces, and volumes of $[C, D]$, respectively, and (h_1, h_2) the depths of the two sides of D (Fig. 11). The characteristics of the geometric parameters (L_c, h_1, h_2) are listed in Table I. The COV for the portion $[C, D]$ is called the partial COV (PCOV). With this treatment, the drag and lift forces and torques at the two parts C and D can be computed separately [36].

4) Sediment Resistance: In the 2-D models (IMPACT25/28) the pertinent parameters are sediment density and bearing strength. The bearing strength is calculated simply by ten times the shear strength, which is not very realistic. In fact, when the mine impacts and penetrates into the sediment, it will create a large transient pore pressure in the sediment that causes

TABLE I
GEOMETRIC PARAMETERS DURING THE CYLINDER PENETRATION (AFTER [36])

	L_c	h_1	h_2
Upper & Lower Parts of Fig.9a	>0	2R	0
Upper Part of Fig. 9b	>0	2R	0 ~ 2R
Lower Part of Fig.9b	0	0 ~ 2R	0
Upper & lower Parts of Fig. 9c	0	0 ~ 2R	0 ~ 2R

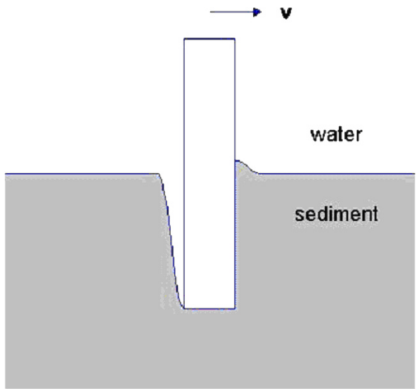

Fig. 12. Impact (resistant) force exerted on the part of the mine surface moving towards the sediment (after [36]).

ruptures in the sediment and influences the resistance force on the mine surface [11], [36], which is not simply ten times the shear strength. In 3-D model (IMPACT35), two distinct methods (delta and bearing factor) are used to compute total sediment resistance force and torque.

a) Delta method: The delta method is developed on the assumption that the mine pushes the sediment and leaves space in the wake as it impacts and penetrates into the sediment. This space is refilled by water and the water cavity is produced (Fig. 12). At the instance of the penetration, the total sediment shear resistant force on the mine surface is calculated by [36]

$$\begin{aligned}\mathbf{F}^s = &\int_{\sigma_{\text{sed}}} \boldsymbol{\tau}\,[\delta\mu G(V)S(z)]\,d\sigma \\ &- \int_{\sigma_{\text{sed}}} \mathbf{n}\left[\left(\delta\int_z^{z_{ws}} \rho_s(z')g dz'\right) + \rho_w g(z_{ws}-z)\right] d\sigma \\ &+ \mathbf{k}\frac{\pi}{8}\rho_s(z)\left(\frac{gw}{k_p} + \frac{1+e_v}{e_v}\frac{dw}{dt}\right)B^3 \end{aligned} \tag{58}$$

where, in the right-hand side, the first term is the shear resistance force, the second term is the buoyancy force, and the third term is the pore water pressure. $S(z)$ is the sediment shear strength, $G(V)$ is the impact function, V is the mine translation speed, $\rho_s(z)$ is the sediment wet density (usually obtained from the sediment data), $(\mathbf{n}, \boldsymbol{\tau})$ are unit vectors normal (outward positive) and tangential to the mine surface, z_{ws} represents the vertical coordinate of the water–sediment interface, k_p is the permeability coefficient (10^{-4} m s^{-1}, Hansen *et al.*, 1994***[AU: Please add this to the reference list]***), e_v (~0.50)

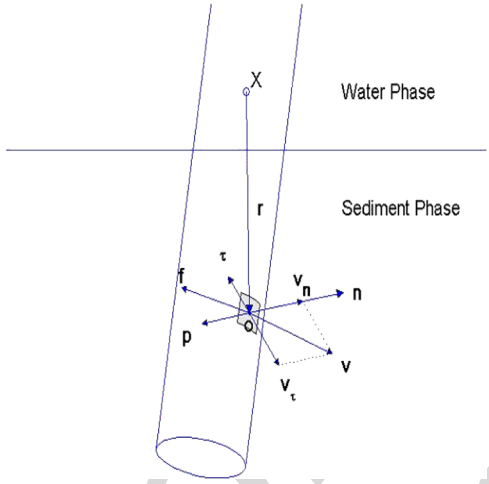

Fig. 13. Momentum and angular momentum balance for mine penetration through the water–sediment interface.

is the void ratio, and B is the length of the rupture line. The step function δ is defined by

$$\delta = \begin{cases} 1 & \mathbf{v}\bullet\mathbf{n} \geq 0 \\ 0 & \mathbf{v}\bullet\mathbf{n} \leq 0 \end{cases} \tag{59}$$

which shows that the sediment buoyancy and shear resistance forces act when the cylinder moves towards them. Let $\mathbf{v}_n$ be the normal velocity. The tangential velocity is represented by

$$\mathbf{v}_\tau = \mathbf{v} - \mathbf{v}_n. \tag{60}$$

The tangential unit vector $(\boldsymbol{\tau})$ is defined by

$$\boldsymbol{\tau} = -\frac{\mathbf{v}_\tau}{|\mathbf{v}_\tau|} \tag{61}$$

which is opposite to $\mathbf{v}_\tau$ (Fig. 13).

The sediment resistance torque $(\mathbf{M}^s)$ is calculated by

$$\begin{aligned}\mathbf{M}^s = &\int_{\sigma_{\text{sed}}} (\mathbf{r}\times\boldsymbol{\tau})\,[\delta\mu G(V)S(z)]\,d\sigma \\ &+ \int_{\sigma_{\text{sed}}} (\mathbf{r}\times\mathbf{n})\left[\left(\delta\int_z^{z_{ws}} \rho_s(z')g dz'\right) + \rho_w g(z_{ws}-z)\right] d\sigma \\ &+ (\mathbf{r}_{pw}\times\mathbf{k})\frac{\pi}{8}\rho_s(z)\left(\frac{gw}{k} + \frac{1+e_v}{e_v}\frac{dw}{dt}\right)B^3. \end{aligned} \tag{62}$$

where $\mathbf{r}_{pw}$ is the position vector (in the M-coordinate) indicating the location of the cylinder's rupture line.

b) Bearing factor method: The bearing factor method is based on the fact that the shear resistance force $(\mathbf{F}_r^s)$ is in the opposite direction of $\mathbf{v}$ and acts on the mine. Its magnitude is proportional to the product of the sediment shear strength (S) and the rupture area (A, projection of sediment-contacting area perpendicular to the velocity $\mathbf{V}$) with a nonnegative bearing factor N [43]

$$\mathbf{F}_r^s = -\int_{\sigma_{\text{sed}}} \boldsymbol{\tau} N(p,v) S A d\sigma, \qquad N \geq 0. \tag{63}$$

TABLE II
PHYSICAL PARAMETERS OF THE MODEL MINES IN THE NSWC—CARDEROCK EXPERIMENT (AFTER [46])

Mine	Mass (kg)	ρ (10^3 kg m^{-3})	L (m)	J_1 (kg m^2)	J_2 (J_3) (kg m^2)	χ (m)
1	16.96	1.60	0.505	0.0647	0.356	0
2	22.27	2.10	0.505	0.0806	0.477	0
3	34.93	1.60	1.010	0.1362	2.900	0
4	45.85	2.10	1.010	0.1696	3.820	0
5	45.85	2.10	1.010	0.1693	3.940	0.0045
6	45.85	2.10	1.010	0.1692	4.570	-0.077

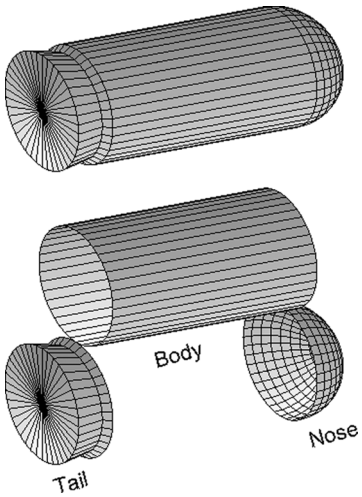

Fig. 14. Mine with nose, tail, and cylindrical body (after [35]).

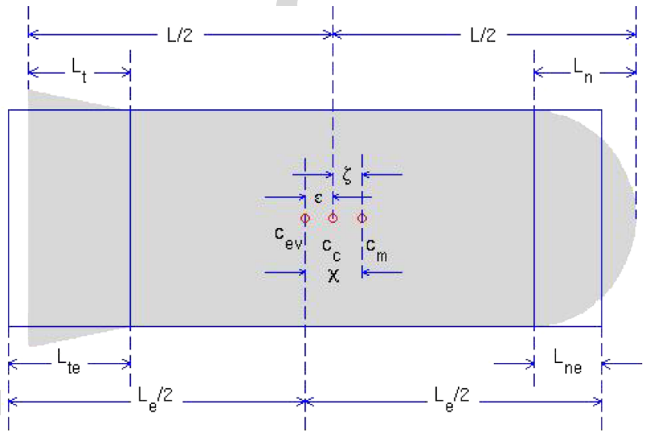

Fig. 15. Location of c_v, c_{ev}, and c_m. Here, ε is the distance between c_v and c_m and χ is the distance between c_{ev} and c_m (after [35]).

The sediment resistance torque includes the hydrodynamic and shearing resistance torques

$$\mathbf{M}^s = \int_{\sigma_{\text{sed}}} \{\mathbf{r} \times \mathbf{f}_h^s - [N(p,v)SA]\mathbf{r} \times \boldsymbol{\tau}\}\, d\sigma. \tag{64}$$

Here, p is the nondimensional penetration depth scaled by the diameter $(2R)$. The sediment density and shear strength (S) in (63) and (64) are measured. The bearing factor increases with p and decreases with the decreasing speed

$$N(p,v) = [\mu_1 p^{\mu_2}]\left[1 + \lambda \log\left(\frac{v}{v_{cri}}\right)\right] \tag{65}$$

where λ is the v-effect parameter, (μ_1, μ_2) are the p-effect parameters [16], and v_{cri} is the critical speed.

5) Pseudocylinder Parameterization: The Navy operational mines are usually not cylindrical. It is important to develop a model with more general shapes such as with nose and tail. Ppseudocylinder parameterization was proposed for noncylindrical mines [35]. For a near-cylindrical mine with nose and tail falling through a single medium or multiple media, the buoyancy force and torque are relatively easy to calculate. However, the hydrodynamic forces (lift, drag) and torques are difficult to compute. A feasible way is to transform a mine with nose and tail to a cylindrical mine (i.e., called the pseudocylinder parameterization). An axially symmetric mine usually consists of three parts: cylindrical body with radius of R, nose, and tail (Fig. 14). The lengths of the mine, nose, and tail are L, L_n, and L_t, respectively. A pseudocylinder is defined with the following features: the same radius (R) of the mine's cylindrical body and the same volume as the original mine (Fig. 15). It consists of the following three parts: original cylindrical body and equivalent cylinders for nose and tail. Let (Π, Π_n, Π_t) be the volumes of the mine, nose, and tail. The equivalent cylinder has length

$$L_{ne} = \frac{\Pi_n}{\pi R^2}$$

for the nose, and

$$L_{te} = \frac{\Pi_t}{\pi R^2}$$

for the tail. Let (c_c, c_m) be the mine's midpoint on the main axis and the COM position, and let c_{ev} be the COV of the pseudocylindrical mine (Fig. 15). The gravity is downward and passing through c_m. The buoyancy force is upward and passing through c_{ev}. Let ε_1 be the distances between c_c and c_m

$$\varepsilon_1 = \frac{L_n - L_{ne}}{2} - \frac{L_t - L_{te}}{2}. \tag{66}$$

Let ε_2 be the displacement from c_c to c_m that is easy to determine if COM is given. Let χ be the displacement from c_{ev} to c_m that is calculated as

$$\chi = \varepsilon_1 + \varepsilon_2. \tag{67}$$

Both χ and ε_2 can be positive and negative. The positive values refer to nose-down case, i.e., the point c_m is lower than the point c_{ev} for positive χ and the point c_c is lower than the point c_{ev} for positive ε_2.

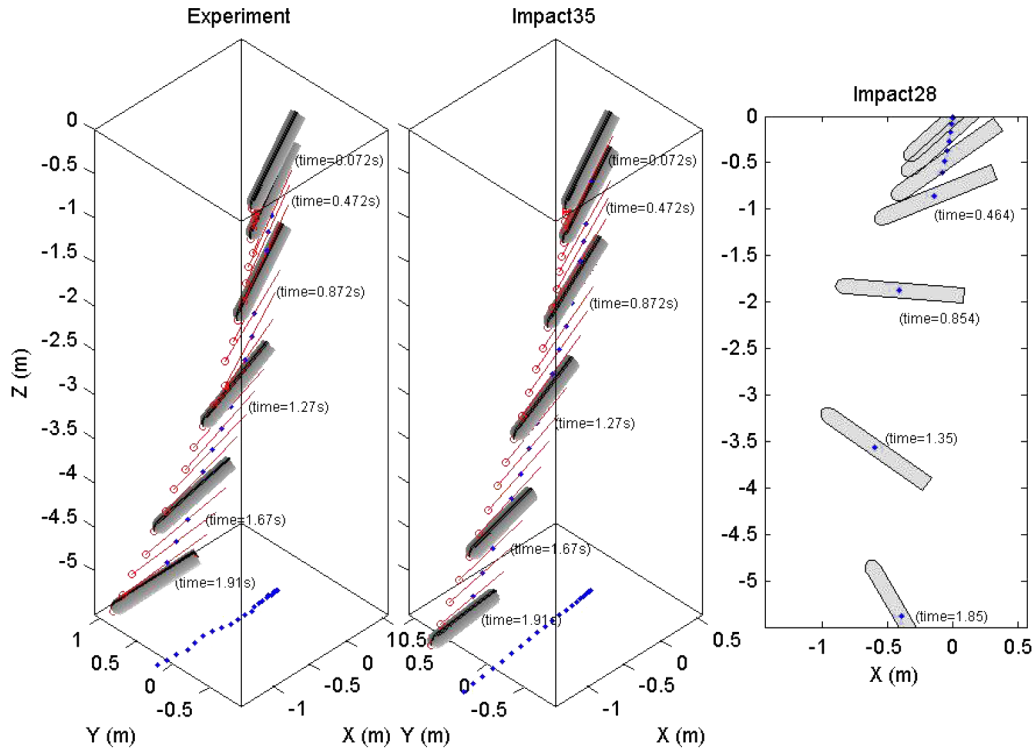

Fig. 16. Movement of mine #6 ($L = 1.01$ m, $\rho = 2.1 \times 10^3$ kg m^{-3}) with $\chi = -0.0077$ m and $\psi_2 = -14.0°$ obtained from (a) experiment, (b) 3-D model (IMPACT35), and (c) 2-D model (IMPACT25/28).***[AU: Please add space between unit and number in Figs. 16-18]***

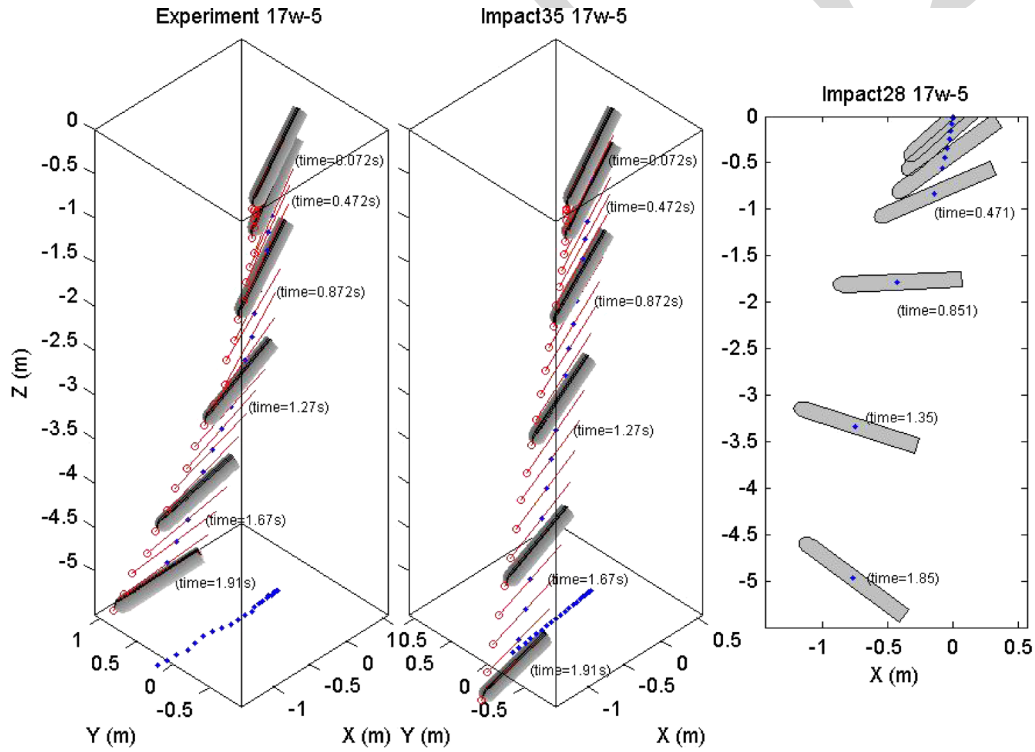

Fig. 17. Movement of mine #5 ($L = 1.01$ m, $\rho = 2.1 \times 10^3$ kg m^{-3}) with $\chi = 0.0045$ m and $\psi_2 = 42.2°$ obtained from (a) experiment, (b) 3-D model (IMPACT35), and (c) 2-D model (IMPACT25/28).

C. Mine Impact Burial Experiment for Model Verification

The added value of 3-D model (IMPACT35) versus 2-D model (IMPACT25/28) is verified by several recent experiments: mine impact burial experiment (MIBEX) at Monterey Bay, CA, on May 22, 2000 [9], [31], [32], mine drop experiment (MIDEX) at the Naval Postgraduate School (NPS) swimming pool in June 2001 [6], [10], [13], [16], [34] [44], MIDEX at NSWC—Carderock Explosion Test Pond on September

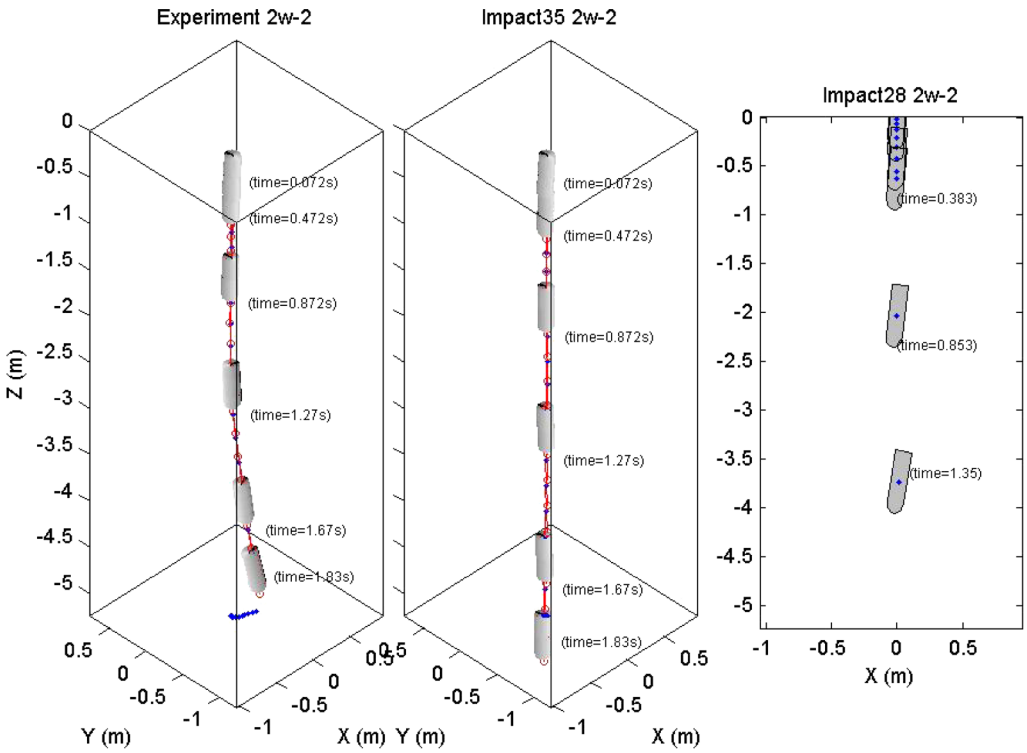

Fig. 18. Movement of cylinder #2 ($L = 0.505$ m, $\rho = 2.1 \times 10^3$ kg m^{-3}) with $\chi = 0$ and $\psi_2 = 87.0°$ obtained from (a) experiment, (b) 3D IMPACT35 model, and (c) 2D IMPACT25/28 model.

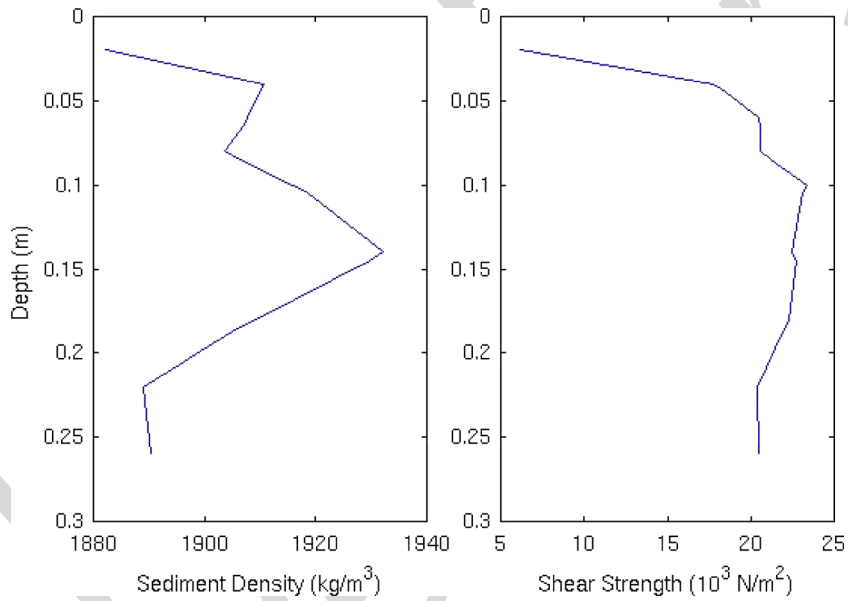

Fig. 19. Mean sediment density $\rho_s(z)$ and shear strength $S(z)$ profiles in the Monterey Bay collected during the cylinder drop experiment on May 31, 2000.

[AU: Please change units so they correspond with the text]

10–14, 2001, MIDEX at NSWC—Corpus Christi, TX, [46], [47], and the Baltic Sea experiment conducted in June 2003 by the German Federal Armed Forces Underwater Acoustic and Marine Geophysics Research Institute (FWG, Kiel, Germany) [48], [49] with the full-size optical mine which is allowed to free fall from the wench. During these experiments, various model mines (most cylinders) were released into the water. The mine trajectories were recorded by underwater high-speed video cameras. The mine burial depths were also observed by the diver (in MIBEX—Monterey Bay) and optical instruments (in MIDEX—Baltic Sea).

D. Model-Data Comparison

The 2-D model (IMPACT25/28) and 3-D model (IMPACT35) are integrated using the same mine parameters (such as the density ratio, length, radius, and distance between

COV and COM) and mine drop initial conditions (speed and orientation) as in the mine drop experiments. Added value ***[AU: "Value-added" was changed to "added value" throughout. Please check.]*** of IMPACT35 versus IMPACT25/28 is verified through comparison between modeled and observed mine trajectories and burial depths.

1) Trajectory in Water Column: Data from MIDEX at NSWC—Caderock is used as illustration. The physical parameters of the six mines are presented in Table II. Three cases are presented as follows: 1) near-horizontal release ($\psi_2^{(0)} = -14°$) with model mine #6, 2) near-45° release ($\psi_2^{(0)} = 42.2°$) with model mine #6, and 3) near-vertical release ($\psi_2^{(0)} = 87°$) with model mine #2. The other initial conditions are given by

$$x^{(0)} = y^{(0)} = z^{(0)} = 0 \quad u^{(0)} = v^{(0)} = w^{(0)} = 0$$
$$\psi_1^{(0)} = \psi_3^{(0)} = 0 \quad \omega_1^{(0)} = \omega_2^{(0)} = \omega_3^{(0)} = 0. \tag{68}$$

For near-horizontal release (Fig. 16), the 3-D model (IMPACT35) simulated trajectory agrees well with the observed trajectory with the same travel time (1.91 s) for the mine passing through the water column. For near-45° release, the 3-D model (IMPACT35) simulated trajectory and travel time agree well with the observed trajectory (Fig. 17). However, the 2-D model (IMPACT28) has less capability to predict the cylinder trajectory in the water column.

For near-vertical release (Fig. 18), the 3-D model (IMPACT35) simulated trajectory agrees well with the observed trajectory. Both show the same straight pattern and the same travel time (1.83 s) for the cylinder passing through the water column. However, the existing 2-D model (IMPACT28) does not predict the travel time well.

2) Burial Depth: MIBEX—Monterey Bay was conducted on the R/V John Martin on May 23, 2000 [9], [31]. The barrel with density ratio of 1.8 was treated as model mine and released horizontally while touching the surface. The initial conditions were

$$x^{(0)} = y^{(0)} = z^{(0)} = 0 \quad u^{(0)} = v^{(0)} = w^{(0)} = 0$$
$$\psi_2^{(0)} = 90° \quad \psi_1^{(0)} = \psi_3^{(0)} = 0 \quad \omega_1^{(0)} = \omega_2^{(0)} = \omega_3^{(0)} = 0. \tag{69}$$

This would eliminate any chance of inertial effects caused by uneven introduction into the air–sea interface. This also set the initial velocity parameter in the code to zero. The barrel was to be released 17 times. The diver would snap the quick-release shackle on the barrel, and then, dive down to conduct measurements. The average depth of the water was 13 m. Since the path the barrel would follow was uncertain, both the releasing diver and a second safety diver would stay on the surface until after the barrel was dropped. Once reaching the bottom, one diver would take penetration measurements using a meter stick marked at millimeter increments while the other would take a gravity core. After 17 drops, the divers began to run out of air and results were not varying greatly so the decision was made to end the experiment. The gravity cores were taken immediately to the United States Geological Survey (USGS) Laboratories in Menlo Park, CA, to get the sediment density and shear strength profiles (Fig. 19).

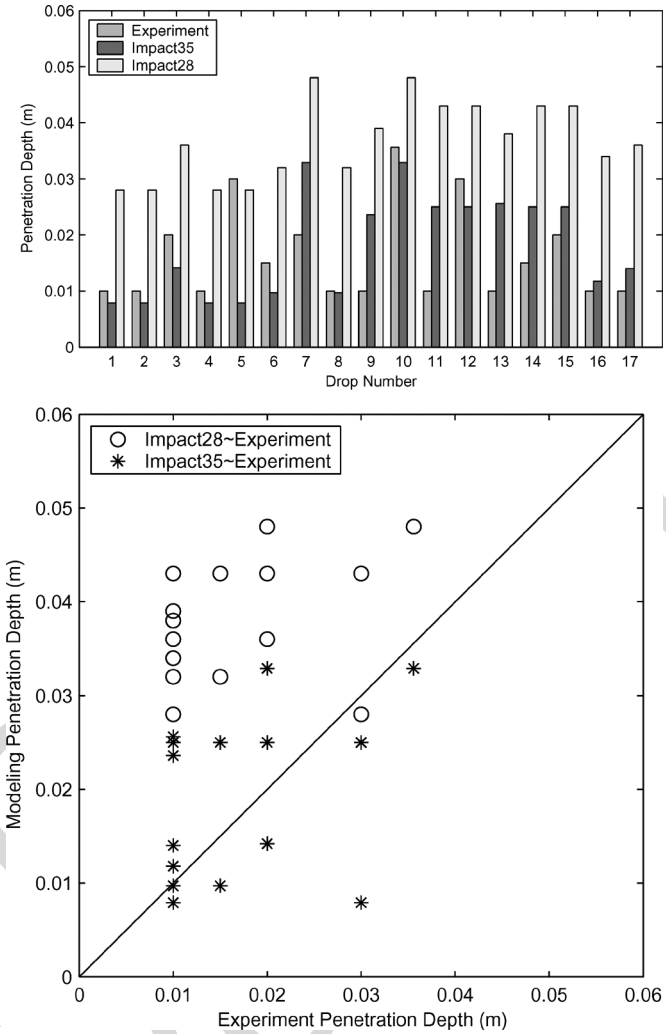

Fig. 20. Observed (MIBEX—NPS) and predicted (IMPACT25/28 and IMPACT35 with delta method) burial depths: (a) direct comparison and (b) scatter diagram. Note that the 2-D model (IMPACT25/28) predicts the burial depth 5–10 times larger than the observed depth, and IMPACT35 with dDelta method performs much better than IMPACT25/28 (after [36]).

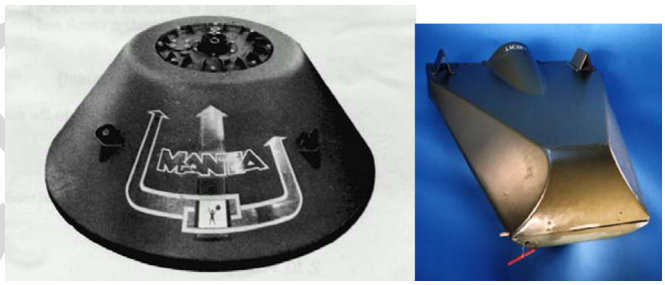

Fig. 21. Operational mines: (a) Manta and (b) Rockan (after [50]).

For sediment resistance force, the 2-D model (IMPACT25/28) uses ten times shear strength as the bearing strength. The 3-D model (IMPACT35) uses the delta or bearing factor method (see Section VI-B4). After running the two models (IMPACT35 and IMPACT25/28) for each gravity core regime $[\rho_s(z), S(z)]$ from the initial conditions (69), the burial depths were compared with measured burial depth data (Fig. 20). As evident, IMPACT35 improves the prediction

capability. The existing 2-D model (IMPACT25/28) overpredicts actual burial depth by an order of magnitude on average. However, the 3-D model (IMPACT35) predicts the burial depth reasonably well without evident overprediction. Since the gravity cores were taken for approximately 2–3 m from the impact location, several cores were taken for each drop. This allowed an average to be calculated to yield more accurate data for each drop. Recently, Chu and Fan [11] compared the delta and bearing factor methods in IMPACT35 for sediment resistance using the Baltic Sea experiment data and found that the bearing factor method is better than the delta method.

E. Weakness and Future Improvement

The main limitation of the current iteration of IMPACT 35 is its utilization for cylindrical and near-cylindrical mines only. The effect of shape is a significant issue if the model is to be used operationally, as the most widely used bottom mines such as Manta and Rockan are not cylindrical (near-cylindrical). Determination of the hydrodynamic force and torque for noncylindrical mines is crucial, but there are no existing formulas for these shapes.

The shape effect is more tenuous and will have less test data. Shape is a significant issue if the model is used operationally, because the most popular mines such as Rockan and Manta are not cylindrical (Fig. 21). The most important issue is to determine the hydrodynamic (drag and lift) force and torque for noncylindrical mines since there is no existing formula for calculating the drag and lift forces and torques for noncylindrical objects. MIDEX-II at NPS, conducted in September 2005, is the direct continuation of mine drop experiments with operational mine shapes [50], [51]. In that experiment, the overall shape of the mine was varied from cylindrical mines to see how the water phase trajectory would be affected. In addition to a sphere and semihemispherical "Gumdrop" shape, two shapes were specifically chosen to represent real-world bottom mines: Manta and Rockan [50], [51].

With the data collected at MIDEX-II at NPS, IMPACT35 for Manta and Rockan mines are developing. In the model development, the nonlinear instability and model sensitivity should be studied. Within the correct physics there is a possibility of chaotic behavior in the model. The chaotic features will be handled by the instability and predictability analyses.

VII. Conclusion

Advances in the mine impact burial prediction are reviewed in this paper. The 1-D model (IBPM) was developed to predict the vertical position of the mine's COM. The model provides useful information such as higher falling velocity for vertical release than for horizontal release, strong dependence of water and vertical impact velocity on the attitude for light mines (not for heavy mines), and strong dependence of the mine's falling velocity in water column on attitude, wet weight, mine's length, and mine's radius. For the same mine, the falling velocity in the water has a minimum in horizontal orientation and a maximum in vertical orientation. Major weakness is the constant falling angle assumption through a single fluid.

The 2-D model (IMPACT25/28) was developed to overcome the major weakness of the 1-D model and to predict the COM position in the (x, z)-plane and the rotation around the y-axis. Major weakness is the difficulty to include the fluid's motion in the model because it is impossible to lay a mine in the same direction of the fluid velocity. In littoral zone, the water velocity is not negligible. The application of the 2-D model for the operational use is limited. Other weaknesses are as follows: 1) a similar dependence of the axial and cross drag coefficients on the Reynolds number Re and the aspect ratio and 2) crude parameterization for sediment bearing strength.

The 3-D model (IMPACT35) has been developed to predict the COM position in (x, y, z)-space and the rotation around x-, y-, and z-axes. Althogh IMPACT35 shows great improvements versus IMPACT25/28 using the recent mine drop experimental data, it is used only for the cylindrical and near-cylindrical mines (major weakness). Mine shape is a significant issue if the model is used operationally, because the most mines such as Manta and Rockan are not cylindrical. The most important thing for future improvement of IMPACT35 is to determine the drag and lift laws for noncylindrical mines. With the data collected during MIDEX-II at NPS for operational mine shapes such as Manta and Rockan, IMPACT35 for operational mine shapes should be developed.

Acknowledgment

The author would like to thank Drs. P. Valent, M. D. Richardson, P. Elmore, T. Holland, and A. Abelev at the Naval Research Laboratory, and Dr. T. Weaver at FWG for fruitful discussions that benefited this paper.

References

[1] R. A. Arnone and L. E. Bowen, "Prediction model of the time history penetration of a cylinder through the air-water-sediment phases," Naval Coast. Syst. Ctr., Panama City, FL, Tech. Note 734-36, 1980.

[2] L. J. Satkowiak, "Modifications to the NCSC impact burial prediction model," Naval Coast. Syst. Ctr., Panama City, FL, Tech. Note 883-87, 1987.

[3] ——, "User's guide for the modified impact burial prediction model," Naval Coast. Syst. Ctr., Panama City, FL, Tech. Note 884-87, 1987.

[4] R. B. Hurst, "Mine impact burial prediction model—Technical description of recent changes and developments (U)," Def. Sci. Establishment, Auckland, New Zealand, DSE Rep. 149, 1992, (Restricted).

[5] P. J. Mulhearn, "Experiments on mine burial on impact—Sydney Harbour," *U.S. Navy J. Underwater Acoust.*, vol. 43, pp. 1271–1281, 1992.

[6] P. C. Chu, A. F. Gilles, C. W. Fan, and P. Fleischer, "Hydrodynamics of falling mine in water column," in *Proc. 4th Int. Symp. Technol. Mine Problem*, 2000, CD-ROM.

[7] P. C. Chu, V. L. Taber, and S. D. Haeger, "Environmental sensitivity studies on mine impact burial prediction model (two-dimensional)," in *Proc. 4th Int. Symp. Technol. Mine Problem*, 2000, CD-ROM.

[8] ***[AU: Please provide department]***V. L. Taber, "Environmental sensitivity studies on mine impact burial prediction model," M.S. thesis, Naval Postgrad. School, Monterey, CA, 1999.

[9] ***[AU: Please provide department]***T. B. Smith, "Validation of the mine impact burial model using experimental data," M.S. thesis, Naval Postgrad. School, Monterey, CA, 2000.

[10] P. C. Chu, A. D. Evans, A. F. Gilles, T. Smith, and V. Taber, "Development of Navy's 3D mine impact burial prediction model (IMPACT35)," in *Proc. 6th Int. Symp. Technol. Mine Problem*, 2004, DVD-ROM.

[11] ***[Page range to come!]***P. C. Chu and C. W. Fan, R. H. Wilkens and M. D. Richardson, Eds., "Mine impact burial model (IMPACT35) verification and improvement using sediment bearing factor method," *IEEE J. Ocean. Eng.*, vol. 32, no. 1, pp. XXX–XXX, Jan. 2007.

[12] P. C. Chu, "Hydrodynamics of mine impact burial," presented at the ONR Impact Burial Annu. Workshop, La Jolla, CA, Jan. 15–17, 2002.

[13] P. C. Chu, C. W. Fan, A. D. Evans, A. F. Gilles, and P. Fleischer, "Three-dimensional hydrodynamic model for prediction of falling cylinder through water column," in *Proc. MTS/IEEE Conf. OCEANS*, San Diego, CA, 2003, pp. 2047–2057.

[14] P. C. Chu, C. W. Fan, and A. D. Evans, "Three-dimensional rigid body impact burial model (IMPACT35)," *Adv. Fluid Mech.*, vol. 5, pp. 43–52, 2004.

[15] ***[AU: Please provide department]***A. D. Evans, "Hydrodynamics of mine impact burial," M.S. thesis, Naval Postgrad. School, Monterey, CA, 2002.

[16] P. C. Chu, C. W. Fan, A. D. Evans, and A. F. Gilles, "Triple coordinate transforms for prediction of falling cylinder through the water column," *J. Appl. Mech.*, vol. 71, pp. 292–298, 2004.

[17] H. Lamb, *Hydrodynamics*. Cambridge, U.K.: Cambridge Univ. Press, 1932.

[18] L. M. Milne-Thomson, *Theoretical Hydrodynamics*. New York: Macmillian, 1968.

[19] H. Aref and S. W. Jones, "Chaotic motion of a solid through ideal fluid," *Phys. Fluids A—Fluid Dyn.*, vol. 5, no. 12, pp. 3026–3028, 1993.

[20] ——, "Motion of a solid body through an ideal fluid," College Eng., Univ. Illinois Urbana-Champaign, Urbana, IL, Rep. No. 772, 1994.

[21] P. Holmes, J. Jenkins, and N. E. Leonard, "Dynamics of the Kirchhoff equations I: Coincident centers of gravity and buoyancy," *Physica D*, vol. 118, no. 3–4, pp. 311–342, 1998.

[22] S. B. Field, M. Klaus, M. G. Moore, and F. Nori, "Chaotic dynamics of falling disks," *Nature*, vol. 388, no. 6639, pp. 252–254, 1997.

[23] L. Mahadevan, W. S. Ryu, and D. T. S. Aravinthan, "Tumbling cards," *Phys. Fluids*, vol. 11, no. 1, pp. 1–3, 1999.

[24] N. E. Kochin, I. A. Kibel, and N. V. Roze, *Theoretical Hydromechanics*. New York: Interscience, 1964.

[25] V. V. Kozlov, "Heavy rigid body falling in an ideal fluid," *Izv AN SSSR, Mekhanika Tverdogo Tela*, vol. 24, no. 5, pp. 10–17, 1989.

[26] L. J. Satkowiak, "Modified NCSC impact burial prediction model with comparisons to mine drop tests," Naval Coast. Syst. Ctr., Panama City, FL, Tech. Note 486-88, 1988.

[27] P. C. Chu, "Ensemble mine impact burial prediction," presented at the ONR Impact Burial Modeling Workshop, Phoenix, AZ, Mar. 5–7, 2002.

[28] P. C. Chu, V. L. Taber, and S. D. Haeger, " Mine impact burial model sensitivity study," Naval Postgrad. School, Monterey, FL, NPS-IJWA-00-003, 2000, pp. 1–48.

[29] E. M. Stanley, "Viscosity of sea water at moderate temperatures and pressures," *J. Geophys. Res.*, vol. 74, pp. 3415–3420, 1969.

[30] R. B. Krone, "A study of rheological properties of estuarine sediments," U.S. Army Corps Eng., Vicksburg, MS, Tech. Bulletin No.7, 1963.

[31] P. C. Chu, T. B. Smith, and S. D. Haeger, "Mine impact burial prediction experiment," Naval Postgrad. School, Monterey, CA, NPS-IJWA-01-007, 2001, pp. 1–161.

[32] ——, "Mine impact burial prediction," in *Proc. 4th Int. Symp. Technol. Mine Problem*, 2002, CD-ROM.

[33] C. T. Crowe, J. A. Roberson, and D. F. Elger, *Engineering Fluid Mechanics*, 7th ed. New York: Wiley, 2001, pp. 1–714.

[34] P. C. Chu, A. F. Gilles, C. W. Fan, J. Lan, and P. Fleischer, "Hydrodynamics of falling cylinder in water column," *Adv. Fluid Mech.*, vol. 4, pp. 163–181, 2002.

[35] P. C. Chu and C. W. Fan, "Pseudo-cylinder parameterization for mine impact burial prediction," *J. Fluids Eng.*, vol. 127, pp. 1515–1520, 2005.

[36] ——, "Prediction of falling cylinder through air-water-sediment columns," *J. Appl. Mech.*, vol. 73, pp. 300–314, 2006.

[37] P. C. Chu and G. Ray, "Prediction of high speed rigid body maneuvering in air-water-sediment column," *Adv. Fluid Mech.*, vol. 6, pp. 123–132, 2006.

[38] P. C. Chu, G. Ray, P. Fleischer, and P. Gefken, "Development of three dimensional bomb maneuvering model," in *Proc. 7th Int. Symp. Technol. Mine Problems*, 2006, DVD-ROM.

[39] H. Rouse, *Fluid Mechanics for Hydraulic Engineers*, 1st ed. New York: Mcgraw-Hill, 1938.

[40] R. Von Mises, *Theory of Flight*. New York: Dover, 1959, pp. 564–585.

[41] B. M. Sumer and J. Fredsøe, *Hydrodynamics Around Cylindrical Structures*. Singapore: World Scientific, 1997.

[42] F. M. White, *Viscous Fluid Flow*. New York: McGraw-Hill, 1974.

[43] ***[Page range to come!]***C. P. Aubeny and H. Shi, R. H. Wilkens and M. D. Richardson, Eds., "Effect of rate-dependent soil strength on cylinders penetrating into soft clay," *IEEE J. Ocean. Eng.*, vol. 32, no. 1, pp. XXX–XXX, Jan. 2007.

[44] ***[AU: Please provide department]***A. F. Gilles, "Mine drop experiment," M.S. thesis, Naval Postgrad. School, Monterey, CA, 2001.

[45] P. C. Chu, A. F. Gilles, and C. W. Fan, "Experiment of falling cylinder through the water column," *Exp. Thermal Fluid Sci.*, vol. 29, pp. 555–568, 2005.

[46] ***[Page range to come!]***A. V. Abelev, P. J. Valent, and K. T. Holland, R. H. Wilkens and M. D. Richardson, Eds., "Behavior of a large cylinder in free fall through water," *IEEE J. Ocean. Eng.*, vol. 32, no. 1, pp. XXX–XXX, Jan. 2007.

[47] K. T. Holland, A. W. Green, A. Abelev, and P. J. Valent, "Parameterization of the in-water motions of falling cylinders using high-speed video," *Exp. Thermal Fluid Sci.*, vol. 37, pp. 690–770, 2004, doi: 10.1007/800348-004-0859-2.

[48] ***[AU: Please provide page range]***P. A. Elmore, R. Wilkens, T. Weaver, and M. D. Richardson, "IMPACT 28 and 35 simulations of 2003 Baltic Sea cruise: model results and comparison with data," in *Proc. 5th Annu. ONR Workshop Mine Burial Prediction*, Kona, HI, Jan. 31–Feb. 2 2005.

[49] ***[Page range to come!]***P. A. Elmore, M. D. Richardson, and R. H. Wilkens, R. H. Wilkens and M. D. Richardson, Eds., "Exercising the Monte Carlo mine burial prediction system for impact and scour burial for operational Navy use," *IEEE J. Ocean. Eng.*, vol. 32, no. 1, pp. XXX–XXX, Jan. 2007.

[50] P. C. Chu, C. R. Allen, and P. Fleischer, "Non-cylindrical mine impact experiment," in *Proc. 7th Int. Symp. Technol. Mine Problems*, 2006, DVD-ROM.

[51] ***[AU: Please provide department]***C. R. Allen, "Mine drop experiment II with operational mine shapes (MIDEX-II)," M.S. thesis, Naval Postgrad. School, Monterey, CA, 2006.

Peter C. Chu received the Ph.D. degree in geophysical fluid dynamics from the University of Chicago, Chicago, IL, in 1985.

He is a Professor of Oceanography and Head of the Naval Ocean Analysis and Prediction (NOAP) Laboratory at the Naval Postgraduate School, Monterey, CA. His research interests include ocean analysis and prediction, coastal modeling, littoral zone oceanography for mine warfare, mine impact burial prediction, mine acoustic detection, and satellite data assimilation for undersea warfare.

Mine Impact Burial Prediction From One to Three Dimensions

Peter C. Chu

***Abstract*—The Navy's mine impact burial prediction model (IBPM) creates a time history of a cylindrical (or near-cylindrical) mine as it falls through air, water, and sediment. The output of the model is the predicted burial depth and orientation of the mine in the sediment, as well as height, area, and volume protruding. Model inputs consist of environmental parameters and mine characteristics, as well as parameters describing the mine's release. This paper reviews the following model advances from one to three dimensions: 1) 1-D models predict the vertical position of the mine's center of mass (COM) with the assumption of constant falling angle, 2) 2-D models predict the COM position in the (x, z)-plane and the rotation around the y-axis, and 3) 3-D models predict the COM position in (x, y, z)-space and the rotation around x-, y-, and z-axes. These models are verified using the data collected from recent mine impact burial experiments. The 1-D model only solves one momentum equation (in the z-direction); it cannot predict the mine trajectory and burial depth well. The 2-D model restricts the mine motion in the (x, z)-plane (which requires motionless *[AU: Requires motionless what?]* for the environmental fluids), and uses incorrect drag coefficients and inaccurate sediment dynamics. The prediction errors are large in the mine trajectory and burial depth prediction (6–10 times larger than the observed depth in sand bottom of the Monterey Bay, CA). The 3-D model predicts the trajectory and burial depth relatively well for cylindrical and near-cylindrical mines, but not for the operational mines such as Manta and Rockan. Future improvements should include the shape effects, especially the operational mines.**

***Index Terms*—Burial depth, drag and lift forces and torques, impact burial prediction model (IBPM), IMPACT25/28, IMPACT35, Kirchhoff–Kelvin equation, mine impact burial prediction, orientation, sediment dynamics, translation velocity, triple coordinate system.**

NOMENCLATURE

(C_{d1}, C_{d2})	Drag coefficients along and across the cylinder.
C_l	Lift coefficient.
C_{tl}	Translational lift coefficient (kg s^{-1}).
e_v	Void ratio.
(f_1, f_2, f_3)	Added-mass ratios for drag and lift forces.
f_r	Added-mass ratio for moment of drag and lift forces.
(f_{rd2}, f_{rd3})	Rotational drag force (N).
$\mathbf{F}_b$	Buoyancy force (N).
$\mathbf{F}_d$	Drag force (N).
$(\mathbf{F}_{d1}, \mathbf{F}_{d2}, \mathbf{F}_{d3})$	Drag force in the F-coordinate (N).
$\mathbf{F}_l$	Lift force (N).
$(\mathbf{F}_{l1}, \mathbf{F}_{l2}, \mathbf{F}_{l3})$	Lift force in the F-coordinate (N).
$(\mathbf{i}_E, \mathbf{j}_E, \mathbf{k}_E)$	Unit vectors in the E-coordinate.
$(\mathbf{i}_F, \mathbf{j}_F, \mathbf{k}_F)$	Unit vectors in the F-coordinate.
$(\mathbf{i}_M, \mathbf{j}_M, \mathbf{k}_M)$	Unit vectors in the M-coordinate.
(J_1, J_2, J_3)	Moments of gyration (kg m^2).
$(J_1^{(i)}, J_2^{(i)}, J_3^{(i)})$	Moments of gyration for cylindrical part-i (kg m^2).
L	Length of the cylinder (m).
$\mathbf{M}_b$	Torque due to the buoyancy force (kg m^2 s^{-2}).
$\mathbf{M}_h$	Torque due to the hydrodynamic force (kg m^2 s^{-2}).
$(\mathbf{M}_{d1}, \mathbf{M}_{d2}, \mathbf{M}_{d3})$	Torques due to the drag force in the M-coordinate (kg m^2 s^{-2}).
$\mathbf{r}$	Position vector (in the M-coordinate) of point on the cylinder's surface.
R	Radius of the cylinder.
Re	Reynolds number.
$\mathbf{V}$	Translation velocity (m s^{-1}).
$\mathbf{V}_r$	Water-to-cylinder velocity (m s^{-1}).
$\mathbf{V}_1$	Component of $\mathbf{V}_r$ along the cylinder (m s^{-1}).
$\mathbf{V}_2$	Component of $\mathbf{V}_r$ perpendicular to the cylinder (m s^{-1}).
$\mathbf{V_w}$	Water velocity (m s^{-1}).

Manuscript received June 5, 2005; revised October 4, 2005; accepted October 15, 2005. This work was supported by the U.S. Office of Naval Research Coastal Geosciences Program under the Grants N0001403WR20178 and N0001404WR20067, by the Naval Oceanographic Office, and by the Naval Postgraduate School. **Guest Editor: M. D. Richardson**.

The author is with the Naval Ocean Analysis and Prediction Laboratory, Naval Postgraduate School, Monterey, CA 93943 USA (e-mail: pcchu@nps.edu).

Color versions of one or more of the figures in this paper are available online at http://ieeexplore.ieee.org.

Digital Object Identifier 10.1109/JOE.2007.890941

ν	Molecular viscosity of the water ($m^2\ s^{-1}$).
Π	Volume of the cylinder (m^3).
ρ	Density of the cylinder (kg m^3).
ρ_w	Density of the water (kg m^3).
χ	Distance between COM and COV (m).
(ψ_1, ψ_2, ψ_3)	Angles determining the cylinders' orientation.
$\boldsymbol{\omega}$	Angular velocity (s^{-1}).
$(\omega_1, \omega_2, \omega_3)$	Angular velocity components in the M-coordinate (s^{-1}).
$(\omega_1^F, \omega_2^F, \omega_3^F)$	Angular velocity components in the F-coordinate (s^{-1}).

I. Introduction

In mine hunting, success often hinges on knowing as much as possible about the mines that have been placed and the effects the environment has had on that placement. Since bottom mines cannot be searched visually, and are often difficult to locate with conventional sonar, an estimate of area or height of the mine protruding from the sediment, or the burial depth, is crucial information for the planning and execution of mine clearance operations. Determining the likely mine burial depth requires numerical models of the burial process and knowledge of the environment, including sediment properties, waves, tides, and water depth.

Sea-deployed mines currently used by the United States and other nations fall into three general categories: bottom, moored, and drifting mines. Bottom mines rest on the ocean floor and are generally deployed in littoral regions. Common placements for bottom mines include shipping channels, harbors, anchorages, rivers, and estuaries. Bottom mines are deployed in one of three ways: aircraft, surface ship, or submarine. Mine impact burial models have been developed to predict mine's motion in air and water and to determine the burial depth when the mine comes to rest in the sediment.

The 1-D impact burial prediction model (IBPM) was developed by Arnone and Bowen [1] to predict the vertical position of the cylindrical mine's center of mass (COM) as it falls through air, water, and sediment. The burial depth of the mine in marine sediment is then calculated from the mine's velocity and the sediment characteristics. IBPM only solves the vertical momentum equation with the assumption of an unchanged orientation in the fluid.

Satkowiak [2], [3] modified Arnone and Bowen's [1] pioneering work including corrected reference flow used in drag calculation and corrected added-mass term in equations; reworked equations for sediment-cavity regime, drag due to cylindrical and rounded noses, and retarding forces in semisolid sediment; and included water temperature effect on the water viscosity. The major weakness of the 1-D model is the mine's orientation (or the falling angle) assumed constant as it falls through the fluid.

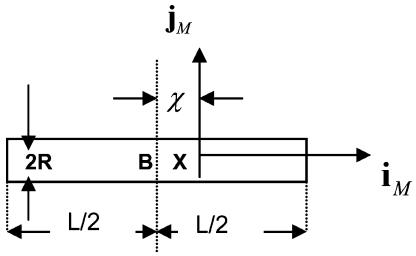

Fig. 1. M-coordinate with the COM as the origin $\mathbf{X}$ and (i_m, j_m) as the two axes. Here, χ is the distance between the COV ($\mathbf{B}$) and COM ($\mathbf{X}$) and (L, R) are the cylinder's length and radius (after [13]).

The 2-D models were developed first by Hurst to overcome major weakness of IBPM (constant falling angles) ([4]), and written in Basic (IMPACT25) and in Matlab (IMPACT28). The models contain three equations with two momentum equations (in x- and z-directions) and a moment-of-momentum equation (in y-direction), and predict mine COM position in the (x, z)-plane and the rotation (i.e., mine orientation) around the y-axis. The models include Mulhearn's [5] formulation for sediment bearing strength and uses multilayered sediments.

Although the 2-D (x, z)-models advance our knowledge on the mine by including mine rotation around the y-axis, it is very difficult to include the motion of fluid. This is because it is hard to assume the fluid (air, water, and sediment) movement strictly in the (x, z)-plane. Any fluid motion in the y-direction induces drag force, and in turn, causes the mine movement (in the y-direction), which breaks the 2-D scenario [6], [7]. In fact, it is impossible to lay a mine in the same vertical plane of the fluid velocity. Sensitivity studies on IMPACT25/28 burial depth show the insensitivity of the mine-releasing height and the water temperature ([8]). A mine drop experiment at Monterey Bay, CA ([9]–[11]) shows that IMPACT25/28 overpredicts the burial depth.

The 3-D model (IMPACT35) has been developed with the support from the U.S. Office of Naval Research (ONR, Arlington, VA) through mine burial prediction program [12]–[15]. The model contains six equations with three momentum equations and three moment-of-momentum equations, and predicts the mine's COM position in the (x, y, z)-space and the rotation (i.e., mine's orientation) around the three axes. Several mine drop experiments conducted at the Naval Postgraduate School (Monterey, CA), Naval Undersea Warfare Center—Carderock (West Bethesda, MD), and Baltic Sea (by the German Navy) are used to evaluate the 2-D and 3-D models. The results show great improvement of the 3-D modeling.

The 1-D, 2-D, and 3-D models are reviewed in the following sections. Basic physics, formulation, strength, and weakness of each model are presented. The purpose is to provide an overall picture of more than two decades' effort on predicting the mine movement in air, water, and sediment.

II. Mine Location and Orientation

Consider an axially symmetric cylinder with the COM $\mathbf{X}$ [or called gravity center (GC) in literature] and center of volume (COV) $\mathbf{B}$ on the main axis (Fig. 1). Let (L, R, χ) represent cylinder length, radius, and the distance between the two points

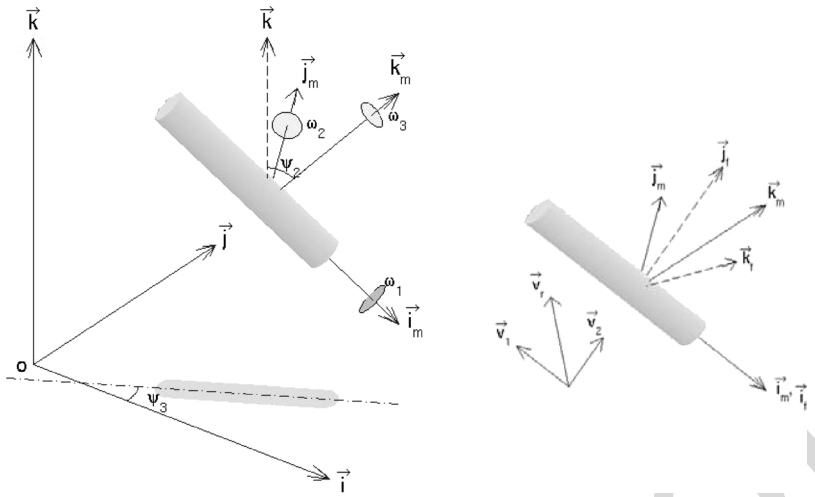

Fig. 2. Mine's COM position (x, z) and orientation ψ_2 (after [16]).

$(\mathbf{X}, \mathbf{B})$. The positive χ-values refer to nose-down case, i.e., the point $\mathbf{X}$ is lower than the point $\mathbf{B}$. Let $F_E(O, \mathbf{i}, \mathbf{j}, \mathbf{k})$ be the earth-fixed coordinate (E-coordinate) with the origin "O", and three axes: x- and y-axes (horizontal) with the unit vectors $(\mathbf{i}, \mathbf{j})$ and z-axis (vertical) with the unit vector $\mathbf{k}$ (upward positive). The position of the cylinder is represented by the position of the COM

$$\mathbf{X} = x\mathbf{i} + y\mathbf{j} + z\mathbf{k} \tag{1}$$

which is translation of the cylinder. The translation velocity is given by

$$\frac{d\mathbf{X}}{dt} = \mathbf{V}, \qquad \mathbf{V} = (u, v, w). \tag{2}$$

The orientation of the cylinder main axis (pointing downward) is given by $\mathbf{i}_M$. The angle between $\mathbf{i}_M$ and $\mathbf{k}$ is denoted by $\psi_2 + \pi/2$ (Fig. 2). The angle ψ_2 is the mine-falling angle. In the 1-D and 2-D modeling, only the E-coordinate system is used. In 3-D modeling, two extra-coordinate systems (main-axis-following and force-following coordinates) are also used.

III. Triple Coordinate Systems

The following three coordinate systems are used in mine impact burial prediction modeling: earth-fixed coordinate (E-coordinate), main-axis-following coordinate (M-coordinate), and force-following coordinate (F-coordinate) systems. All three coordinate systems are 3-D, orthogonal, and right-handed [16]. Projection of the mine's main-axis vector $\mathbf{i}_M$ onto the (x, y)-plane creates angle (ψ_3) between the projection and the x-axis (Fig. 2). The M-coordinate is represented by $F_M(\mathbf{X}, \mathbf{i}_M, \mathbf{j}_M, \mathbf{k}_M)$ with the origin "$\mathbf{X}$" (i.e., the COM location), unit vectors $(\mathbf{i}_M, \mathbf{j}_M, \mathbf{k}_M)$, and coordinates (x_M, y_M, z_M). The unit vectors of the M-coordinate system are given by

$$\mathbf{j}_M = \mathbf{k} \times \mathbf{i}_M \quad \mathbf{k}_M = \mathbf{i}_M \times \mathbf{j}_M. \tag{3}$$

The M-coordinate system is solely determined by orientation of the cylinder's main axis $\mathbf{i}_M$.

The F-coordinate is represented by $F_F(X, i_F, j_F, k_F)$ with the origin $\mathbf{X}$, unit vectors $(\mathbf{i}_F, \mathbf{j}_F, \mathbf{k}_F)$, and coordinates (x_F, y_F, z_F). Let $\mathbf{V}_w$ be the fluid velocity. The water-to-mine velocity is represented by

$$\mathbf{V}_r = \mathbf{V}_w - \mathbf{V} \tag{4}$$

which can be decomposed into two parts

$$\mathbf{V}_r = \mathbf{V}_1 + \mathbf{V}_2 \quad \mathbf{V}_1 = (\mathbf{V}_r \cdot \mathbf{i}_F)\mathbf{i}_F \quad \mathbf{V}_2 = \mathbf{V}_r - (\mathbf{V}_r \cdot \mathbf{i}_F)\mathbf{i}_F \tag{5}$$

where $\mathbf{V}_1$ is the component paralleling to the cylinder's main axis (i.e., along $\mathbf{i}_M$), and $\mathbf{V}_2$ is the component perpendicular to the cylinder's main-axial direction. The unit vectors for the F-coordinate are defined by (column vectors)

$$\mathbf{i}_F = \mathbf{i}_M \quad \mathbf{j}_F = \mathbf{V}_2/|\mathbf{V}_2| \quad \mathbf{k}_F = \mathbf{i}_F \times \mathbf{j}_F. \tag{6}$$

Transforms among the three coordinate systems can be found in [16].

IV. The 1-D Modeling

The 1-D models assume that the cylinder is not rotating about any axis, nor is there a net fluid dynamic lift; consequently, it can be reasonably applied to stable motion of the body along one of its major axes (horizontal or vertical). The models predict the COM location (i.e., z) using the Kirchhoff–Kelvin theory. Only the E-coordinate system is used for 1-D modeling.

A. Kirchhoff–Kelvin Theory

In the later half of the 19th century, Kirchhoff and Lord Kelvin showed that the motion of a solid moving through an ideal fluid could be represented by a compact system of equations describing the coupled fluid-body dynamics [17], [18]. Publications about the implications and extensions of this theory (cited as the Kirchhoff–Kelvin equations hereafter) were frequent from the 1870s until the 1900s, when experimental aerodynamics showed the limitations of the idealized models in representing the coupled dynamics of bodies and complex turbulent boundary layer regimes. Interest in the subject also

waned due to the daunting nonlinearity of the governing equations. Recently, there has been a resurgence of interest in the Kirchhoff–Kelvin theory, since the widespread availability of highly capable computers has allowed numerical analysis of problems involving nonlinear dynamics [19]–[21]. Even when analytical closure is not practical, the general results of the Kirchhoff–Kelvin equations aid heuristic explanations of the observed dynamics of more complex shapes, such as coins (very short cylinders) sinking in water [22] and tumbling cards [23]. In [24], excellent introductory can be found to the Kirchhoff–Kelvin equations and implications.

In general, the Kirchhoff–Kelvin equations predict the coupled dynamic response of arbitrary solid bodies to various forces and torques within inviscid, incompressible flow. For high Reynolds number regimes ($\mathrm{Re} = UD/\nu > 10^4$, where U is velocity, D is either the length or diameter of the cylinder depending on release orientation, and ν is kinematic viscosity), the direct effect of viscosity is small such that coherent structures of the turbulent boundary layer diminish. The typical value of Re for mine falling through the water column is around 10^5 [15]. This condition allows the generalized dynamics of falling bodies to be characterized in terms of a simplified form of the Kirchhoff–Kelvin theory where buoyancy forces and turbulent drag are balanced by the inertia of the cylinder and displaced water. For a freely sinking cylinder of diameter d and length l, the combined effect of gravity and buoyancy per unit volume is

$$B = (\rho - \rho_w)g \tag{7}$$

where g is the gravity and $(\rho - \rho_w)$ is the density difference of the cylinder and the water. The flow over the cylinder surface yields pressure distributions that result in a net drag force on the body, empirically represented as proportional to the square of the body's speed through the water

$$F \approx \frac{1}{2}\rho_w C_d U^2 \Lambda \tag{8}$$

where C_d is the drag coefficient, U is mine's fall speed, and Λ is an effective cross-sectional area normal to the flow. Under the assumption that the torques exerted by wake pressure fluctuations are insignificant, the phenomenological representation of the total drag force on the cylinder can be used in an approximation for the falling motion where the rate of change in kinetic energy is parameterized by the rate of change of the cylinder momentum and the acceleration of the "virtual mass" of the displaced water (which depends upon the geometric characteristics of the body). Thus, the force balance on the cylinder is given by

$$\frac{d^2z}{dt^2} = \frac{\rho_w C_d \Lambda}{2\rho\Pi(1+f)}\left(\frac{dz}{dt}\right)^2 - \frac{(\rho - \rho_w)}{\rho}g + \frac{F}{\rho\Pi} \tag{9}$$

where Π is the volume of the mine, f is the effective added-mass factor or the virtual mass coefficient of the system due to the acceleration of water around the moving body, and F is the additional sediment force which is zero in air and water.

Full implementation of the theory is not the focus of this paper; however, stability analysis of particular variants of the Kirchhoff–Kelvin equation provide useful insights. We can characterize the generalized dynamics governing the motions of mines falling through water under the following hypothetical situations: vertical descent with the axis of the cylinder aligned parallel to the flow or vertical descent with the axis of the cylinder aligned perpendicular to the flow. For the simplest case where the axis of the cylinder is aligned with the fall direction, body motions will be stable unless they are significantly disturbed in a direction normal to the motion. This means that a vertically oriented cylinder dropped freely will maintain this orientation until external forces, such as variable turbulent drag, cause the motion to become unstable resulting in changes in orientation. With the axis of the cylinder oriented horizontally, or normal to the trajectory, the motion is also stable. An alterative scenario where the axis of the cylinder is not initially aligned either parallel or perpendicular to the flow makes application of the above equations difficult, but has been addressed in [25] where it is established that with time, the falling body will assume a horizontal orientation where the torque exerted on the body by the water turns the main axis of the cylinder, so that it is normal to the relative flow (broadside). This configuration is stable when the exposed area is normal to the flow and is significantly greater than the cross-sectional area of the "nose-on" attitude. Slight variations of this stable mode also exist including regular oscillations, glide tumble motions, and helical motions.

B. IBPM

The 1-D model is the first generation of the U.S. Navy's mine impact burial model [1]–[3], called the IBPM. This model is used to predict the vertical location and orientation of a cylindrical mine falling through air, water, and sediment through solving the Kirchhoff–Kelvin equation (9). The model consists of four major components: 1) steady falling attitude (ψ_2), 2) drag computation, 3) cavity regimes, and 4) additional sediment forces.

1) Constant Falling Angle in Single Media: IBPM does not use the moment-of-momentum equation to predict the mine orientation. After the mine passes the interface of two contacted media, the falling angle is assumed [1] to have a steady value determined by the moments of the vertical force $(\rho g - f_1\rho_w \cos^2\psi_2)$ and of the horizontal force $(\rho g - f_2\rho_w \sin^2\psi_2)$,

$$\tan\psi_2 = \frac{\mathrm{moment}(\rho g - f_1\rho_w\cos^2\psi_2)}{\mathrm{moment}(\rho g - f_2\rho_w\sin^2\psi_2)}. \tag{10}$$

An iteration method is used to calculate the attitude ψ_2. Equation (10) is not correct since the orientation of the moment is not the same as the orientation of mine.

In IBPM, the falling angle is treated as a given parameter, which means that the orientation of the mine does not change in the single medium. The effective cross-sectional area (or sometimes called projected area) Λ is calculated by

$$\Lambda = 2LR\sin\psi_2 + \pi R^2\cos\psi_2. \tag{11}$$

For an attitude of 0° (vertical), Λ equals πR^2. For an attitude of 90° (horizontal), Λ is the product of the length (L) and diameter $(2R)$.

The effective added-mass factors in the along and across mine's axis direction f_1 and f_2 are given by

$$f_1 = \frac{\alpha_0}{2-\alpha_0} \quad f_2 = \frac{\beta_0}{2-\beta_0} \tag{12}$$

where

$$\begin{aligned} \alpha_0 &\equiv \frac{4}{\delta}\left(\frac{4}{\delta^2}-1\right) - \left[\frac{1}{2}\ln\left(\frac{2+\delta}{2-\delta}\right) - \frac{\delta}{2}\right] \\ \beta_0 &\equiv \frac{4}{\delta^2} - \frac{1}{\delta}\left(\frac{4}{\delta^2}-1\right)\ln\left(\frac{2+\delta}{2-\delta}\right) \\ \delta &\equiv \frac{2R}{L}. \end{aligned} \tag{13}$$

δ is the aspect ratio. The effective added-mass factor is computed by

$$f = f_2 \sin\psi_2 + f_1 \cos\psi_2. \tag{14}$$

For an attitude of 0° (vertical), f equals f_1. For an attitude of 90° (horizontal), f equals f_2.

2) Drag Coefficient: Drag on a cylinder is proportional to the forces acting on the cylinder as if it were falling both vertically and horizontally. Thus, attitude during fall is important. Simply put, the total drag coefficient is a sum of the drag coefficient due to flow plus the drag coefficient due to cross flow as a function of attitude. This becomes somewhat more complicated because the character of the flow across the cylinder changes based on the magnitude of the Reynolds number of the cylinder. When the Reynolds number is small (<1), skin friction dominates but as the Reynolds number increases, a more laminar flow occurs and pressure drag dominates. At a certain and critical Reynolds number (10^4), flow becomes turbulent and drag abruptly decreases. Reynolds number is thus dependent on velocity of the cylinder and must be constantly recalculated as the cylinder falls through each medium. Let the Reynolds number (Re) be defined by

$$\mathrm{Re} = \frac{2UR}{\nu} \tag{15}$$

where ν is the kinematic viscosity of the fluid.

The axial and cross drag coefficients (C_{da}, C_{dc}) are calculated by [1]

$$C_{dc} = 1.1\eta C_{d\infty}\sin^2\psi_2 \quad C_{da} = 1.1C_{d*}\frac{\Lambda}{2RL} \tag{16}$$

where (17), shown at the bottom of the page, is the cross flow drag coefficient for the cylinder with infinite length $(C_{d\infty})$, and

$$C_{d*} = 0.33\delta + \frac{3.984}{\sqrt{\mathrm{Re}}}\left[\frac{1}{\delta} + \delta^{1/2}\right] \tag{18}$$

is the axial drag coefficient with no surface imperfections. The coefficient of 1.1 in (16) is used to account for imperfections of the cylinder with the correction factor η given by

$$\eta = 0.52238 + 0.02119\frac{1}{\delta} - 0.00048\left(\frac{1}{\delta}\right)^2. \tag{19}$$

The total drag coefficient (C_d) for computing the drag force on a mine moving through the fluid is calculated by

$$C_d = C_{da} + C_{dc}\sin^2\psi_2. \tag{20}$$

3) Air–Water Cavity: Upon impacting the water, the cylindrical mine enters the air–water cavity. The properties of the fluid in the water cavity are combination of air and water fluid properties and are continuously changing with time. Thus, it becomes extremely difficult to accurately predict the forces acting on a body in a fluid of changing properties [1], [26]. The changing properties around the cylinder through the cavity are the fluid density and kinematic viscosity. For example, the fluid density changes from air ($\rho_a = 1.29$ kg m^{-3}) to seawater ($\rho_w = 1025$ kg m^{-3}).

Within the air–water cavity regime, a percentage of each of these densities is used in determination of the resulting average density. This is represented by the ratio (called the void ratio) of the volume of water in the cavity to the total cavity volume. Although it is difficult to actually determine these volumes, the trend of this ratio is known. For example, the void ratio equals 0 for the cylinder in the air, and equals 1 for the cylinder totally wetted in the water. The void ratio n_0 is calculated by

$$n_0(t) = \sqrt{\frac{p_D(t)}{p_S(t)}} \tag{21}$$

in the IBPM. Here

$$p_D(t) = p_a + \frac{1}{2}\rho_w\left[U(t)\right]^2 \quad p_S(t) = p_a - \rho_w g z(t) \tag{22}$$

are the dynamic and static pressures, $z = 0$ denotes the air–water interface, and $p_a(= 100$ kPa) is the atmospheric pressure at the air–water interface. The air–water cavity density (ρ_w^{cav}) and viscosity (ν_w^{cav}) are calculated by

$$\rho_w^{\mathrm{cav}} = \rho_a(1-n_0) + \rho_w n_0, \quad \frac{1}{\rho_w^{\mathrm{cav}}\nu_w^{\mathrm{cav}}} = \frac{(1-n_0)}{\rho_a\nu_a} + \frac{n_0}{\rho_w\nu_w}. \tag{23}$$

The dynamic effect of cavitation on the body is through the change of the Reynolds number (in turn the change of the drag coefficient). The Reynolds number for the air–water cavity is calculated by

$$\mathrm{Re}_w^{\mathrm{cav}} = \frac{2UR}{\nu_w^{\mathrm{cav}}}$$

$$C_{d\infty} = \begin{cases} 0.84864 + 5.81939/\mathrm{Re}, & \text{if } \mathrm{Re} \le 4\times 10^3 \\ (0.5833\times 10^{-4})\mathrm{Re} + 0.61677, & \text{if } 4\times 10^3 < \mathrm{Re} \le 10^4 \\ 1.2, & \text{if } 10^4 < \mathrm{Re} \le 8\times 10^4 \\ 1.19381 + (0.65828\times 10^{-6})\mathrm{Re} - 10^{-11}\mathrm{Re}^2, & \text{if } 8\times 10^4 < \mathrm{Re} \le 5\times 10^5 \\ 8\times 10^{-7}\mathrm{Re} - 0.15, & \text{if } \mathrm{Re} \ge 5\times 10^5 \end{cases} \tag{17}$$

Substitution of $\mathrm{Re}_w^{\mathrm{cav}}$ into (16)–(20) leads to the drag coefficient for the air–water cavity.

4) Water–Sediment Cavity: Upon impacting the sediment, the cylindrical mine enters the water–sediment cavity. Similar to the air–water cavity regime, the properties of the water–sediment cavity are combination of water and sediment properties and are continuously changing with time. In the water–sediment cavity regime, the fluid density changes from water ($\rho_w = 1025$ kg m^{-3}) to sediment ρ_s. Within the water–sediment cavity, the void ratio n_1 is calculated by

$$n_1(t) = \sqrt{\frac{p_D(t)}{p_S(t)}} \tag{24}$$

where

$$\begin{aligned} p_D(t) &= p_a + \rho_w g h + \frac{1}{2}\rho_s \left[U(t)\right]^2 \\ p_S(t) &= p_a + \rho_w g h - \rho_s g \left[z(t) + h\right] \end{aligned} \tag{25}$$

are the dynamic and static pressures and h is the water depth. The water–sediment cavity density (ρ_s^{cav}) and viscosity (ν_s^{cav}) are calculated by

$$\rho_s^{\mathrm{cav}} = \rho_w(1-n_1) + \rho_s n_1 \quad \frac{1}{\rho_s^{\mathrm{cav}}\nu_s^{\mathrm{cav}}} = \frac{(1-n_1)}{\rho_w \nu_w} + \frac{n_1}{\rho_s \nu_s}. \tag{26}$$

The kinematic viscosity of the sediment is determined by

$$\nu_s = \nu_w + \frac{S}{\rho_s dU/dz} \tag{27}$$

where S is the shear strength of the sediment. Substitution of ν_s into (15) leads to a new Reynolds number; and then, use of (16)–(20) leads to the drag coefficient for the water–sediment cavity.

5) Additional Sediment Forces: It is noted that there are forces acting on the mine in the sediment which are different from those forces determined in the air and water. The hydrodynamic forces do not impose or account for the retarding force on a mine moving in sediment. The compressive and shearing stress forces of a sediment, which are not included in the hydrodynamic forces, are important in affecting the mine movement. The following equations

$$F = F_C + F_S \quad F_C = 2S\Lambda_f \quad F_S = S\Lambda_s \tag{28}$$

are used to compute the sediment resistant force [1]. Here, Λ_f and Λ_s are the frontal and side areas of the cylinder. The sediment resistant force is also dependent on the velocity of cylinder [3]

$$F = E_s S(N_b\Lambda_f + S_{af}\Lambda_s/S_t) \tag{29}$$

where E_s is the sediment strain effect (i.e., ratio of the sediment strength for a given velocity of the cylinder), $N_b(=10)$ is the bearing capacity factor, S_{af} is the side adhesive factor (0.3 for the cavity and 1.0 for sediment), and $S_t(=3)$ is the sediment sensitivity coefficient.

Thus, the sediment shear strength and density data are required to solve the Kirchhoff–Kelvin equation (9) for mine movement in the sediment since they are needed for determination of the sediment's compressive and shearing forces, buoyancy force, added-mass, drag force, and kinematic viscosity. Since the properties of sediment change with depth, the sediment density and shear strength profiles with 5-cm vertical resolution are used in the IBPM.

C. Sensitivity Studies

For a single medium, after the attitude (ψ_2) is determined from (10), the effective cross-sectional area Λ and effective added-mass factor f can be calculated using (11) and (12), and then, the total drag coefficient C_d can be computed using (20). For sediment, the compressive and shear stress forces (F) are computed from the density and shear strength. With the known parameters (Λ, f, C_d, F), the Kirchhoff–Kelvin equation (9) can be solved for mine movement. For mine penetration into the air–water and water–sediment interfaces, the total drag coefficient C_d^{cav} is calculated from the cavity density (ρ_w^{cav} or ρ_s^{cav}) and viscosity (ν_w^{cav} or ν_s^{cav}).

Arnone and Bowen [1] conducted a model sensitivity study on the mine air weight (or wet weight), length, and radius. The model (9) was integrated with various combinations of these parameters and the following three different attitudes: $\psi_2 = 0°$ (horizontal), 45°, abd 90° (vertical). The water impact velocity has the following features: 1) For mine movement in the air, as one would expect, the more streamlined the falling attitude is (i.e., $\psi_2 = 90°$, vertical), the higher velocity of the cylindrical mine falls; 2) the water impact velocity varies drastically with the attitude for light mines; such an effect reduces as the mass increases; and 3) the water impact velocity is not sensitive to mine length and radius.

The mine-falling velocity in water has the following characteristics.

1) It varies drastically with attitude and wet weight. For the same wet weight, the mine falls faster for $\psi_2 = 90°$ (vertical) than for $\psi_2 = 0°$ (horizontal). For the same ψ_2, the mine falls faster for heavier wet weight.
2) It is not sensitive to attitude for short mines and is very sensitive to attitude for long mines.
3) It is not sensitive to mine length for horizontal release $(\psi_2 = 0°)$ and is very sensitive to mine length for vertical release $(\psi_2 = 90°)$.
4) It is not sensitive to attitude for small R and is very sensitive to attitude for large R.***[AU: Last item of this list was removed, because it was exactly the same as point 4). Please check.]***

D. Strength and Weakness

IBPM can simulate mine-falling velocity in the air and water columns. As mentioned in Section IV-C, the model provides the following useful results: 1) the mine has higher falling velocity for vertical release $(\psi_2 = 90°)$ than for the horizontal release $(\psi_2 = 0°)$; 2) the water impact velocity varies drastically with the attitude for light mines, but does not for heavy mines; and 3) the mine-falling velocity in water column is sensitive to attitude, wet weight, mine length, and mine radius. For the same mine, the falling velocity in the water has a minimum in horizontal orientation and a maximum in vertical orientation.

Weakness of the IBPM is to assume the constant attitude (ψ_2) during the mine falling through air, water, and sediment (Fig. 3),

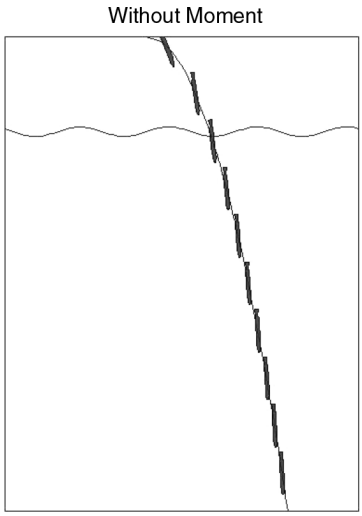

Fig. 3. Mine's orientation is assumed constant by the 1-D model when it falls through a single fluid (after [12]).

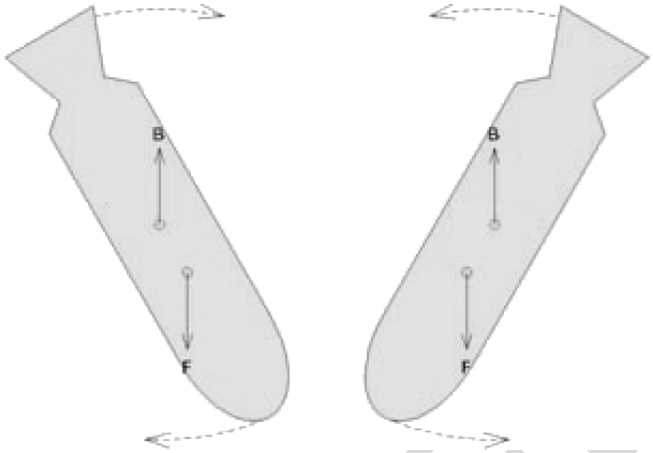

Fig. 4. Change of mine orientation caused by moment of momentum due to the buoyancy force (after [27]).

which is not physically realistic [12]. In fact, the orientation changes for any solid object falling through fluid (air and water). When COV is not colocated with COM, the buoyancy force ($\mathbf{B}$) has a moment of momentum exerted on mine (Fig. 4) [27]. If the mine slants toward left (right), the moment of momentum due to the buoyancy force will rotate the mine clockwise (counterclockwise), respectively. This causes the spiral motion for mine falling through fluid.

V. The 2-D Modeling

To overcome the major weakness of the 1-D model (i.e., constant falling angle), Hurst [4] modified the IBPM model allowing the cylinder to move both vertically and horizontally [in (x, z)-plane] as well as rotating about y-axis. These changes mandated the use of more complicated dynamical system than the IBPM. Two coordinate systems (E- and M-coordinates) are used in the 2-D modeling.

A. Dynamical System

Let the cylinder be moving in (x, z)-plane. The momentum equations in the (x, z)-directions are given by

$$\frac{d^2x}{dt^2} \equiv \frac{du}{dt} = \frac{F_h^x}{\rho\Pi} \tag{30}$$

$$\frac{d^2z}{dt^2} \equiv \frac{dw}{dt} = -g + \frac{B + F_h^z}{\rho\Pi} \tag{31}$$

where B is the buoyancy force, and F_h^x and F_h^z are the components of the hydrodynamic force $\mathbf{F}_h$. Since the cylinder is in the (x, z)-plane, the only possible rotation is around y-axis, which is described by the attitude ψ_2. The moment-of-momentum equation in the M-coordinate is given by

$$J_2 \frac{d^2\psi_2}{dt^2} = B\chi \cos\psi_2 + M_h^y \tag{32}$$

where J_2 is the moment of inertia in the y-axis and M_h^y is called the braking torque in [4].

B. IMPACT25/28

The 2-D models, usually called IMPACT25 (written in Basic) and IMPACT28 (written in Matlab), are the second generation of the Navy's mine IBPMs and were based on (30)–(32) for obtaining x, z, and ψ_2. The external forcing for IMPACT25/28 consists of drag force (F_h^x and F_h^z) and braking torque (M_h^y). Since the mine movement is restricted in the (x, z)-plane, it is very hard to include the motion of the fluids (air or water). If the fluid has velocity in the y-direction, the mine's motion cannot be 2-D. Thus, in IMPACT25 and IMPACT28, the fluid (air or water) is assumed motionless.

1) Drag Force: The drag force for the whole cylinder is calculated in two directions: along the cylinder's main axis ($\mathbf{i}_M$) and across the cylinder ($\mathbf{k}_M$)

$$\mathbf{F}_d = -F_d(\mathbf{i}_M \sin\psi_2 - \mathbf{k}_M \cos\psi_2) \tag{33}$$

where F_d is computed using the drag law

$$F_d = \frac{1}{2}\rho_w \hat{C}_d(u^2 + w^2)\Lambda. \tag{34}$$

The drag coefficient $\hat{C}_d$ is computed by

$$\hat{C}_d = C_d + C_{dn} \tag{35}$$

where C_d is computed in the same way as in the 1-D model [i.e., (20)] and C_{dn} is the drag coefficient for the nose.

2) Braking Torque: The braking torque M_h^y in (32) is calculated by

$$M_h^y = -\frac{1}{6} C_{dc} R \rho_w \omega_2 L^3 V_c \tag{36}$$

where

$$V_c = u\cos\psi_2 + w\sin\psi_2 \tag{37}$$

is the cross-cylinder velocity. Equation (36) is only used when the mine is fully immersed in a single fluid. During the cavity regimes, a different calculation is applied. Furthermore, the torque is opposite in sign to rotation, and thus, it acts to brake the rotation of mine. For a single fluid, the basic (30)–(32) are integrated with (33) and (36).

3) Sediment: In the 1-D models, IPBM and its modifications treat the sediment as fluid that is characterized by the following two parameters: sediment density and shear strength. Different from the 1-D models, the 2-D model treats the sediment as a solid that undergoes plastic deformation [4]. The pertinent parameters become sediment density and bearing strength. Bearing strength is the load bearing capacity of the sediment and defined as the pressure in front of the object penetrating the sediment. It is related to the shear strength, typically larger by a factor of about ten. The following three mechanisms contributing to the sediment resistance on the penetration of a falling mine are included in IMPACT25/28: bearing strength of the sediment (70%), hydrodynamic drag (25%), and buoyancy (5%) [4].

As the mine penetrates the sediment, the hydrodynamic drag that retards the penetration is calculated by

$$F_d = \frac{\rho_s \Lambda (u^2 + w^2)}{2} \left(C_1 \frac{h}{L} + C_2 \right) \tag{38}$$

where C_1 and C_2 are drag coefficients for low Reynolds number and h is the depth in sediment. The buoyancy force comes into play when the mine impacts the sediment. A crater is formed and the force that is required to create and enlarge the crater is given by [4]

$$B = \pi g h (\rho_w - \rho) \Lambda. \tag{39}$$

Two assumptions are made regarding the mine. First, the buoyancy force acts uniformly on the portion of the mine in contact with the sediment. Second, cavity is formed, and remains at the aft end of the mine, leading the mine surface to the buoyancy force. The second is not always true. For some cases, the cavity collapses under the weight of the sediment. The collapse limit is defined and approximated as the depth where the buoyancy force is 20% of the bearing force. Besides, the drag, buoyancy, and bearing strength of sediment all depend on the mine contact area Λ.

4) Air–Water Cavity: As mentioned before, when the mine penetrates the air–water interface, it forms a cavity behind the mine that changes the drag forces. Throughout the cavity regimes, nonsymmetric forces are acting on the mine that generate torque and affect the rate of rotation. The cavity parameterization is different between the 2-D models (IMPACT25/28) and 1-D model (IPBM). The cavity formation in the 2-D models is controlled by a cavitation number (N_{cav}) defined by

$$N_{\text{cav}} = \frac{2(p_{\text{out}} - p_{\text{in}})}{\rho_w (u^2 + w^2)} \tag{40}$$

where p_{out} and p_{in} are the hydrodynamic pressure outside (i.e., water) and inside the cavity, respectively. Pressure difference between outside and inside of the cavity increases or the mine's velocity decreases; the cavitation number increases until the eventual collapse of the cavity. The drag coefficient of the cavity is the function of the cavitation number

$$C_d(N_{\text{cav}}) = \hat{C}_d(1 + bN_{\text{cav}}). \tag{41}$$

When the air–water cavity collapses, $N_{\text{cav}} = 0$, $C_d(0)$ is the water drag coefficient. The torque in the air–water cavity can be computed after the drag coefficient is determined.

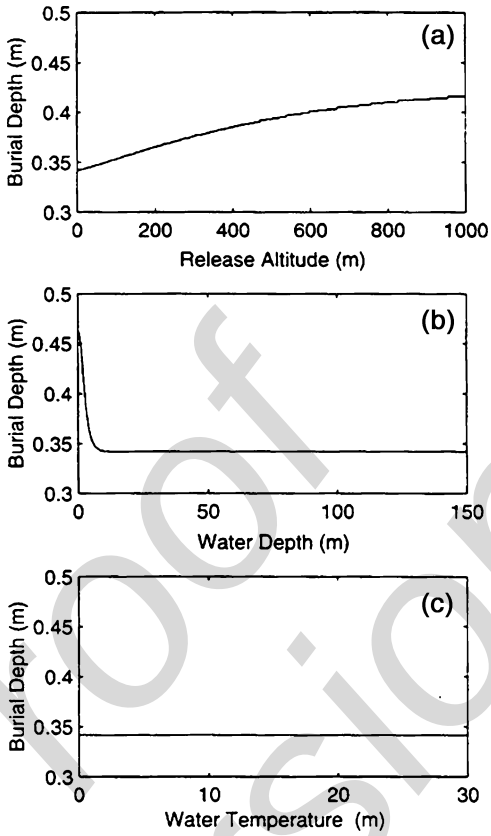

Fig. 5. Effect of (a) release attitude, (b) water depth, and (c) water temperature on burial depth. Values are preliminarily chosen to represent all conditions under which IMPACT25 and IMPACT28 may be used (after [28]).

C. Sensitivity Study

Sensitivity studies [8], [28] were conducted on the 2-D model (IMPACT25/28) to ascertain which parameters the model is most sensitive to and which can be simplified or eliminated to simplify its use. The model was altered to allow most parameters to be set and a loop run for one variable at a time. All model runs were made with preset mine profile, which has a dry weight of 538 kg, a wet weight of 251 kg, and a uniform diameter of 0.475 m.

1) Sensitivity to Release Parameters: Fig. 5 demonstrates the sensitivity of the release altitude and model parameters such as water depth and water temperature. Altitude, when varied from 0 to 1000 m, has a small effect on burial depth (relative difference of 18%). When a more realistic upper limit of 300 m for a mine laying aircraft is applied, the relative difference drops to just 9%. Water depth affects the burial depth only if a mine reaching the terminal velocity (in this case, about 20 m). Although temperature varies the water density up to 3%, and in

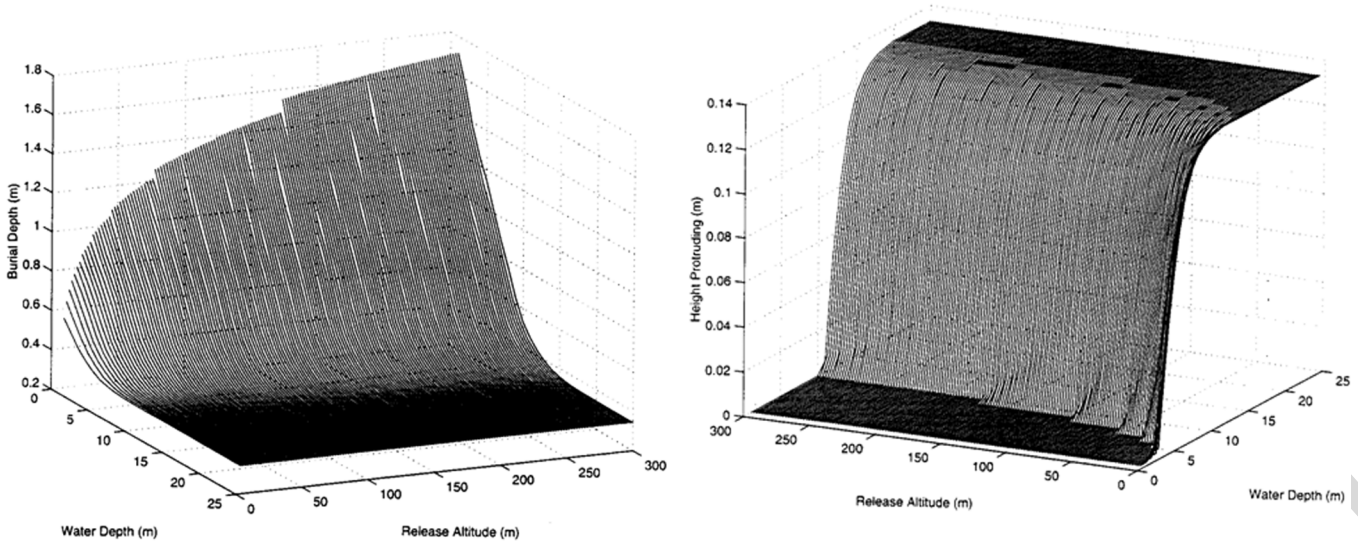

(a) (b)

Fig. 6. Dependence of (a) burial depth and (b) height protruding on release altitude and water depth (all in meters). Protruded height is illustrated here to clarify the levels at which these parameters become less influential in the 2-D models (after [28]).

turn, changes the viscosity [29], it does not affect the burial depth and orientation.

For vertical initial falling angle (Fig. 6) with zero rotation rate, the mine is heading directly downward, resulting in the maximum burial depth. When the release height is 150 m, the mine burial depth is 2.405 m for the vertical initial falling angle and 0.359 m for the horizontal initial falling angle. Such a difference in burial depth decreases as the release height decreases. When the release height is 1.5 m, the mine burial depth is 0.977 m for the vertical initial falling angle and 0.342 m for the horizontal initial falling angle.

2) Sensitivity to Sediment Characteristics: Fig. 7 shows the sensitivity of sediment density and shear strength on burial depth. For the shear strength of 1 kPa (extremely soft sediment), the burial depth changes 37% for sediment density varying from 1000 to 2000 kg m^{-3} ***[AU: "kg/m^{3}" was changed to "kg m^{-3}" to be consistent. Please check.]***. At the more common values of shear strength (5–15 kPa), the sediment density has very little effect, just 3.7% Fig. 7(a). As shear strength increases, the influence of sediment density reduces. For constant sediment density (1.5 kg m^{-3}), the impact burial depth drastically reduces from 0.55 m for the shear strength of 1 kPa to 0.1 m for shear strength of 10 kPa [Fig. 7(b)].

A power law is used

$$S = \alpha \rho_s^{\beta} \tag{42}$$

to represent the relationship between sediment density (ρ_s) and shear strength (S) [30]. Here, the two coefficients α and β are determined experimentally. Considering a homogeneous sediment layer $(\rho_s = \text{const})$, the shear strength is a function of (α, β). For a given ρ_s, increasing α or β enhances the shear strength (S), and in turn, decreases the burial depth. These features are well simulated by the model (Fig. 8).

D. Strength and Weakness

The improvement of the 2-D model versus the 1-D model is its capability to predict the mine rotation in the (x, z)-plane, i.e., ψ_2. In the 2-D model, the momentum equation for the (x, z)-directions and the moment-of-momentum equation for the y-direction are used to predict the position and orientation around the y-axis [i.e., in the (x, z)-plane]. The basic physics for the spiral motion described in Fig. 4 is included in the 2-D model, but strictly in the (x, z)-plane [31], [32].

Since the mine movement is strictly in the (x, z)-plane, it is very hard to include the motion of fluid in the 2-D model, because it is impossible to lay a mine in the same direction of the fluid velocity. In littoral zone, the water velocity is not negligible. The application of the 2-D model for the operational use is limited. Besides, the drag coefficients for the axial and cross directions have similar dependence on the Reynolds number Re and the aspect ratio (δ) [see (17) and (18)]. However, the drag coefficients in the axial and cross directions are independent [33]. Besides, a mine drop experiment shows that IMPACT25/28 overpredicts (5–10 times larger) the mine burial in the sandy bottom [9], [31], [32]. This indicates that the sediment dynamics is too simple in the 2-D model.

VI. The 3-D Modeling

To overcome the major weaknesses of the 2-D model, i.e., 1) environmental fluid assumed motionless, 2) similar drag coefficients in the axial and cross directions, and 3) nonrealistic sediment dynamics, Chu *et al.*[10]–[16], [34]–[38] modified IMPACT25/28 allowing the cylinder to move in 3-D space. These changes mandated the use of more complicated dynamical system than IMPACT25/28. The three coordinate systems (E-, F-, and M-coordinates) are used in the 3-D modeling.

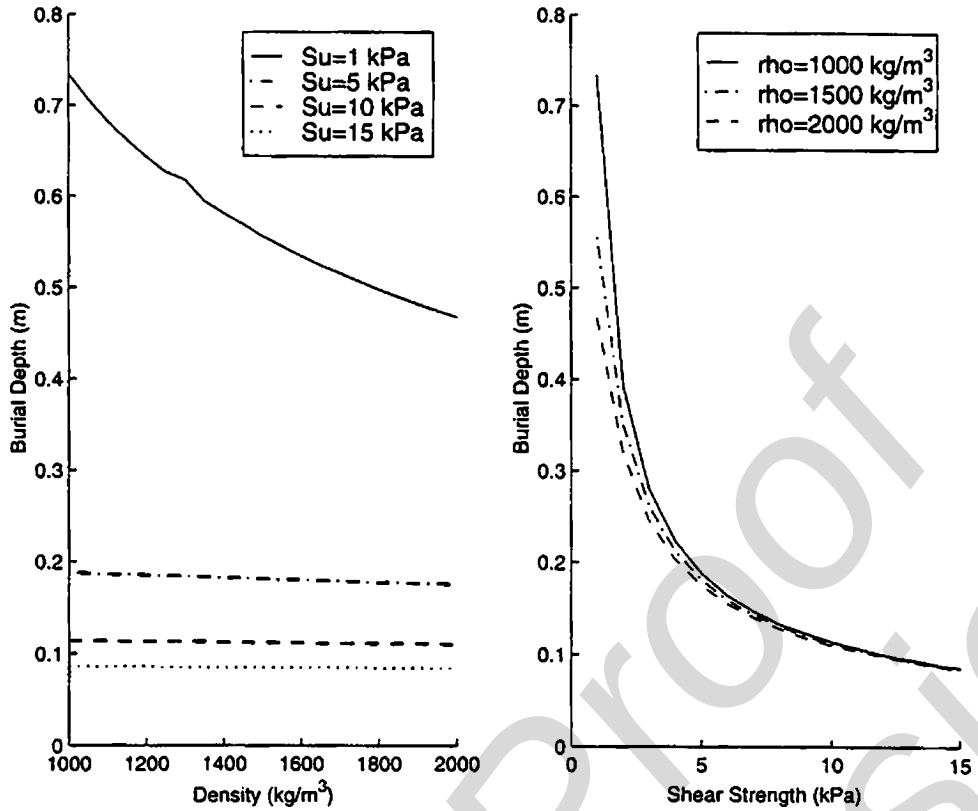

Fig. 7. Effect of sediment (a) density and (b) shear strength on burial depth. Density change only impacts the predicted burial depth in very soft sediments. As expected, shear strength has a dramatic impact on predicted burial depth (after [31]).***[AU: Please change units in the fig. to be consistent with the text]***

A. Dynamical System

The three momentum equations (in the E-coordinate system) are given by

$$\frac{d}{dt}\begin{bmatrix} u \\ v \\ w \end{bmatrix} = -\begin{bmatrix} 0 \\ 0 \\ g \end{bmatrix} + \frac{\mathbf{F}_b + \mathbf{F}_h}{\rho \Pi} \tag{43}$$

and the three moment-of-momentum equations (in the M-coordinate system) are written in vector form

$$\mathbf{J} \bullet \frac{d\boldsymbol{\omega}}{dt} = -2\mathbf{J} \bullet (\boldsymbol{\Omega} \times \boldsymbol{\omega}) + \mathbf{M}_b + \mathbf{M}_h. \tag{44}$$

Here, $(\mathbf{F}_b, \mathbf{M}_b)$ are the buoyancy force and torque and $(\mathbf{F}_h, \mathbf{M}_h)$ are the hydrodynamic force and torque including drag, lift, and impact ($\mathbf{F}_d$, $\mathbf{F}_l$, $\mathbf{F}_i$; $\mathbf{M}_d$, $\mathbf{M}_l$, $\mathbf{M}_i$). The vectors $(\boldsymbol{\omega}, \boldsymbol{\Omega})$ are the angular velocity of mine and M-coordinate system

$$\boldsymbol{\Omega} = \omega_2 \mathbf{j}_M + \omega_3 \mathbf{k}_M. \tag{45}$$

The first term in the right-hand side of (44) is an apparent torque (similar to the Corilois term in Earth science) due to the use of the rotating coordinate system (i.e., the M-coordinate). If $\omega_1 = 0$, then $\boldsymbol{\Omega} = \boldsymbol{\omega}$. The apparent torque is given by

$$-2\mathbf{J} \bullet (\boldsymbol{\Omega} \times \boldsymbol{\omega}) = \begin{cases} 0, & \text{if } \omega_1 = 0 \text{ (i.e., } \boldsymbol{\Omega} = \boldsymbol{\omega}) \\ -2J_2\omega_1\omega_3\mathbf{j}_M & \\ \quad +2J_3\omega_1\omega_2\mathbf{k}_M, & \text{if } \omega_1 \neq 0. \end{cases} \tag{46}$$

The gravitational force, passing the COM, does not induce the moment. In the M-coordinate system, the moment of gyration tensor for the axially symmetric cylinder is a diagonal matrix

$$\mathbf{J} = \begin{bmatrix} J_1 & 0 & 0 \\ 0 & J_2 & 0 \\ 0 & 0 & J_3 \end{bmatrix} \tag{47}$$

where J_1, J_2, and J_3 are the moments of inertia. The buoyancy force induces the moment in the $\mathbf{j}_M$ direction if the COM does not coincide with the COV (i.e., $\chi \neq 0$)

$$\mathbf{M}_b = |\mathbf{F}_b| \chi \cos\psi_2 \mathbf{j}_M. \tag{48}$$

B. IMPACT35

The 3-D model, usually called IMPACT35 (written in Matlab), is the third generation of the Navy's mine IBPM. It was developed to solve the six scalar (43) and (44) to obtain (x, y, z, ω_1, ω_2, ω_3). From the angular velocity (ω_1, ω_2, ω_3), the three angles determining the mine orientation (ψ_1, ψ_2, ψ_3) can be obtained

$$\frac{d\psi_1}{dt} = \omega_1 \quad \frac{d\psi_2}{dt} = \omega_2 \quad \frac{d\psi_3}{dt} = \omega_3.$$

The external forcing for IMPACT35 consists of drag force $\mathbf{F}_d$ and torque $\mathbf{M}_d$, as well as lift force $\mathbf{F}_l$ and torque $\mathbf{M}_l$. All these external forces and torques are calculated in the F-coordinate system. The model includes cylindrical and noncylindrical

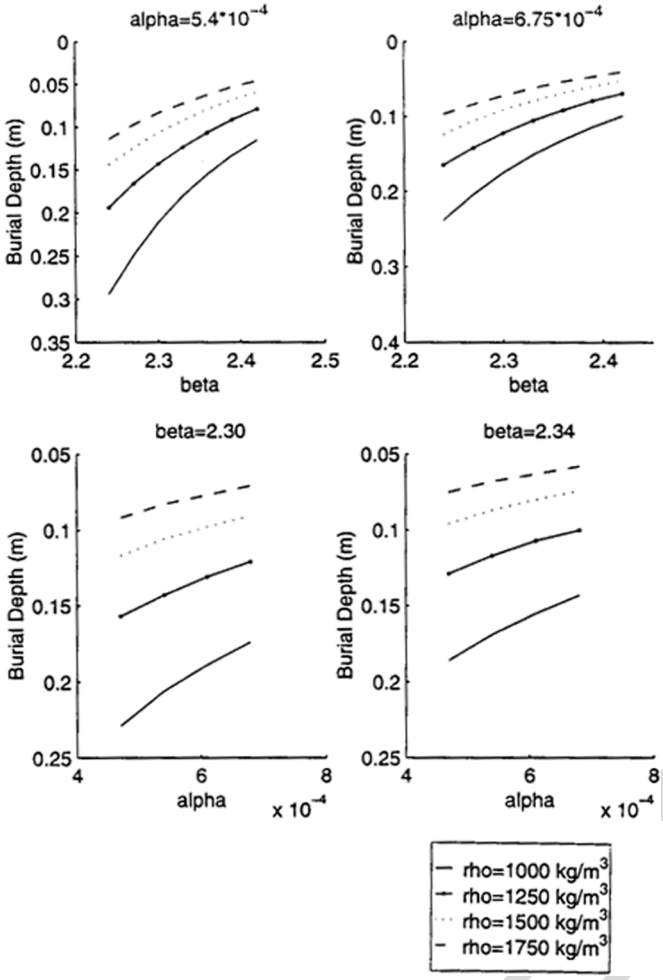

Fig. 8. Effect of α and β on predicted burial depth (meters) for different values of sediment density (after [31]). ***[AU: Please change units in the figure to as they are in text]***

mines. In this section, the cylindrical mine is taken as an example for illustration.

1) Drag and Lift Forces: Two features of the drag and lift coefficients (Reynolds-number-dependent and asymmetry in along- and across-mine main axis) distinguish IMPACT35 from IMPACT25/28. The drag and lift forces are calculated using the F-coordinate system. Let (C_{d1}, C_{d2}) be the drag coefficients along- and across-mine main axis and (f_1, f_2, f_3) be the added-mass corrections (f_1, f_2, f_3) in the three directions of the F-coordinate system.

The total drag force along-$\mathbf{i}_F$ (i.e., relative flow along the cylinder's main axis) is calculated by

$$F_{d1} = C_{td1}(t)V_1, \quad C_{td1}(t) \equiv C_{d1}\frac{\pi R^2}{2}\frac{\rho_w}{(1+f_1)}\left|V_1(t)\right|. \tag{49}$$

C_{d1} is almost independent on the axial Reynolds number (Re) when $Re > 10^4$, but dependent on the cylinder's aspect ratio [33],

$$C_{d1} = \begin{cases} 1.0, & \text{if } \delta > 8 \\ 0.75 + \delta/32.1934 + 0.09612/\delta^2, & \text{if } 8 \geq \delta > 0.5 \\ 1.15, & \text{if } \delta \leq 0.5. \end{cases} \tag{50}$$

The total drag force along-$\mathbf{j}_F$ (i.e., relative flow across the cylinder) is calculated by

$$F_{d2} = R\int_{-\frac{L}{2}-\chi}^{\frac{L}{2}-\chi} C_{d2}\left(V_2'\right)^2\frac{\rho_w}{(1+f_2)}d\eta \quad V_2'(\eta) = V_2 - \omega_3^F\eta$$

where V_2' is the water-to-cylinder velocity at the surface in the $\mathbf{j}_F$ direction and an empirical formula is used for calculating C_{d2} [39], as shown in (51) at the bottom of the page.

The drag force along-$\mathbf{k}_F$ is calculated by

$$\mathbf{F}_{d3} = \left[C_{d2}R\frac{\rho_w}{(1+f_2)}\omega_2^F\left|\omega_2^F\right| \times\left(\int_0^{\frac{L}{2}-\chi}\eta^2 d\eta - \int_{-\frac{L}{2}-\chi}^{0}\eta^2 d\eta\right)\right]\mathbf{k}_F. \tag{52}$$

The water-to-cylinder velocity determines the lift force [40],

$$\mathbf{F}_l = \left[\frac{C_{tl}(t)}{L}\int_{-\frac{L}{2}-\chi}^{\frac{L}{2}-\chi} V_2'(\eta)d\eta\right]\mathbf{k}_F$$
$$C_{tl}(t) \equiv C_l LR\frac{\rho_w}{(1+f_2)}|V_2| \tag{53}$$

where C_l is the lift coefficient. An empirical formula is used for calculating C_l [41]

$$C_l = \begin{cases} 2\omega_1 R/V_2, & \text{if } \omega_1 R/V_2 \leq 4 \\ 8 + 0.24(\omega_1 R/V_2 - 4), & \text{if } \omega_1 R/V_2 > 4. \end{cases} \tag{54}$$

2) Drag and Lift Torques: For an axially symmetric cylinder, the moment of the hydrodynamic force in $\mathbf{i}_F$ direction is not

$$C_{d2} = \begin{cases} 1.9276 + 8/\mathrm{Re}, & \text{if } \mathrm{Re} \leq 12 \\ 1.261 + 16/\mathrm{Re}, & \text{if } 12 < \mathrm{Re} \leq 180 \\ 0.855 + 89/\mathrm{Re}, & \text{if } 180 < \mathrm{Re} \leq 2000 \\ 0.84 + 0.00003\mathrm{Re}, & \text{if } 2000 < \mathrm{Re} \leq 12\,000 \\ 1.2 - 4/\delta & \text{if } 12\,000 < \mathrm{Re} \leq 150\,000, \quad \delta \geq 10 \\ 0.835 - 0.35/\delta, & \text{if } 12\,000 < \mathrm{Re} \leq 150\,000, \quad 2 \leq \delta < 10 \\ 0.7 - 0.08/\delta, & \text{if } 12\,000 < \mathrm{Re} \leq 150\,000, \quad \delta < 2 \\ 1.875 - 0.0000045\mathrm{Re}, & \text{if } 150\,000 < \mathrm{Re} \leq 350\,000 \\ 1/(641\,550/\mathrm{Re} + 1.5), & \text{if } \mathrm{Re} > 350\,000. \end{cases} \tag{51}$$

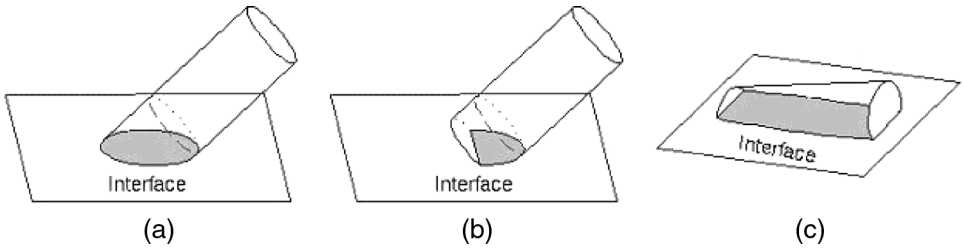

Fig. 9. Three patterns of cylinder penetration with the cross section being (a) a complete ellipse, (b) a cutoff ellipse with one side straight line, and (c) a cutoff ellipse with two sides straight lines (after [36]).

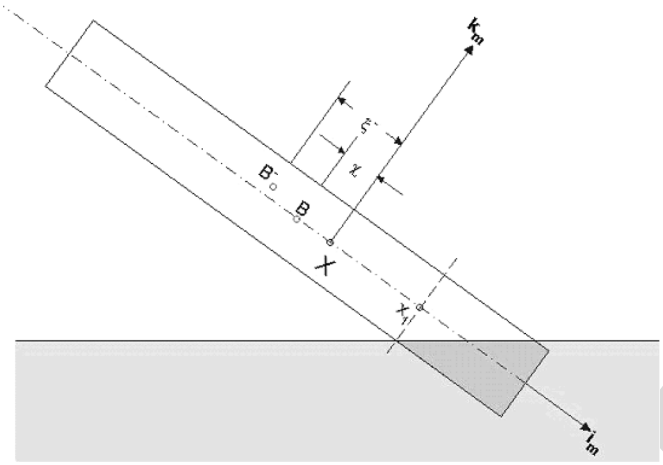

Fig. 10. Illustration of PCOV (B^-), x_1, and ξ^- for the tail part $[C^{(1)}, D^{(1)}]$ for the case in Fig. 9(a) (after [36]).

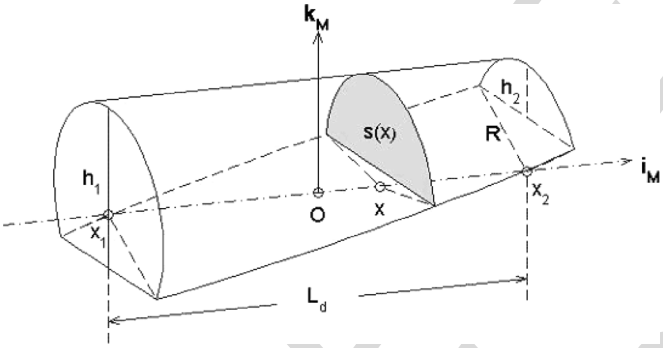

Fig. 11. Geometry of the part $D^{(1)}$ (after [36]).

caused by the drag and lift forces, but by the viscous fluid. The moment of the viscous force of steady flow between two rotating cylinders with the common axis is calculated by [42]

$$M = 4\pi\mu \frac{r_1^2 \cdot r_0^2}{r_1^2 - r_0^2}(\omega_1 - \omega_0)$$

where (r_1, r_0) and (ω_1, ω_0) are the radii and angle velocities of the inner and outer cylinders and μ is the viscosity. Moment of the viscous force on one rotating cylinder is the limit case of the two rotating cylinders as $r_0 \to \infty$ and $\omega_0 = 0$. The moment of the viscous force around $\mathbf{i}_F$ is calculated by

$$\mathbf{M}_{v1} = -C_{m1}\omega_1 \mathbf{i}_F \quad C_{m1} \equiv \pi\mu L d^2. \tag{55}$$

Same as the hydrodynamic forces, the torques along $\mathbf{j}_F$ and $\mathbf{k}_F$ axes, ($\mathbf{M}_{d1}$, $\mathbf{M}_{d2}$, $\mathbf{M}_l$), are calculated. When the cylinder rotates around $\mathbf{j}_F$ with the angular velocity ω_2^F, the drag force causes a torque on the cylinder in the $\mathbf{j}_F$ direction

$$\mathbf{M}_{d2} = \left[-\omega_2^F \left|\omega_2^F\right| \int_{-\frac{L}{2}-\chi}^{\frac{L}{2}-\chi} C_{d2} R \frac{\rho_w}{(1+f_r)} \eta^2 |\eta| d\eta \right] \mathbf{j}_F \tag{56a}$$

where f_r is the added-mass factor for the moment of drag and lift forces. If the water-to-cylinder velocity or the cylinder mass distribution is nonuniform ($\chi \neq 0$), the drag force causes a torque on the cylinder in the $\mathbf{k}_F$ direction

$$\mathbf{M}_{d3} = \left[\int_{-\frac{L}{2}-\chi}^{\frac{L}{2}-\chi} C_{d2} R \frac{\rho_w}{(1+f_r)} \left(V_2 - \omega_3^F \eta\right)^2 \eta d\eta \right] \mathbf{k}_F. \tag{56b}$$

The lift force exerts a torque on the cylinder in the $\mathbf{j}_F$ direction

$$\mathbf{M}_{l2} = \left[-\int_{-\frac{L}{2}-\chi}^{\frac{L}{2}-\chi} C_l R \frac{\rho_w}{f_{kr}} \left(V_2 - \omega_3^F \eta\right) \eta d\eta \right] \mathbf{j}_F. \tag{57}$$

3) Interfacial Treatment: Computation of buoyancy and hydrodynamic forces ($\mathbf{F}_b$, $\mathbf{F}_h$) and torques ($\mathbf{M}_b$, $\mathbf{M}_h$) is more complicated for a cylinder penetrating through air–water and water–sediment interfaces than falling through a single medium such as water. At the instance when the cylinder penetrates into an interface, three situations may exist as follows: 1) the cross section is a complete ellipse [Fig. 9(a)], 2) a cutoff ellipse with one side straight line [Fig. 9(b)], or 3) a cutoff ellipse with two straight lines [Fig. 9(c)]. The interface separates the cylinder to two parts. Each part contains a noncylinder D and a subcylinder C (Fig. 10). Let (L_c, L_d), (Ω_c, Ω_d), and (Π_c, Π_d) be the lengths, surfaces, and volumes of $[C, D]$, respectively, and (h_1, h_2) the depths of the two sides of D (Fig. 11). The characteristics of the geometric parameters (L_c, h_1, h_2) are listed in Table I. The COV for the portion $[C, D]$ is called the partial COV (PCOV). With this treatment, the drag and lift forces and torques at the two parts C and D can be computed separately [36].

4) Sediment Resistance: In the 2-D models (IMPACT25/28) the pertinent parameters are sediment density and bearing strength. The bearing strength is calculated simply by ten times the shear strength, which is not very realistic. In fact, when the mine impacts and penetrates into the sediment, it will create a large transient pore pressure in the sediment that causes

TABLE I
GEOMETRIC PARAMETERS DURING THE CYLINDER PENETRATION (AFTER [36])

	L_c	h_1	h_2
Upper & Lower Parts of Fig.9a	>0	2R	0
Upper Part of Fig. 9b	>0	2R	0 ~ 2R
Lower Part of Fig.9b	0	0 ~ 2R	0
Upper & lower Parts of Fig. 9c	0	0 ~ 2R	0 ~ 2R

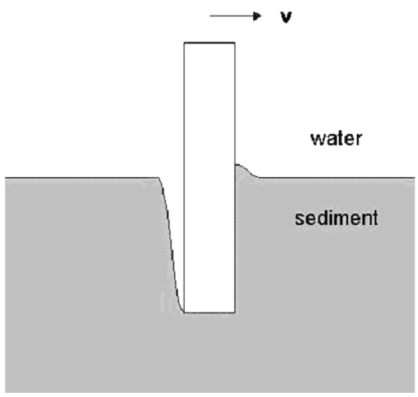

Fig. 12. Impact (resistant) force exerted on the part of the mine surface moving towards the sediment (after [36]).

ruptures in the sediment and influences the resistance force on the mine surface [11], [36], which is not simply ten times the shear strength. In 3-D model (IMPACT35), two distinct methods (delta and bearing factor) are used to compute total sediment resistance force and torque.

a) Delta method: The delta method is developed on the assumption that the mine pushes the sediment and leaves space in the wake as it impacts and penetrates into the sediment. This space is refilled by water and the water cavity is produced (Fig. 12). At the instance of the penetration, the total sediment shear resistant force on the mine surface is calculated by [36]

$$\begin{aligned}\mathbf{F}^s = &\int_{\sigma_{\text{sed}}} \boldsymbol{\tau}\,[\delta\mu G(V)S(z)]\,d\sigma \\ &- \int_{\sigma_{\text{sed}}} \mathbf{n}\left[\left(\delta\int_z^{z_{ws}} \rho_s(z')g dz'\right) + \rho_w g(z_{ws}-z)\right] d\sigma \\ &+ \mathbf{k}\frac{\pi}{8}\rho_s(z)\left(\frac{gw}{k_p} + \frac{1+e_v}{e_v}\frac{dw}{dt}\right)B^3 \end{aligned} \tag{58}$$

where, in the right-hand side, the first term is the shear resistance force, the second term is the buoyancy force, and the third term is the pore water pressure. $S(z)$ is the sediment shear strength, $G(V)$ is the impact function, V is the mine translation speed, $\rho_s(z)$ is the sediment wet density (usually obtained from the sediment data), $(\mathbf{n}, \boldsymbol{\tau})$ are unit vectors normal (outward positive) and tangential to the mine surface, z_{ws} represents the vertical coordinate of the water–sediment interface, k_p is the permeability coefficient (10^{-4} m s^{-1}, Hansen *et al.*, 1994***[AU: Please add this to the reference list]***), e_v (~0.50)

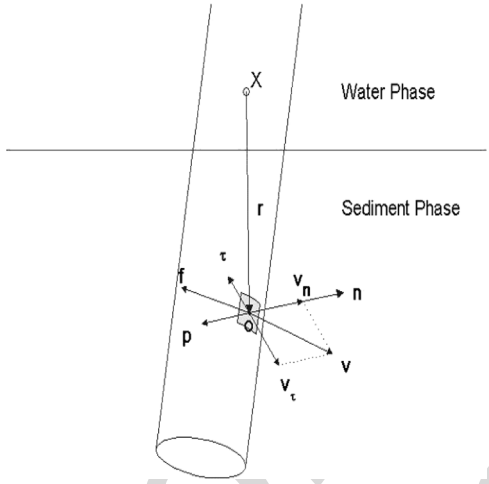

Fig. 13. Momentum and angular momentum balance for mine penetration through the water–sediment interface.

is the void ratio, and B is the length of the rupture line. The step function δ is defined by

$$\delta = \begin{cases} 1 & \mathbf{v}\bullet\mathbf{n} \geq 0 \\ 0 & \mathbf{v}\bullet\mathbf{n} \leq 0 \end{cases} \tag{59}$$

which shows that the sediment buoyancy and shear resistance forces act when the cylinder moves towards them. Let $\mathbf{v}_n$ be the normal velocity. The tangential velocity is represented by

$$\mathbf{v}_\tau = \mathbf{v} - \mathbf{v}_n. \tag{60}$$

The tangential unit vector $(\boldsymbol{\tau})$ is defined by

$$\boldsymbol{\tau} = -\frac{\mathbf{v}_\tau}{|\mathbf{v}_\tau|} \tag{61}$$

which is opposite to $\mathbf{v}_\tau$ (Fig. 13).

The sediment resistance torque $(\mathbf{M}^s)$ is calculated by

$$\begin{aligned}\mathbf{M}^s = &\int_{\sigma_{\text{sed}}} (\mathbf{r}\times\boldsymbol{\tau})\,[\delta\mu G(V)S(z)]\,d\sigma \\ &+ \int_{\sigma_{\text{sed}}} (\mathbf{r}\times\mathbf{n})\left[\left(\delta\int_z^{z_{ws}} \rho_s(z')g dz'\right) + \rho_w g(z_{ws}-z)\right] d\sigma \\ &+ (\mathbf{r}_{pw}\times\mathbf{k})\frac{\pi}{8}\rho_s(z)\left(\frac{gw}{k} + \frac{1+e_v}{e_v}\frac{dw}{dt}\right)B^3. \end{aligned} \tag{62}$$

where $\mathbf{r}_{pw}$ is the position vector (in the M-coordinate) indicating the location of the cylinder's rupture line.

b) Bearing factor method: The bearing factor method is based on the fact that the shear resistance force $(\mathbf{F}_r^s)$ is in the opposite direction of $\mathbf{v}$ and acts on the mine. Its magnitude is proportional to the product of the sediment shear strength (S) and the rupture area (A, projection of sediment-contacting area perpendicular to the velocity $\mathbf{V}$) with a nonnegative bearing factor N [43]

$$\mathbf{F}_r^s = -\int_{\sigma_{\text{sed}}} \boldsymbol{\tau} N(p,v) S A d\sigma, \qquad N \geq 0. \tag{63}$$

TABLE II
PHYSICAL PARAMETERS OF THE MODEL MINES IN THE NSWC—CARDEROCK EXPERIMENT (AFTER [46])

Mine	Mass (kg)	ρ (10^3 kg m^{-3})	L (m)	J_1 (kg m^2)	J_2 (J_3) (kg m^2)	χ (m)
1	16.96	1.60	0.505	0.0647	0.356	0
2	22.27	2.10	0.505	0.0806	0.477	0
3	34.93	1.60	1.010	0.1362	2.900	0
4	45.85	2.10	1.010	0.1696	3.820	0
5	45.85	2.10	1.010	0.1693	3.940	0.0045
6	45.85	2.10	1.010	0.1692	4.570	-0.077

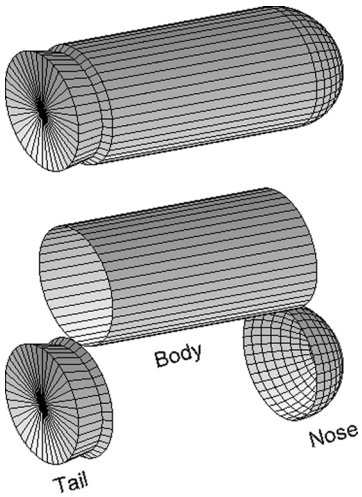

Fig. 14. Mine with nose, tail, and cylindrical body (after [35]).

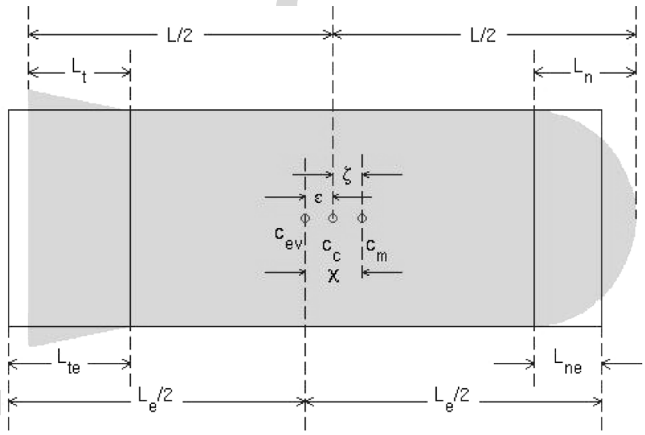

Fig. 15. Location of c_v, c_{ev}, and c_m. Here, ε is the distance between c_v and c_m and χ is the distance between c_{ev} and c_m (after [35]).

The sediment resistance torque includes the hydrodynamic and shearing resistance torques

$$\mathbf{M}^s = \int_{\sigma_{\text{sed}}} \{\mathbf{r} \times \mathbf{f}_h^s - [N(p,v)SA]\mathbf{r} \times \boldsymbol{\tau}\}\, d\sigma. \qquad (64)$$

Here, p is the nondimensional penetration depth scaled by the diameter $(2R)$. The sediment density and shear strength (S) in (63) and (64) are measured. The bearing factor increases with p and decreases with the decreasing speed

$$N(p,v) = [\mu_1 p^{\mu_2}]\left[1 + \lambda \log\left(\frac{v}{v_{cri}}\right)\right] \qquad (65)$$

where λ is the v-effect parameter, (μ_1, μ_2) are the p-effect parameters [16], and v_{cri} is the critical speed.

5) Pseudocylinder Parameterization: The Navy operational mines are usually not cylindrical. It is important to develop a model with more general shapes such as with nose and tail. Ppseudocylinder parameterization was proposed for noncylindrical mines [35]. For a near-cylindrical mine with nose and tail falling through a single medium or multiple media, the buoyancy force and torque are relatively easy to calculate. However, the hydrodynamic forces (lift, drag) and torques are difficult to compute. A feasible way is to transform a mine with nose and tail to a cylindrical mine (i.e., called the pseudocylinder parameterization). An axially symmetric mine usually consists of three parts: cylindrical body with radius of R, nose, and tail (Fig. 14). The lengths of the mine, nose, and tail are L, L_n, and L_t, respectively. A pseudocylinder is defined with the following features: the same radius (R) of the mine's cylindrical body and the same volume as the original mine (Fig. 15). It consists of the following three parts: original cylindrical body and equivalent cylinders for nose and tail. Let (Π, Π_n, Π_t) be the volumes of the mine, nose, and tail. The equivalent cylinder has length

$$L_{ne} = \frac{\Pi_n}{\pi R^2}$$

for the nose, and

$$L_{te} = \frac{\Pi_t}{\pi R^2}$$

for the tail. Let (c_c, c_m) be the mine's midpoint on the main axis and the COM position, and let c_{ev} be the COV of the pseudocylindrical mine (Fig. 15). The gravity is downward and passing through c_m. The buoyancy force is upward and passing through c_{ev}. Let ε_1 be the distances between c_c and c_m

$$\varepsilon_1 = \frac{L_n - L_{ne}}{2} - \frac{L_t - L_{te}}{2}. \qquad (66)$$

Let ε_2 be the displacement from c_c to c_m that is easy to determine if COM is given. Let χ be the displacement from c_{ev} to c_m that is calculated as

$$\chi = \varepsilon_1 + \varepsilon_2. \qquad (67)$$

Both χ and ε_2 can be positive and negative. The positive values refer to nose-down case, i.e., the point c_m is lower than the point c_{ev} for positive χ and the point c_c is lower than the point c_{ev} for positive ε_2.

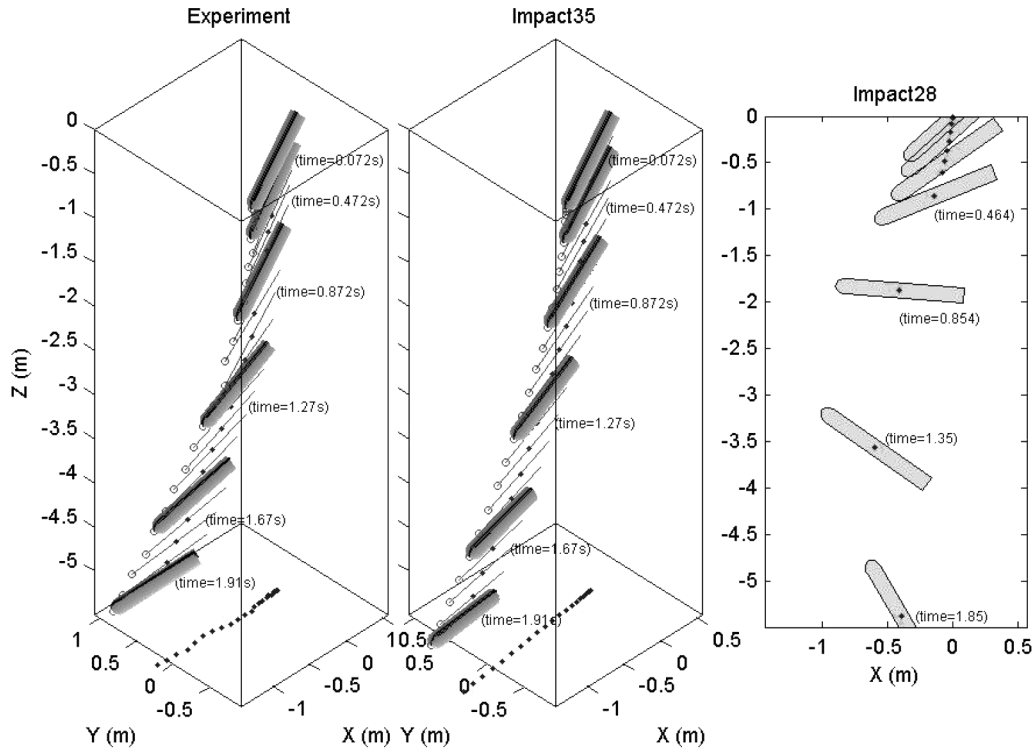

Fig. 16. Movement of mine #6 ($L = 1.01$ m, $\rho = 2.1 \times 10^3$ kg m^{-3}) with $\chi = -0.0077$ m and $\psi_2 = -14.0°$ obtained from (a) experiment, (b) 3-D model (IMPACT35), and (c) 2-D model (IMPACT25/28).***[AU: Please add space between unit and number in Figs. 16-18]***

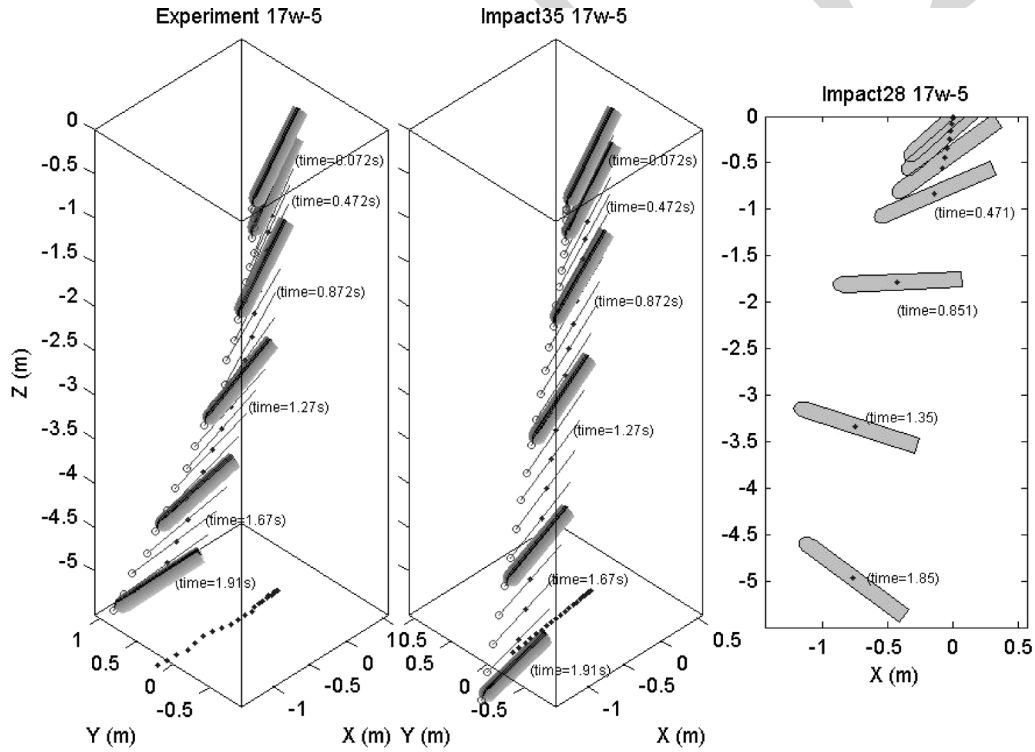

Fig. 17. Movement of mine #5 ($L = 1.01$ m, $\rho = 2.1 \times 10^3$ kg m^{-3}) with $\chi = 0.0045$ m and $\psi_2 = 42.2°$ obtained from (a) experiment, (b) 3-D model (IMPACT35), and (c) 2-D model (IMPACT25/28).

C. Mine Impact Burial Experiment for Model Verification

The added value of 3-D model (IMPACT35) versus 2-D model (IMPACT25/28) is verified by several recent experiments: mine impact burial experiment (MIBEX) at Monterey Bay, CA, on May 22, 2000 [9], [31], [32], mine drop experiment (MIDEX) at the Naval Postgraduate School (NPS) swimming pool in June 2001 [6], [10], [13], [16], [34] [44], MIDEX at NSWC—Carderock Explosion Test Pond on September

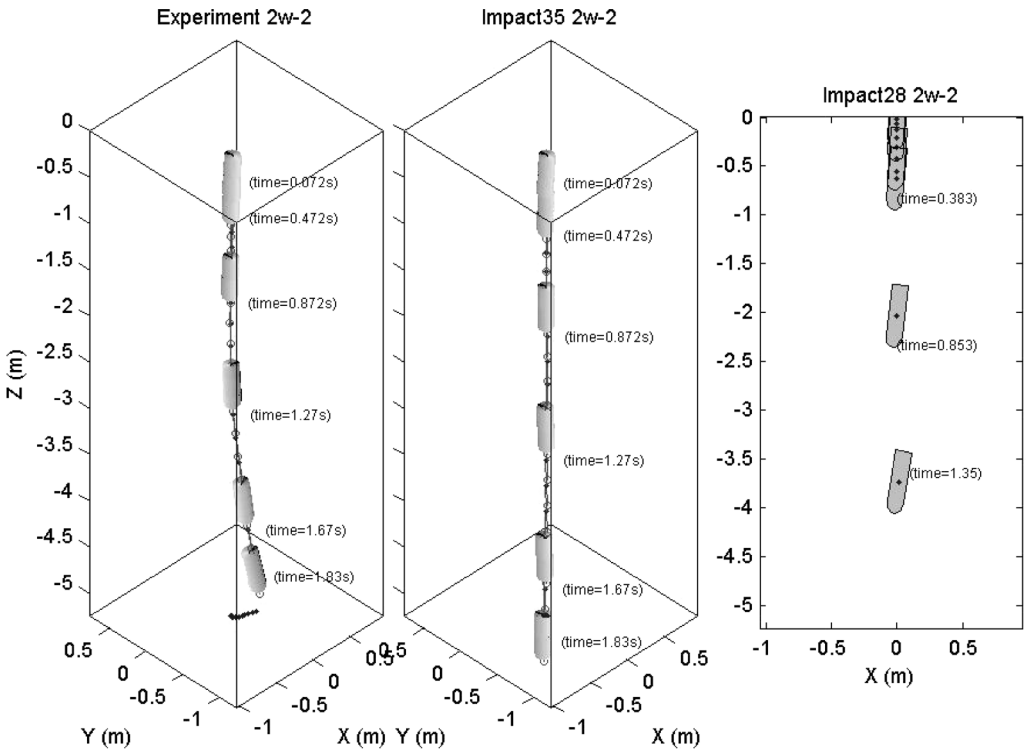

Fig. 18. Movement of cylinder #2 ($L = 0.505$ m, $\rho = 2.1 \times 10^3$ kg m^{-3}) with $\chi = 0$ and $\psi_2 = 87.0°$ obtained from (a) experiment, (b) 3D IMPACT35 model, and (c) 2D IMPACT25/28 model.

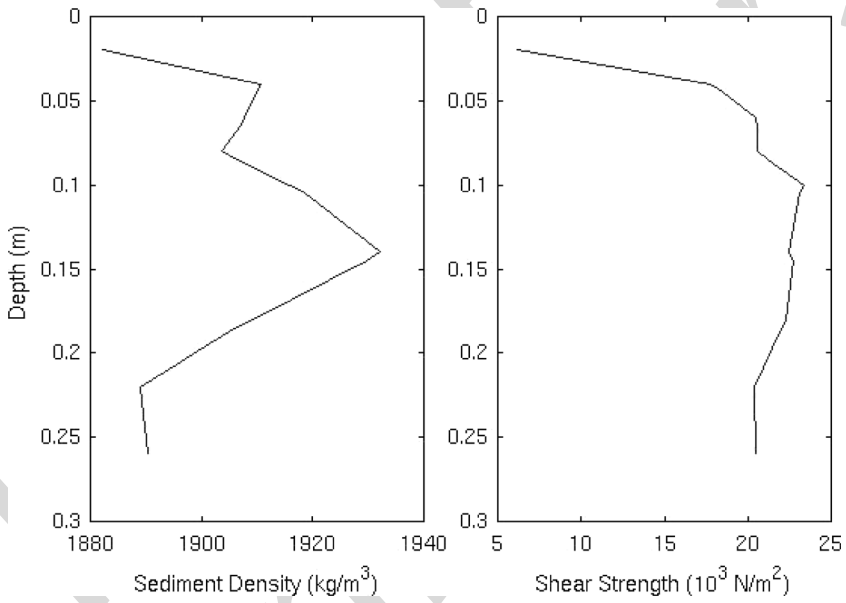

Fig. 19. Mean sediment density $\rho_s(z)$ and shear strength $S(z)$ profiles in the Monterey Bay collected during the cylinder drop experiment on May 31, 2000.

[AU: Please change units so they correspond with the text]

10–14, 2001, MIDEX at NSWC—Corpus Christi, TX, [46], [47], and the Baltic Sea experiment conducted in June 2003 by the German Federal Armed Forces Underwater Acoustic and Marine Geophysics Research Institute (FWG, Kiel, Germany) [48], [49] with the full-size optical mine which is allowed to free fall from the wench. During these experiments, various model mines (most cylinders) were released into the water. The mine trajectories were recorded by underwater high-speed video cameras. The mine burial depths were also observed by the diver (in MIBEX—Monterey Bay) and optical instruments (in MIDEX—Baltic Sea).

D. Model-Data Comparison

The 2-D model (IMPACT25/28) and 3-D model (IMPACT35) are integrated using the same mine parameters (such as the density ratio, length, radius, and distance between

COV and COM) and mine drop initial conditions (speed and orientation) as in the mine drop experiments. Added value ***[AU: "Value-added" was changed to "added value" throughout. Please check.]*** of IMPACT35 versus IMPACT25/28 is verified through comparison between modeled and observed mine trajectories and burial depths.

1) Trajectory in Water Column: Data from MIDEX at NSWC—Caderock is used as illustration. The physical parameters of the six mines are presented in Table II. Three cases are presented as follows: 1) near-horizontal release ($\psi_2^{(0)} = -14°$) with model mine #6, 2) near-45° release ($\psi_2^{(0)} = 42.2°$) with model mine #6, and 3) near-vertical release ($\psi_2^{(0)} = 87°$) with model mine #2. The other initial conditions are given by

$$x^{(0)} = y^{(0)} = z^{(0)} = 0 \quad u^{(0)} = v^{(0)} = w^{(0)} = 0$$
$$\psi_1^{(0)} = \psi_3^{(0)} = 0 \quad \omega_1^{(0)} = \omega_2^{(0)} = \omega_3^{(0)} = 0. \tag{68}$$

For near-horizontal release (Fig. 16), the 3-D model (IMPACT35) simulated trajectory agrees well with the observed trajectory with the same travel time (1.91 s) for the mine passing through the water column. For near-45° release, the 3-D model (IMPACT35) simulated trajectory and travel time agree well with the observed trajectory (Fig. 17). However, the 2-D model (IMPACT28) has less capability to predict the cylinder trajectory in the water column.

For near-vertical release (Fig. 18), the 3-D model (IMPACT35) simulated trajectory agrees well with the observed trajectory. Both show the same straight pattern and the same travel time (1.83 s) for the cylinder passing through the water column. However, the existing 2-D model (IMPACT28) does not predict the travel time well.

2) Burial Depth: MIBEX—Monterey Bay was conducted on the R/V John Martin on May 23, 2000 [9], [31]. The barrel with density ratio of 1.8 was treated as model mine and released horizontally while touching the surface. The initial conditions were

$$x^{(0)} = y^{(0)} = z^{(0)} = 0 \quad u^{(0)} = v^{(0)} = w^{(0)} = 0$$
$$\psi_2^{(0)} = 90° \quad \psi_1^{(0)} = \psi_3^{(0)} = 0 \quad \omega_1^{(0)} = \omega_2^{(0)} = \omega_3^{(0)} = 0. \tag{69}$$

This would eliminate any chance of inertial effects caused by uneven introduction into the air–sea interface. This also set the initial velocity parameter in the code to zero. The barrel was to be released 17 times. The diver would snap the quick-release shackle on the barrel, and then, dive down to conduct measurements. The average depth of the water was 13 m. Since the path the barrel would follow was uncertain, both the releasing diver and a second safety diver would stay on the surface until after the barrel was dropped. Once reaching the bottom, one diver would take penetration measurements using a meter stick marked at millimeter increments while the other would take a gravity core. After 17 drops, the divers began to run out of air and results were not varying greatly so the decision was made to end the experiment. The gravity cores were taken immediately to the United States Geological Survey (USGS) Laboratories in Menlo Park, CA, to get the sediment density and shear strength profiles (Fig. 19).

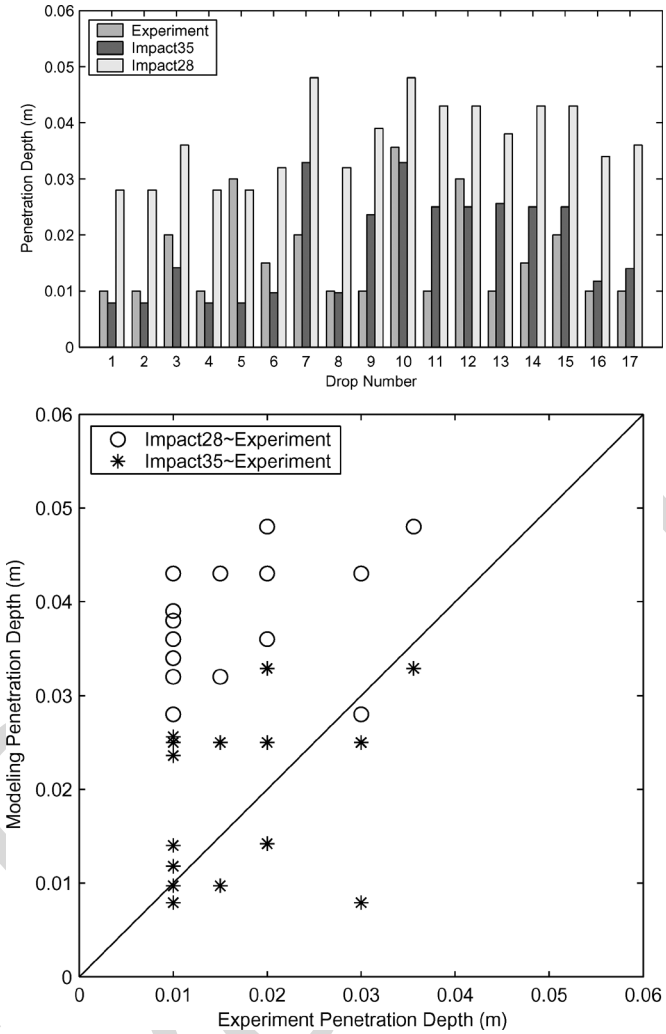

Fig. 20. Observed (MIBEX—NPS) and predicted (IMPACT25/28 and IMPACT35 with delta method) burial depths: (a) direct comparison and (b) scatter diagram. Note that the 2-D model (IMPACT25/28) predicts the burial depth 5–10 times larger than the observed depth, and IMPACT35 with dDelta method performs much better than IMPACT25/28 (after [36]).

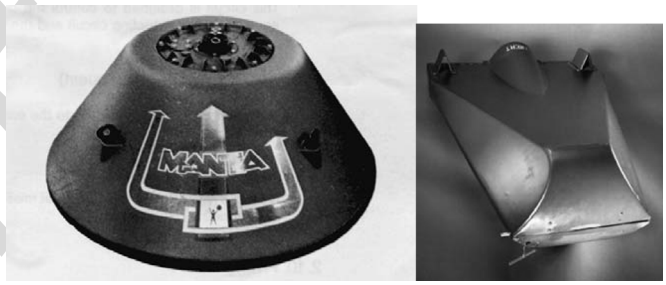

Fig. 21. Operational mines: (a) Manta and (b) Rockan (after [50]).

For sediment resistance force, the 2-D model (IMPACT25/28) uses ten times shear strength as the bearing strength. The 3-D model (IMPACT35) uses the delta or bearing factor method (see Section VI-B4). After running the two models (IMPACT35 and IMPACT25/28) for each gravity core regime $[\rho_s(z), S(z)]$ from the initial conditions (69), the burial depths were compared with measured burial depth data (Fig. 20). As evident, IMPACT35 improves the prediction

capability. The existing 2-D model (IMPACT25/28) overpredicts actual burial depth by an order of magnitude on average. However, the 3-D model (IMPACT35) predicts the burial depth reasonably well without evident overprediction. Since the gravity cores were taken for approximately 2–3 m from the impact location, several cores were taken for each drop. This allowed an average to be calculated to yield more accurate data for each drop. Recently, Chu and Fan [11] compared the delta and bearing factor methods in IMPACT35 for sediment resistance using the Baltic Sea experiment data and found that the bearing factor method is better than the delta method.

E. Weakness and Future Improvement

The main limitation of the current iteration of IMPACT 35 is its utilization for cylindrical and near-cylindrical mines only. The effect of shape is a significant issue if the model is to be used operationally, as the most widely used bottom mines such as Manta and Rockan are not cylindrical (near-cylindrical). Determination of the hydrodynamic force and torque for noncylindrical mines is crucial, but there are no existing formulas for these shapes.

The shape effect is more tenuous and will have less test data. Shape is a significant issue if the model is used operationally, because the most popular mines such as Rockan and Manta are not cylindrical (Fig. 21). The most important issue is to determine the hydrodynamic (drag and lift) force and torque for noncylindrical mines since there is no existing formula for calculating the drag and lift forces and torques for noncylindrical objects. MIDEX-II at NPS, conducted in September 2005, is the direct continuation of mine drop experiments with operational mine shapes [50], [51]. In that experiment, the overall shape of the mine was varied from cylindrical mines to see how the water phase trajectory would be affected. In addition to a sphere and semihemispherical "Gumdrop" shape, two shapes were specifically chosen to represent real-world bottom mines: Manta and Rockan [50], [51].

With the data collected at MIDEX-II at NPS, IMPACT35 for Manta and Rockan mines are developing. In the model development, the nonlinear instability and model sensitivity should be studied. Within the correct physics there is a possibility of chaotic behavior in the model. The chaotic features will be handled by the instability and predictability analyses.

VII. Conclusion

Advances in the mine impact burial prediction are reviewed in this paper. The 1-D model (IBPM) was developed to predict the vertical position of the mine's COM. The model provides useful information such as higher falling velocity for vertical release than for horizontal release, strong dependence of water and vertical impact velocity on the attitude for light mines (not for heavy mines), and strong dependence of the mine's falling velocity in water column on attitude, wet weight, mine's length, and mine's radius. For the same mine, the falling velocity in the water has a minimum in horizontal orientation and a maximum in vertical orientation. Major weakness is the constant falling angle assumption through a single fluid.

The 2-D model (IMPACT25/28) was developed to overcome the major weakness of the 1-D model and to predict the COM position in the (x, z)-plane and the rotation around the y-axis. Major weakness is the difficulty to include the fluid's motion in the model because it is impossible to lay a mine in the same direction of the fluid velocity. In littoral zone, the water velocity is not negligible. The application of the 2-D model for the operational use is limited. Other weaknesses are as follows: 1) a similar dependence of the axial and cross drag coefficients on the Reynolds number Re and the aspect ratio and 2) crude parameterization for sediment bearing strength.

The 3-D model (IMPACT35) has been developed to predict the COM position in (x, y, z)-space and the rotation around x-, y-, and z-axes. Althogh IMPACT35 shows great improvements versus IMPACT25/28 using the recent mine drop experimental data, it is used only for the cylindrical and near-cylindrical mines (major weakness). Mine shape is a significant issue if the model is used operationally, because the most mines such as Manta and Rockan are not cylindrical. The most important thing for future improvement of IMPACT35 is to determine the drag and lift laws for noncylindrical mines. With the data collected during MIDEX-II at NPS for operational mine shapes such as Manta and Rockan, IMPACT35 for operational mine shapes should be developed.

Acknowledgment

The author would like to thank Drs. P. Valent, M. D. Richardson, P. Elmore, T. Holland, and A. Abelev at the Naval Research Laboratory, and Dr. T. Weaver at FWG for fruitful discussions that benefited this paper.

References

[1] R. A. Arnone and L. E. Bowen, "Prediction model of the time history penetration of a cylinder through the air-water-sediment phases," Naval Coast. Syst. Ctr., Panama City, FL, Tech. Note 734-36, 1980.

[2] L. J. Satkowiak, "Modifications to the NCSC impact burial prediction model," Naval Coast. Syst. Ctr., Panama City, FL, Tech. Note 883-87, 1987.

[3] ——, "User's guide for the modified impact burial prediction model," Naval Coast. Syst. Ctr., Panama City, FL, Tech. Note 884-87, 1987.

[4] R. B. Hurst, "Mine impact burial prediction model—Technical description of recent changes and developments (U)," Def. Sci. Establishment, Auckland, New Zealand, DSE Rep. 149, 1992, (Restricted).

[5] P. J. Mulhearn, "Experiments on mine burial on impact—Sydney Harbour," *U.S. Navy J. Underwater Acoust.*, vol. 43, pp. 1271–1281, 1992.

[6] P. C. Chu, A. F. Gilles, C. W. Fan, and P. Fleischer, "Hydrodynamics of falling mine in water column," in *Proc. 4th Int. Symp. Technol. Mine Problem*, 2000, CD-ROM.

[7] P. C. Chu, V. L. Taber, and S. D. Haeger, "Environmental sensitivity studies on mine impact burial prediction model (two-dimensional)," in *Proc. 4th Int. Symp. Technol. Mine Problem*, 2000, CD-ROM.

[8] ***[AU: Please provide department]***V. L. Taber, "Environmental sensitivity studies on mine impact burial prediction model," M.S. thesis, Naval Postgrad. School, Monterey, CA, 1999.

[9] ***[AU: Please provide department]***T. B. Smith, "Validation of the mine impact burial model using experimental data," M.S. thesis, Naval Postgrad. School, Monterey, CA, 2000.

[10] P. C. Chu, A. D. Evans, A. F. Gilles, T. Smith, and V. Taber, "Development of Navy's 3D mine impact burial prediction model (IMPACT35)," in *Proc. 6th Int. Symp. Technol. Mine Problem*, 2004, DVD-ROM.

[11] ***[Page range to come!]***P. C. Chu and C. W. Fan, R. H. Wilkens and M. D. Richardson, Eds., "Mine impact burial model (IMPACT35) verification and improvement using sediment bearing factor method," *IEEE J. Ocean. Eng.*, vol. 32, no. 1, pp. XXX–XXX, Jan. 2007.

[12] P. C. Chu, "Hydrodynamics of mine impact burial," presented at the ONR Impact Burial Annu. Workshop, La Jolla, CA, Jan. 15–17, 2002.

[13] P. C. Chu, C. W. Fan, A. D. Evans, A. F. Gilles, and P. Fleischer, "Three-dimensional hydrodynamic model for prediction of falling cylinder through water column," in *Proc. MTS/IEEE Conf. OCEANS*, San Diego, CA, 2003, pp. 2047–2057.

[14] P. C. Chu, C. W. Fan, and A. D. Evans, "Three-dimensional rigid body impact burial model (IMPACT35)," *Adv. Fluid Mech.*, vol. 5, pp. 43–52, 2004.

[15] ***[AU: Please provide department]***A. D. Evans, "Hydrodynamics of mine impact burial," M.S. thesis, Naval Postgrad. School, Monterey, CA, 2002.

[16] P. C. Chu, C. W. Fan, A. D. Evans, and A. F. Gilles, "Triple coordinate transforms for prediction of falling cylinder through the water column," *J. Appl. Mech.*, vol. 71, pp. 292–298, 2004.

[17] H. Lamb, *Hydrodynamics*. Cambridge, U.K.: Cambridge Univ. Press, 1932.

[18] L. M. Milne-Thomson, *Theoretical Hydrodynamics*. New York: Macmillian, 1968.

[19] H. Aref and S. W. Jones, "Chaotic motion of a solid through ideal fluid," *Phys. Fluids A—Fluid Dyn.*, vol. 5, no. 12, pp. 3026–3028, 1993.

[20] ——, "Motion of a solid body through an ideal fluid," College Eng., Univ. Illinois Urbana-Champaign, Urbana, IL, Rep. No. 772, 1994.

[21] P. Holmes, J. Jenkins, and N. E. Leonard, "Dynamics of the Kirchhoff equations I: Coincident centers of gravity and buoyancy," *Physica D*, vol. 118, no. 3–4, pp. 311–342, 1998.

[22] S. B. Field, M. Klaus, M. G. Moore, and F. Nori, "Chaotic dynamics of falling disks," *Nature*, vol. 388, no. 6639, pp. 252–254, 1997.

[23] L. Mahadevan, W. S. Ryu, and D. T. S. Aravinthan, "Tumbling cards," *Phys. Fluids*, vol. 11, no. 1, pp. 1–3, 1999.

[24] N. E. Kochin, I. A. Kibel, and N. V. Roze, *Theoretical Hydromechanics*. New York: Interscience, 1964.

[25] V. V. Kozlov, "Heavy rigid body falling in an ideal fluid," *Izv AN SSSR, Mekhanika Tverdogo Tela*, vol. 24, no. 5, pp. 10–17, 1989.

[26] L. J. Satkowiak, "Modified NCSC impact burial prediction model with comparisons to mine drop tests," Naval Coast. Syst. Ctr., Panama City, FL, Tech. Note 486-88, 1988.

[27] P. C. Chu, "Ensemble mine impact burial prediction," presented at the ONR Impact Burial Modeling Workshop, Phoenix, AZ, Mar. 5–7, 2002.

[28] P. C. Chu, V. L. Taber, and S. D. Haeger, " Mine impact burial model sensitivity study," Naval Postgrad. School, Monterey, FL, NPS-IJWA-00-003, 2000, pp. 1–48.

[29] E. M. Stanley, "Viscosity of sea water at moderate temperatures and pressures," *J. Geophys. Res.*, vol. 74, pp. 3415–3420, 1969.

[30] R. B. Krone, "A study of rheological properties of estuarine sediments," U.S. Army Corps Eng., Vicksburg, MS, Tech. Bulletin No.7, 1963.

[31] P. C. Chu, T. B. Smith, and S. D. Haeger, "Mine impact burial prediction experiment," Naval Postgrad. School, Monterey, CA, NPS-IJWA-01-007, 2001, pp. 1–161.

[32] ——, "Mine impact burial prediction," in *Proc. 4th Int. Symp. Technol. Mine Problem*, 2002, CD-ROM.

[33] C. T. Crowe, J. A. Roberson, and D. F. Elger, *Engineering Fluid Mechanics*, 7th ed. New York: Wiley, 2001, pp. 1–714.

[34] P. C. Chu, A. F. Gilles, C. W. Fan, J. Lan, and P. Fleischer, "Hydrodynamics of falling cylinder in water column," *Adv. Fluid Mech.*, vol. 4, pp. 163–181, 2002.

[35] P. C. Chu and C. W. Fan, "Pseudo-cylinder parameterization for mine impact burial prediction," *J. Fluids Eng.*, vol. 127, pp. 1515–1520, 2005.

[36] ——, "Prediction of falling cylinder through air-water-sediment columns," *J. Appl. Mech.*, vol. 73, pp. 300–314, 2006.

[37] P. C. Chu and G. Ray, "Prediction of high speed rigid body maneuvering in air-water-sediment column," *Adv. Fluid Mech.*, vol. 6, pp. 123–132, 2006.

[38] P. C. Chu, G. Ray, P. Fleischer, and P. Gefken, "Development of three dimensional bomb maneuvering model," in *Proc. 7th Int. Symp. Technol. Mine Problems*, 2006, DVD-ROM.

[39] H. Rouse, *Fluid Mechanics for Hydraulic Engineers*, 1st ed. New York: Mcgraw-Hill, 1938.

[40] R. Von Mises, *Theory of Flight*. New York: Dover, 1959, pp. 564–585.

[41] B. M. Sumer and J. Fredsøe, *Hydrodynamics Around Cylindrical Structures*. Singapore: World Scientific, 1997.

[42] F. M. White, *Viscous Fluid Flow*. New York: McGraw-Hill, 1974.

[43] ***[Page range to come!]***C. P. Aubeny and H. Shi, R. H. Wilkens and M. D. Richardson, Eds., "Effect of rate-dependent soil strength on cylinders penetrating into soft clay," *IEEE J. Ocean. Eng.*, vol. 32, no. 1, pp. XXX–XXX, Jan. 2007.

[44] ***[AU: Please provide department]***A. F. Gilles, "Mine drop experiment," M.S. thesis, Naval Postgrad. School, Monterey, CA, 2001.

[45] P. C. Chu, A. F. Gilles, and C. W. Fan, "Experiment of falling cylinder through the water column," *Exp. Thermal Fluid Sci.*, vol. 29, pp. 555–568, 2005.

[46] ***[Page range to come!]***A. V. Abelev, P. J. Valent, and K. T. Holland, R. H. Wilkens and M. D. Richardson, Eds., "Behavior of a large cylinder in free fall through water," *IEEE J. Ocean. Eng.*, vol. 32, no. 1, pp. XXX–XXX, Jan. 2007.

[47] K. T. Holland, A. W. Green, A. Abelev, and P. J. Valent, "Parameterization of the in-water motions of falling cylinders using high-speed video," *Exp. Thermal Fluid Sci.*, vol. 37, pp. 690–770, 2004, doi: 10.1007/800348-004-0859-2.

[48] ***[AU: Please provide page range]***P. A. Elmore, R. Wilkens, T. Weaver, and M. D. Richardson, "IMPACT 28 and 35 simulations of 2003 Baltic Sea cruise: model results and comparison with data," in *Proc. 5th Annu. ONR Workshop Mine Burial Prediction*, Kona, HI, Jan. 31–Feb. 2 2005.

[49] ***[Page range to come!]***P. A. Elmore, M. D. Richardson, and R. H. Wilkens, R. H. Wilkens and M. D. Richardson, Eds., "Exercising the Monte Carlo mine burial prediction system for impact and scour burial for operational Navy use," *IEEE J. Ocean. Eng.*, vol. 32, no. 1, pp. XXX–XXX, Jan. 2007.

[50] P. C. Chu, C. R. Allen, and P. Fleischer, "Non-cylindrical mine impact experiment," in *Proc. 7th Int. Symp. Technol. Mine Problems*, 2006, DVD-ROM.

[51] ***[AU: Please provide department]***C. R. Allen, "Mine drop experiment II with operational mine shapes (MIDEX-II)," M.S. thesis, Naval Postgrad. School, Monterey, CA, 2006.

Peter C. Chu received the Ph.D. degree in geophysical fluid dynamics from the University of Chicago, Chicago, IL, in 1985.

He is a Professor of Oceanography and Head of the Naval Ocean Analysis and Prediction (NOAP) Laboratory at the Naval Postgraduate School, Monterey, CA. His research interests include ocean analysis and prediction, coastal modeling, littoral zone oceanography for mine warfare, mine impact burial prediction, mine acoustic detection, and satellite data assimilation for undersea warfare.